Title
Direct-Write Piezoelectric Nanogenerator by Near-Field Electrospinning

Author
Chang, Chieh

Publication Date
2009

Peer reviewed|Thesis/dissertation

Direct-Write Piezoelectric Nanogenerator by Near-Field Electrospinning

by

Chieh Chang

A dissertation submitted in partial satisfaction of the

requirements for the degree of

Doctor of Philosophy

in

Engineering - Mechanical Engineering

in the

Graduate Division

of the

University of California, Berkeley

Committee in charge:

Professor Liwei Lin, Chair

Professor Albert P. Pisano

Professor Seung-Wuk Lee

Fall 2009

Direct-Write Piezoelectric Nanogenerator by Near-Field Electrospinning

by

Chieh Chang

ABSTRACT

Direct-Write Piezoelectric Nanogenerator by Near-Field Electrospinning
by
Chieh Chang
Doctor of Philosophy in Engineering - Mechanical Engineering
University of California, Berkeley
Professor Liwei Lin, Chair

Electrospinning technology based on the electrostatic driving mechanism can construct long and continuous polymeric nanofibers with diameters less than 100 nm. However, conventional electrospinning process is chaotic by nature. The chaos is manifested in the difficulty to control the deposition position and amount of electrospun nanofibers. In this dissertation, a near-field electrospinning (NFES) process has been developed to deposit solid nanofibers in a direct and controllable manner. The process is further extended to continuous and large area deposition and applied to energy harvesting applications by constructing piezoelectric nanogenerators.

In near-field electrospinning process using polyethylene oxide (PEO) as the demonstration example, a tungsten electrode with tip diameter of 25 μm is used to construct nanofibers of 50~500 nm in line-width on silicon based collectors while the liquid polymer solution is supplied in a manner analogous to that of a dip pen. The minimum applied bias voltage is 600 V and minimum electrode-to-collector distance is 500 μm to achieve position controllable deposition. Charged nanofibers can be orderly collected, making NFES a potential tool in direct write nanofabrication for a variety of materials.

The discontinuity issue of the first-generation NFES process is resolved by a continuous NFES process. Before the onset of electrospinning, a bias voltage is applied to a semi-spherical shaped polymer droplet formed outside of a syringe needle. A probe tip is used to mechanically draw a single fiber from the droplet to initiate the continuous NFES process. It is observed that decreasing electrical field in continuous NFES results in smaller line-width deposition which is in contrast to the general understandings from the conventional electrospinning process. Nanofibers can be assembled into controlled, complex patterns such as circular shapes and grid arrays on large and flat areas.

Direct-write polyvinylidene fluoride (PVDF) nanofibers have been constructed as nanogenerators. These nanofibers attain both *in-situ* mechanical stretch and electrical poling to produce piezoelectric characteristics. Under mechanical stretching, nanogenerators have shown repeatable and consistent electrical outputs with energy conversion efficiency of 21.8%, which is an order of magnitude higher than those made of PVDF thin films. The early onset of the nonlinear domain wall motions behavior has been identified as one mechanism responsible for the apparent high piezoelectricity in nanofibers, rendering them potentially advantageous for sensing and actuation applications.

TABLE OF CONTENTS

LIST OF FIGURES

LIST OF TABLES

CHAPTER 1

INTRODUCTION AND BACKGROUND

1.1. Introduction

One-dimensional nanostructures such as nanotubes, nanowires, and nanofibers have attracted tremendous research interests for various potential applications. Among them, the flexible nature of nanofibers could be advantageous in structures such as embedded zero dimensional nanomaterials for sensing and actuation applications. Electrospinning is a versatile method to produce nanofibers of different kinds of materials with diameters ranging from a few micrometers down to a few nanometers. The method can be applied for synthetic and natural polymers, polymer alloys, polymer composites, as well as metals and ceramics [1]. Typical applications of electrospinning include filtrations, membranes, wound dressing, bio-scaffolds and medical implants [2]. In recent years, researchers have further explored the possibilities of using electrospinning for fabrication of micro- and nanodevices such as field effect transistors [3], gas [4] optical sensors [5], and DNA functional chips [6].

In a typical electrospinning process, ultra-thin polymer fibers are formed when a droplet of a viscoelastic polymer solution is subjected to a high voltage electrostatic field [7]. After the jet is emitted from the polymer cone, it bends into a complex path and other changes in shape occur, during which electrical force stretches the fiber [8]. This stretching and whipping process causes the formation of very thin polymer fibers, which are randomly deposited on a counter electrode serving as a collector.

Since the nanofibers formation in an electrospinning process relies on this chaotic whipping of the liquid jet, electrospinning is unstable in nature. Highly aligned nanofibers are therefore difficult to achieve using this method. Several research works have investigated different techniques to achieve alignment of electrospun nanofibers, among others using a rotating collector [9, 10, 11, 12] or modified electrical field [13, 14]. At the same time, numerous studies have been contributed in fundamental physics and chemistry of electrospinning [15] as well as modeling of the process [8, 16] for further improvement and better control of the process.

In this dissertation, a novel idea of controllable electrospinning based on a new type of "near-field" electrospinning (NFES) is presented as shown in Figure 1.1. The electrode-to-collector distance, which is typically in the order of 10 cm in conventional electrospinning, is dramatically reduced to about a half millimeter in order to utilize the stable liquid jet region. At such a shortened distance, electrospinning can be run at a voltage of about one kilovolt, in comparison to several tens kilovolts in conventional electrospinning. With this innovative concept, NFES presents a simple yet powerful method for direct-write deposition of nanofibers with high level of track controllability.

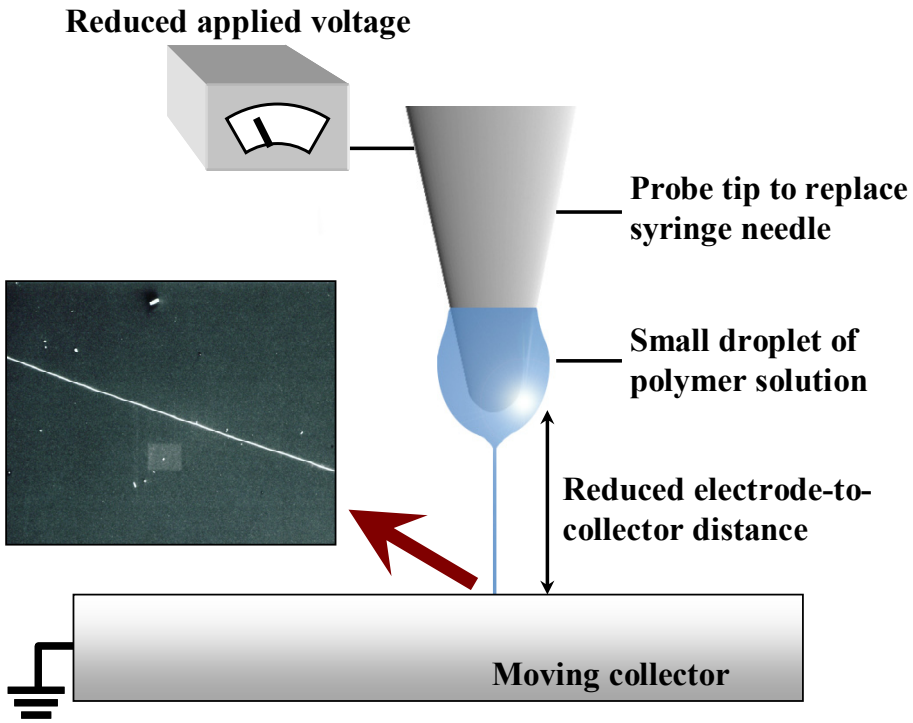

Figure 1.1. Major achievement of NFES.

A second generation of NFES called "continuous NFES" is then developed to further extend its capability to construct large scale patterns and to simply its operation procedure for possible process automation. The main differences between these two generations are the use of syringe needle for continuous polymer solution supply and the probe tip for process initiation as shown in Figure 1.2. With these innovative modifications, continuous NFES maintains the continuous characteristic of conventional electrospinning while the superior controllability is still preserved. The concept and initial demonstrations of NFES suggest that NFES can be extended to new applications previously unachievable by conventional means.

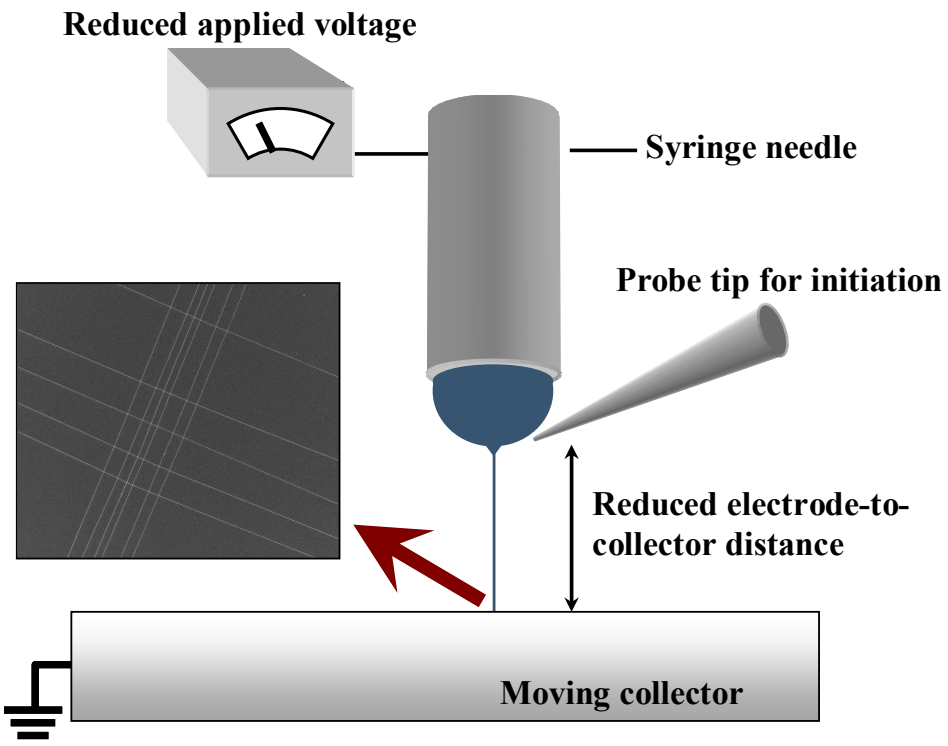

Figure 1.2. Major achievement of continuous NFES.

In the third major accomplishment, we used NFES to make piezoelectric nanogenerators for possible applications of energy harvesting. Electrical power supply generated from scavenging mechanical movements are of great interests for systems of all dimensions [17]. Specifically, a self-powering system that harvests its operating energy directly from the environment is an attractive proposition for sensing, personal electronics and defense technologies [18]. For example, buildings often has constant low frequency vibration (100~200 Hz) and energy could be scavenged to power stand-alone wireless sensors for temperature and humidity measurements [19]. When a car is running, the rotation of wheels could be the power source for wireless tire pressure sensors [20]. Walking dynamics of a human being could be the energy sources from various locations such as heels [21], elbows [22] and clothes [23]. One key element in these energy scavenge schemes is an efficient mechanical-to-electrical energy converter or utilization of piezoelectric material in most cases.

The third part of the dissertation aims to address the mechanical energy scavenge issue by introducing a new architecture – electrospun piezoelectric nanofibers. Piezoelectric nanofibers have never been studied or demonstrated before and it could present interesting potentials in various applications beyond power scavenge, including piezoelectric sensing and actuation. Among the applications, energy conversion represents most fundamental and scientific challenges such that we choose nanogenerators as demonstration examples. Figure 1.3 shows a classical mechanical power distribution diagram from body-driven sources redrawn from Ref [24]. The total powers for each action are included in parentheses while the estimations of possible scavenged power outputs are illustrated using various energy harvesters. It is noted

that these numbers are very optimistic estimations and most of the estimated energy outputs have never been demonstrated experimentally. For example, the footfalls has a theoretical energy scavenge output of 8.3W and a previous project at MIT more than 10 years ago was able to demonstrate 80mW-peak and 1mW-average power outputs – well below the analytical prediction [25]. The MIT project placed polyvinylidene fluoride (PVDF) plates as shown in Figure 1.4 in walking shoes as the mechanical-to-electrical energy harvesters. It is obvious that the dramatically reduction in energy harvesting as compared with the theoretical analyses comes from the very low efficiency of power transformation. After 10 years, there have no great progresses in this issue and we believe that new materials and technologies must be investigated to address this engineering and scientific challenge.

We start our studies on manufacturing protocols, material properties and optimizations and then focus our studies on single nanofiber nanogenerator. With the aids of NFES, PVDF nanofibers could be direct-written and simultaneously polarized to obtain the piezoelectric crystalline structure as shown in Figure 1.5. This principle and the successful experimental demonstration of PVDF nanogenerator could be the basis for new self-powered nanodevices that harvest electricity from the environment for applications such as implantable biomedical devices, wireless sensors, and portable electronics.

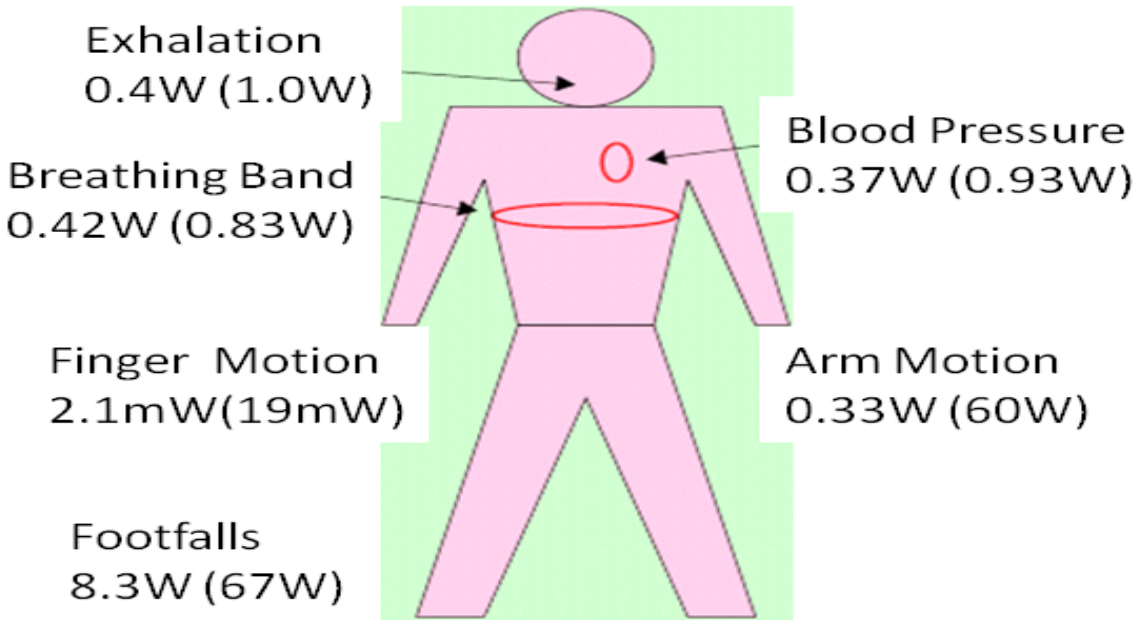

Figure 1.3. Power from body-driven movements. Total power from each action is included in parentheses [24].

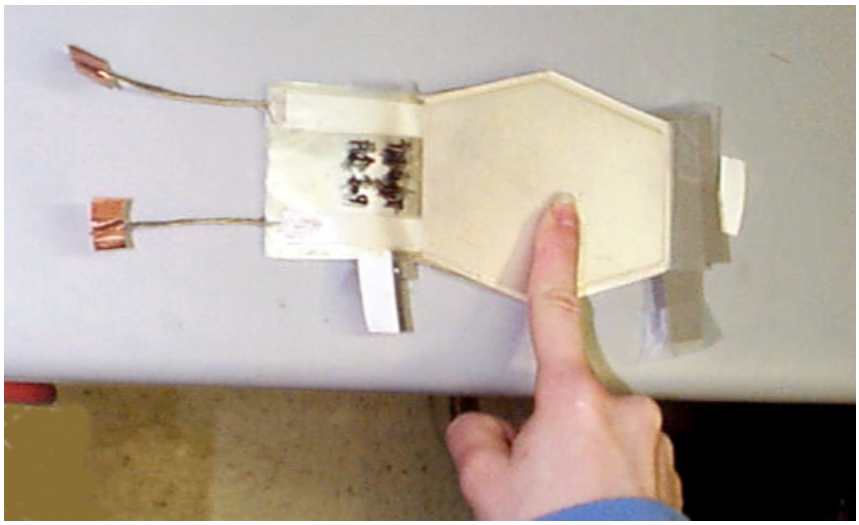

Figure 1.4. The PVDF plates used in walking shoes as the mechanical-to-electrical energy harvesters in the MIT project more than 10 years ago [25].

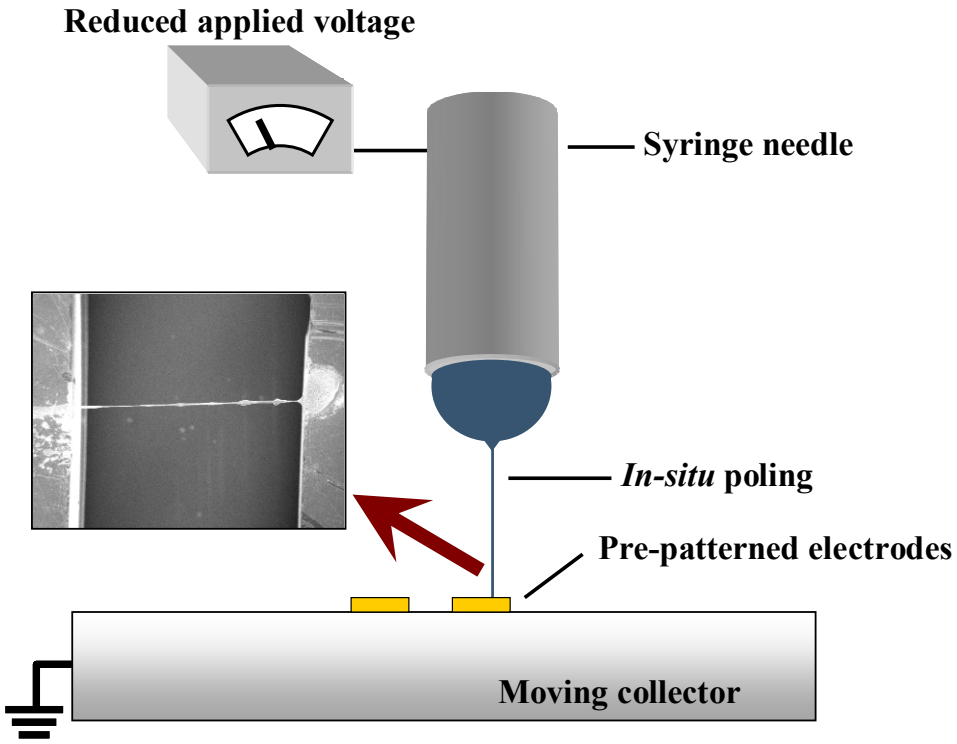

Figure 1.5. Major achievement of direct-write piezoelectric nanogenerator.

1.2. Chapter Overviews

The dissertation is organized in six chapters to describe the research and development efforts. Chapter one briefly introduces the background of electrospinning and nanogenerators, the development of near-field electrospinning and the use of electrospun nanofibers for nanogenerators. Chapter two focuses on the fundamentals of electrospinning process and introduces relevant works on the alignment and assembly of electrospun nanofibers. In chapter three, the details of near-field electrospinning process are presented on how to electrospin nanofibers in a direct and controllable manner. However, the dip-pen like approach has limited deposition length for nanofibers while the fiber thickness is inevitably nonuniform because the polymer droplet is consumed during the process. Therefore, a novel continuous near-field electrospinning is proposed and demonstrated in chapter four, which benefits from the continuity of conventional electrospinning and the superior location control of near-field electrospinning to produce orderly nanofiber patterns over large areas. In chapter five, the development of PVDF piezoelectric nanogenerator via continuous NFES is presented, including fabrication process development, experiments, measurements, and piezoelectric response validation. Chapter six describes the summary of this dissertation and discussions of future research directions, including further expansion of the applications of near-field electrospinning and further improvements on the performance and the functionality of the piezoelectric nanogenerators demonstrated herein.

References

[1] A. Greiner and J. H. Wendorff, "Electrospinning: A fascinating method for the preparation of ultrathin fibers," *Angewandte Chemie*, vol. 46, no. 30, pp. 5670-5703, 2007.

[2] S. Agarwal, J. H. Wendorff, and A. Greiner, "Use of electrospinning technique for biomedical applications," *Polymer*, vol. 49, no. 26, pp. 5603-5621, 2008.

[3] N. J. Pinto, A. T. Johnson, and A. G. MacDiarmid, "Electrospun polyaniline/polyethylene oxide nanofiber field-effect transistor," *Applied Physics Letters*, vol. 83, no. 20, pp. 4244-4246, 2003.

[4] H. Liu, J. Kameoka, D. A. Czaplewski, and H. G. Craighead, "Polymeric Nanowire Chemical Sensor," Nano Letters, vol. 4, no. 4, pp. 671-675, 2004.

[5] X. Wang, C. Drew, S.-H. Lee, K. J. Senecal, J. Kumar, and L. A. Samuelson, "Electrospun Nanofibrous Membranes for Highly Sensitive Optical Sensors," Nano Letters, vol. 2, no. 11, pp. 1273-1275, 2002.

[6] T. Takahashi, M. Taniguchi, and T. Kawai, "Fabrication of DNA Nanofibers on a Planar Surface by Electrospinning," *Japanese Journal of Applied Physics*, vol. 44, no. 27, pp. L860-L862, 2005.

[7] A. Theron, E. Zussman, and A.L. Yarin, "Electrostatic field-assisted alignment of electrospun nanofibers," *Nanotechnology*, vol. 12, no. 3, pp. 384-390, 2001.

[8] D.H. Reneker, A.L. Yarin, H. Fong, and S. Koombhongse, "Bending instability of electrical charged liquid jets of polymer solutions in electrospinning," *Journal of Applied Physics*, vol. 87, no. 9, pp. 4531-4547, 2000.

[9] S. Y. Chew, J. Wen, E. K. F. Yim, and K. W. Leong, "Sustained release of proteins from electrospun biodegradable fibers," *Biomacromolecules*, vol. 6, no. 4, pp. 2017-2024, 2005.

[10] S. F. Fennessey and R. J. Farris, "Fabrication of aligned and molecularly oriented electrospun polyacrylonitrile nanofibers and the mechanical behavior of their twisted yarns," *Polymer*, vol. 45, no. 12, pp. 4217-4225, 2004.

[11] K.W. Kim, K.H. Lee, M.S. Khil, Y.S. Ho, and H.Y. Kim, "The effect of molecular weight and the linear velocity of drum surface on the properties of electrospun poly(ethylene terephthalate) nonwovens," *Fibers and Polymers*, vol. 5, no. 2, pp. 122-127, 2004.

[12] J. A. Matthews, G. E. Wnek, D. G. Simpson, and G. L. Bowlin, "Electrospinning of collagen nanofibers," *Biomacromolecules*, vol. 3, no. 2, pp. 232-238, 2002.

[13] D. Li, Y. Wang, and Y. Xia, "Electrospinning of polymeric and ceramic nanofibers as uniaxially aligned arrays," *Nano Letters*, vol. 3, no. 8, pp. 1167-1171, 2003.

[14] D. Li, Y. Wang, and Y. Xia, "Electrospinning nanofibers as uniaxially aligned arrays and layer-by-layer stacked films," *Advanced Materials*, vol. 16, no. 4, pp. 361-366, 2004.

[15] A. Theron, E. Zussman, and A. L. Yarin, "Experimental investigation of the governing parameters in the electrospinning of polymer solutions," *Polymer*, vol. 45, no. 6, pp. 2017-2030, 2003.

[16] T. A. Kowalewski, S. Blonski, and S. Barral, “Experiments and modelling of electrospinning process,” *Bulletin of the polish academy of sciences*, vol. 53, no. 4, pp. 385-394, 2005.

[17] B. E. White, “Energy-harvesting devices: Beyond the battery,” *Nature Nanotechnology*, vol. 3, pp. 71-72, 2008.

[18] J. A. Paradiso and T. Starner, “Energy scavenging for mobile and wireless electronics,” *IEEE Pervasive Computing*, vol. 4, no. 1, pp. 18-27, 2005.

[19] D. L. Churchill, M. J. Hamel, C. P. Townsend, and S. W. Arms, “Strain Energy Harvesting for Wireless Sensor Networks,” *Smart Structures and Materials, SPIE*, vol. 5005, pp. 319-327, 2003.

[20] C. G. Triplett, “Vehicular Mounted Piezoelectric Generator,” *US patent* 4,504,761, 1985.

[21] N. S. Shenck and J. A. Paradiso, “Energy scavenging with shoe-mounted piezoelectrics,” *IEEE Micro*, vol. 21, no. 3, pp. 30-42, 2001.

[22] P. Niu, P. Chapman, R. Riemer, and X. Zhang, “Evaluation of Motions and Actuation Methods for Biomechanical Energy Harvesting,” *IEEE Power Electronics Specialists Conference*, pp. 2100-2106, 2004.

[23] Y. Qin, X.Wang, and Z. L. Wang, “Microfibre-nanowire hybrid structure for energy scavenging,” *Nature*, vol. 451, pp. 809-813, 2008.

[24] T. Starner, “Human powered wearable computing,” *IBM Systems Journal*, vol. 35, no. 3-4, pp. 618-629, 1996.

[25] J. Kymissis, C. Kendall, J. Paradiso, and N. Gershenfeld, “Parasitic power harvesting in shoes,” *Second IEEE International Symposium on Wearable Computers*, pp. 132-139, 1998.

CHAPTER 2

FUNDAMENTALS IN ELECTROSPINNING TECHNOLOGY

2.1. Introduction to Electrospinning

Conventional tools for spinning and weaving to make yarn and fabrics may be dated back to the earliest relics of human habitations. For example, Linen fabrics dating from 5000 B.C. have been discovered in Egypt; woolen textiles have been found in Scandinavia and Switzerland from the early Bronze Age; cotton has been spun and woven in India since 3000 B.C, and silk has been woven in China since at least 1000 B.C. By the 14th century, splendid fabrics were being woven on the hand looms of the Mediterranean countries in practically all the basic structures known to modern artisans, and there has been no change in fundamental processes since that time, although methods and equipment have been radically altered. Figure 2.1 illustrates a "modern" mechanical spinning machined used by Mahatma Gandhi – known as the "Father of India," as the illustration that not too long ago, mechanical spinning using traditional tools was the main instrument to make fabrics [1]. Today, industrialized machineries are used to make fabrics with fundamental knowledge from ancient history while advanced electrical machinery tools and control algorithms have replaced the old fashion tools to increase the manufacturing speed and lower the manufacturing cost of fabrics.

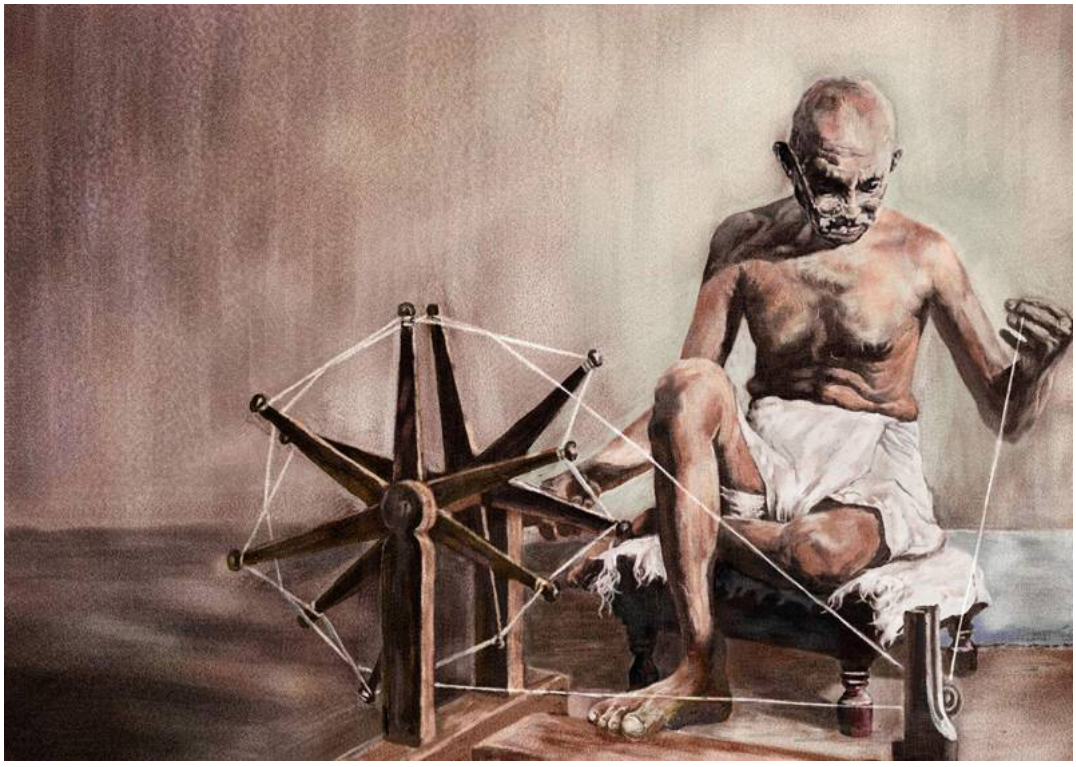

Figure 2.1. Conventional mechanical spinning has used to make yarns as shown in this illustration [1].

Electrospinning, on the other hand, has been emerging as an interesting material processing and manufacturing process. Electrospinning is a simple but highly versatile method to process solutions or melts into ultra thin fibers. The diameters of electrospun fibers range from a few micrometers to a few nanometers, therefore they are commonly known as nanofibers. Electrospinning can be versatilely applied for synthetic and natural polymers, polymer alloys, polymer composites, as well as metals and ceramics [2]. Typical applications of electrospinning include filtrations [3], wound dressing [4], bio-scaffolds [5] and medical implants [6]. In the later years, with the surging interest in nanotechnology, there have been a number of innovative applications of electrospinning for fabrication of micro/nanodevices, such as field effect transistors [7], gas [8] and optical sensors [9], and DNA functional chips [10].

A typical setup for conventional electrospinning contents four main components:

1. A syringe pump to maintain a constant flow rate of the polymer solution
2. A dispense tip that is connected to the high voltage to serve as a cathode, through which the polymer is squirted. Although it is often referred as needle, nozzle or spinneret in literatures, it is to remark that the hollow needle that is commonly used with a syringe is not always suitable for solution dispensing in electrospinning because of the bevels. In most cases of electrospinning, the dispense tip needs to have a flat edge.
3. A high voltage power supply
4. A counter electrode which serves as a collector for the electrospun fibers

Figure 2.2 illustrates schematically a typical setup for conventional electrospinning with vertical feeding direction. Horizontal or angular feeding for specific processing is also common. The inner diameter of the dispense tip usually range on the order of several hundreds micrometers (needle size 32 to 20 gauge). The applied voltage ranges in the order of several tens kilovolts. Typical electrode-to-collector distance ranges in the order of 10 cm.

The formation of thin fibers in an electrospinning process is based on the uniaxial stretching of a viscoelastic solution by electrostatic force [11]. Such a polymer solution can be prepared using a suitable solvent. Additives can be added for certain purposes, commonly salts to increase the conductivity, and/or surfactants to decrease the surface tension. In a typical electrospinning process, a polymer solution is fed through the tip by means of a syringe pump. In idle condition, the droplet that is formed at the opening of the tip has a spherical shape due to the surface tension of the solution. When a voltage is applied on the solution, the electrostatic field causes a conical deformation of the droplet in the direction of the counter electrode into a so-called Taylor cone as shown in Figure 2.3 [12, 13, 14]. At a sufficiently high voltage, the electrostatic force can overcome the surface tension of the polymer droplet and thus initiate the ejection of a thin jet. For a very short distance immediately at the tip, whose length is individual for every polymer and solvent system, the jet goes on a more or less stable path, after that it begins to swing up. The jet then undergoes a stretching and whipping process in the electrical field towards the counter electrode. The solvent evaporates along the way, during that the polymer stream solidifies. Thin solid polymer fibers are deposited on the counter electrode, also referred as collector, often as randomly oriented non-woven mesh.

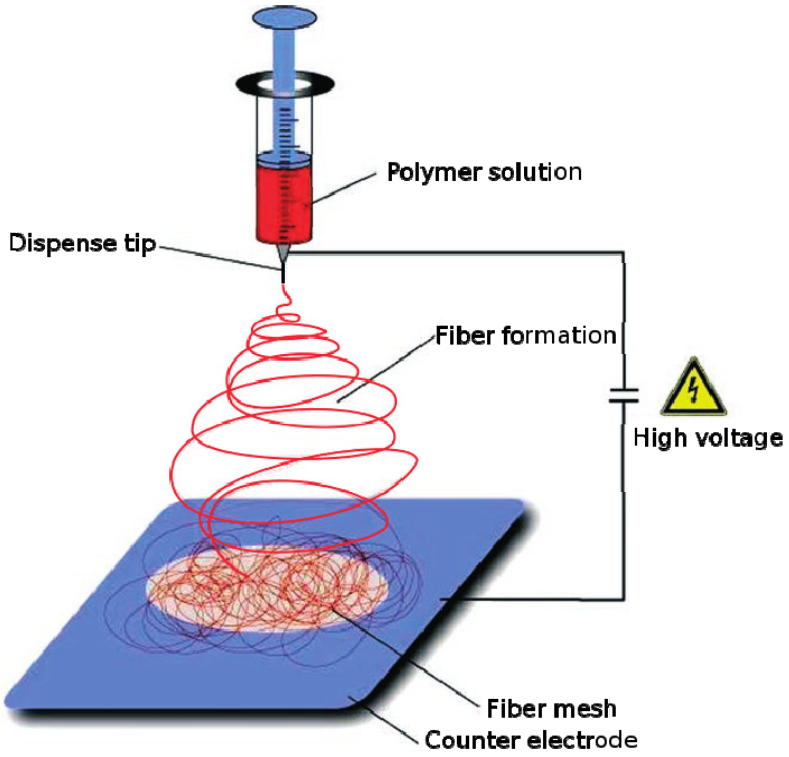

Figure 2.2. Schematic illustration of a typical laboratory setup for conventional electrospinning with vertical solution feeding [2].

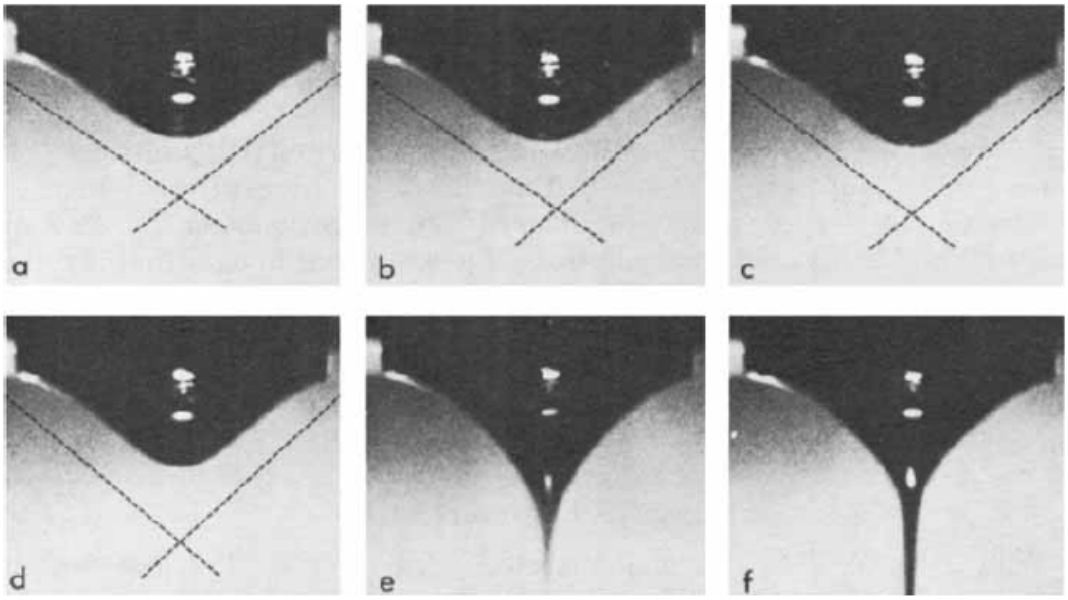

Figure 2.3. Photographs showing the meniscus at the end of the needle developing into a jet as the voltage is progressively increased [13].

Nanofibers of more than fifty different types of organic polymers, including engineering plastics, biopolymers, and those with electrical, optical, or electro-optical activity, have been successfully fabricated with electrospinning [15]. A comprehensive summary of polymers which have been successfully electrospun into nanofibers is presented in the review of Huang *et al.* [16]. More recently, the technique was developed further to the fabrication of metal oxides, ceramic and composite nanofibers with various compositions and properties [17]. All of these nanofibers are of great importance for application in textiles, membranes, composite reinforcement, drug-delivery-systems, tissue engineering, and not least, actuators and sensors technologies.

2.2. Alignment and Assembly of Nanofibers

As described above, in a typical electrospinning process, fibers are deposited randomly on the collector due to the bending instability of the charged polymer jet in an electrical field. Alignment of electrospun fibers has been a long-standing challenge. Research groups from all over the world have experimented different methods to fabricate continuous aligned fibers. The most prevalently studied techniques is using an at high speed rotating collector, including the use of a drum [18, 19, 20, 21], a wheel-like disk [22, 23, 24], a wire drum [25], and further modifications of mechanical devices [26, 27, 28, 29]. The first electrospinning experiment using a rotating collector was introduced by Boland *et al.* [30]. In their experiments, poly(glycolic acid) and collagen were electrospun on a cylinder collector rotating at a speed of 1000 rpm and 4500 rpm, respectively. Although their results in fiber alignment were less successful, this study motivated researchers for further improvements. For instance, Pan *et al.* [27] has developed a modified electrospinning setup using a rotating collector, as illustrated in Figure 2.4. Two horizontal dispense tips were placed oppositely and connected to positive and negative voltages, respectively, as shown in Figure 2.4A. Fibers coming out of the two needles combined in a yarn, which was wound by a cylinder collector rotating at high speed. It was shown that fibers manufactured by this method were continuous, well-aligned, and could be deposited over a large area. Figure 2.4B shows the yarn obtained from two polymer jets coming from two needles which were placed 14 cm apart. The vertical distance between the needles and collector was set to several centimeters. The collector rotated at a very high speed from hundreds to thousands rpm. It was observed that with increasing rotation speed, the degree of alignment became better, as shown in SEM images in Figure 2.4C and D of poly(vinyl alcohol) fibers at 1.3 m/s surface velocity and 4.3 m/s surface velocity, respectively. The average fiber diameter of the fibers was about 350 nm. This method suggests good potential for manufacture of continuous aligned nanofibers using electrospinning [27].

Besides techniques with mechanical devices, manipulation of electrical field has also been exploited to achieve aligned fibers from electrospinning. Investigated techniques include the use of one or several positive charged rings as auxiliary electrodes [31, 32, 33, 34], and parallel ordered counter electrodes [15, 35]. For instance, Li *et al*. [35] demonstrated that two electrodes placed in parallel were able to collect aligned fibers in the gap, as illustrated in Figure 2.5. Figure 2.5A shows a schematic illustration of the setup with the typical grounded electrode being replaced by a collector consisting of two parallel silicon strips separated by a void gap. Figure 2.5B shows a dark-field optical micrograph of nanofibers that were electrospun from a

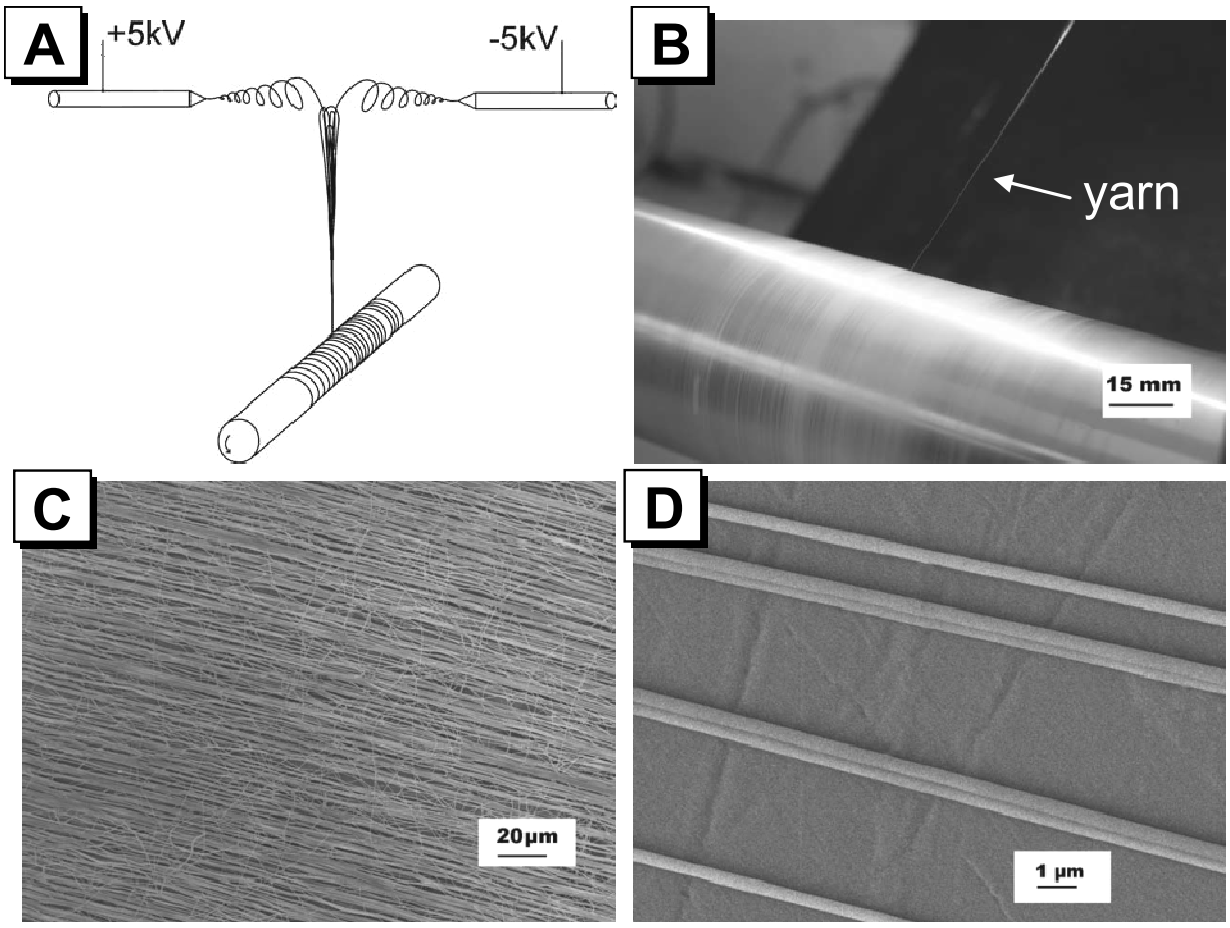

Figure 2.4. (A) Schematic electrospinning setup for collection continuous aligned fibers. (B) A yarn of fibers is formed between the needle and a rotating aluminum shaft. (C) Well-aligned PVA fibers electrospun from a 10% wt solution collected on a Teflon tube at a surface velocity of 1.3 m/s. (D) Well-aligned PVA fibers (13%) collected at the surface velocity of 4.3 m/s [27].

poly(vinyl pyrrolidone) solution and directly deposited on the collector. This image evidently demonstrates a good alignment of the nanofibers with their longitudinal axes oriented perpendicular to the edges of the silicon strips. It was suggested that the fiber arrays could also be stacked layer-by-layer into a multilayered structure. Figure 2.5C shows such an array of 2x2 crossbar junctions obtained by transferring two layers of uniaxially aligned PVP fibers onto the same substrate.

More recently, a new idea of a controllable electrospinning was introduced taking advantage of a very close electrode-to-collector distance. The first experiment of electrospinning at a reduced distance was reported by Kameoka *et al.* in 2003 [36]. The method used a microfabricated scanned tip as an electrospinning source. Figure 2.6 shows the schematic operation of fiber fabrication. As a first step, the tip was dipped in a polymer solution to gather a droplet as source material (Figure 2.6A, B). The arrow shape of the tip helped to establish a droplet located on the tip. For observation of the electrospinning process, the tip then placed horizontally 2 cm from the counter electrode, which was connected to an optical chopper motor

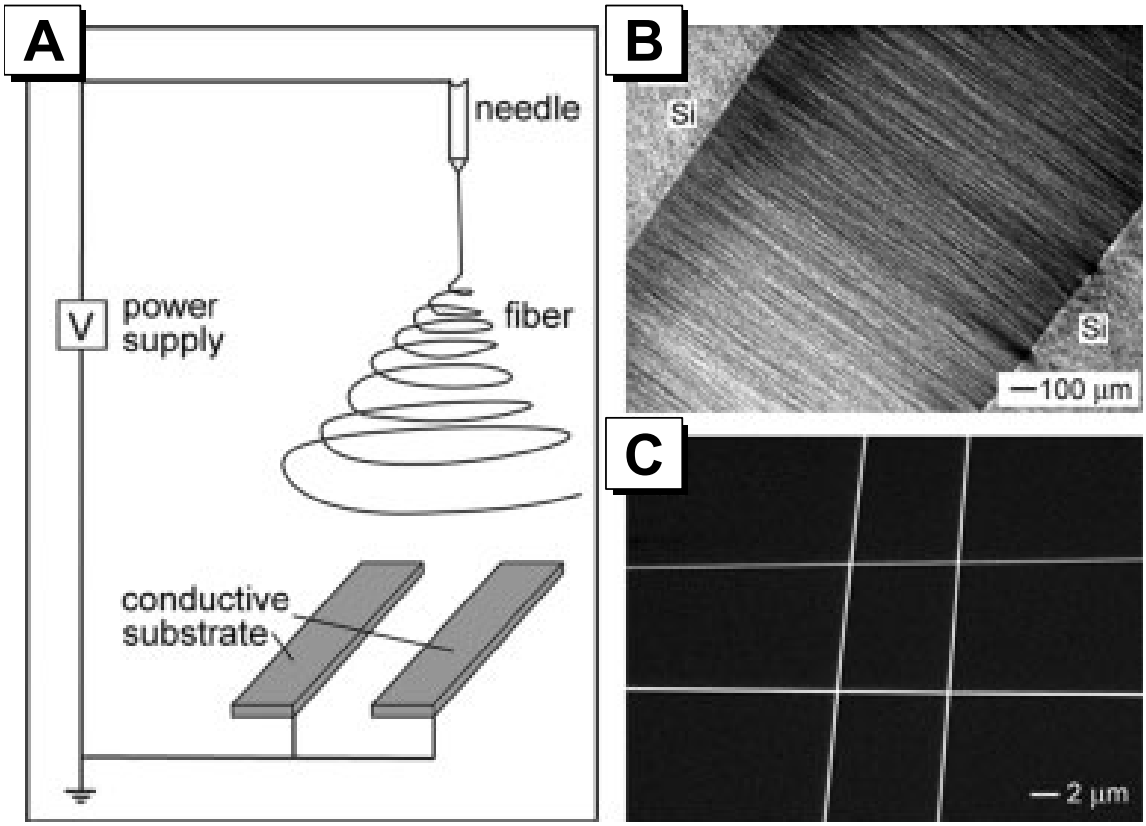

Figure 2.5. (A) Schematic illustration of the setup used to electrospin nanofibers as uniaxially aligned arrays. The collector was composed of two conductive substrates separated by a void gap. (B) Dark-field optical micrograph of PVP nanofibers collected across a void gap formed between two silicon strips. (C) SEM image of a 2 × 2 array of crossbar junctions constructed by sequentially transferring two layers of PVP nanofibers onto the same substrate [35].

to control the motion of the tip relative to the substrate (Figure 2.6C). As a sufficient high voltage, which was about 4 – 6 kV, was applied to the tip, a polymer jet was extracted from the droplet (Figure 2.6D). By moving the tip relative to a surface, oriented nanofibers can be deposited. Figure 2.6E shows scanning electron micrograph (SEM) of a straightened electrospun PEO fiber with diameter of about 150 nm suspended over a 3 μm wide trench.

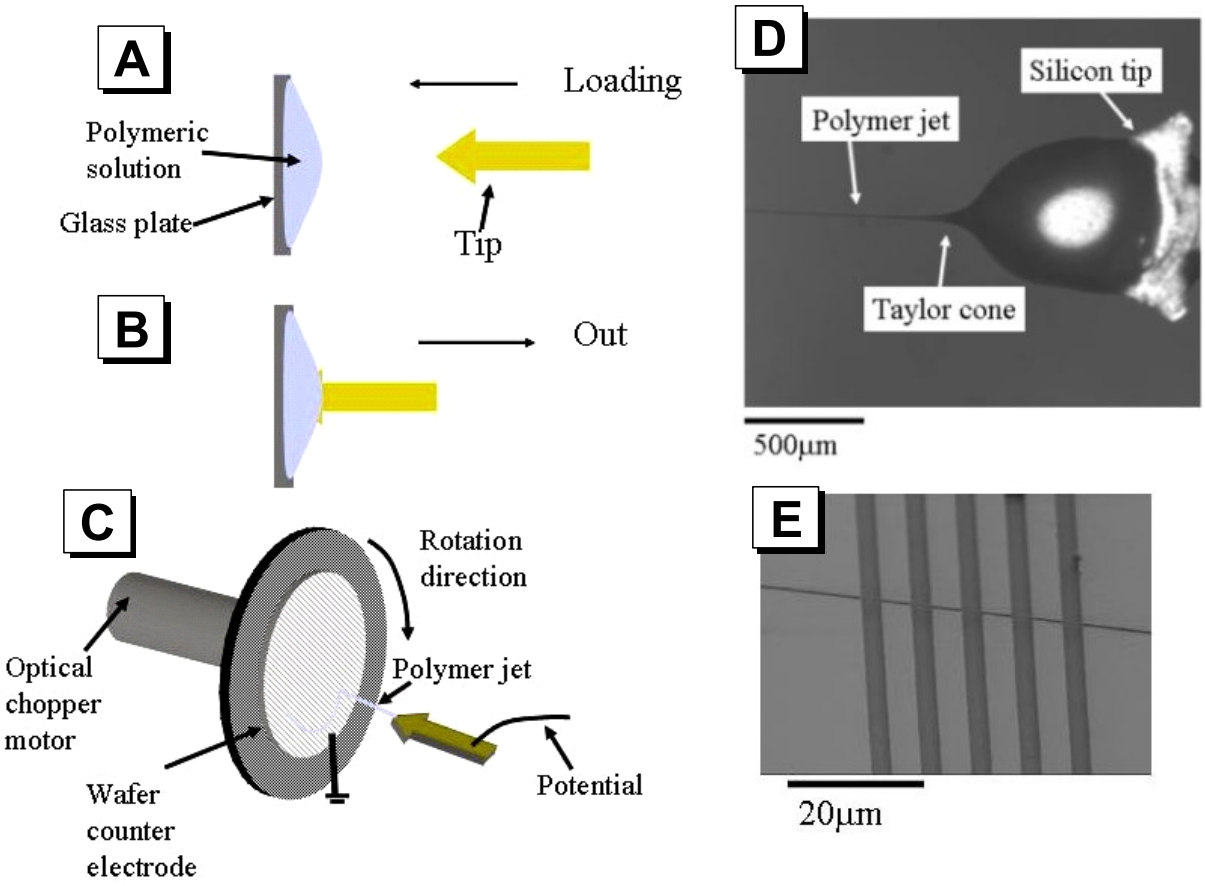

Figure 2.6. (A-C) Schematic operation of a horizontal electrospinning process. (A) Scanning tip was dipped in a polymer solution. (B) Scanning tip was taken out of the polymer solution. (C) The potential was applied to a gold wire connected to the scanning tip and the liquid jet was extracted. The fiber jet was deposited on a counter electrode that was attached to an optical chopper motor for controlling nanofibers orientation. (D) Optical image of polymer liquid jet extracted from an apex of a Taylor cone established on a silicon scanning tip. (E) Scanning electron micrograph of a suspended PEO nanofiber over a 3 μm wide trench [36].

References

[1] Biography of Mahatma Gandhi: http://www.geocities.com/CapitolHill/Lobby/8522/gand_eng.html

[2] A. Greiner and J. H. Wendorff, "Electrospinning: A fascinating method for the preparation of ultrathin fibers," *Angewandte Chemie*, vol. 46, no. 30, pp. 5670-5703, 2007.

[3] P. W. Gibson, H. L. Schreuder-Gibson, and D. Rivin, "Electrospun fiber mats: Transport properties," *AlChE Journal*, vol. 45, no. 1, pp. 190-195, 1999.

[4] H. J. Jin, S. V. Fridrikh, G. C. Rutledge, and D. L. Kaplan, "Electrospinning Bombyx mori silk with poly(ethylene oxide)," *Biomacromolecules*, vol. 3, no. 6. pp. 1233-1239, 2002.

[5] U. Boudriot, R. Dersch, B. Goetz, P. Griss, A. Greiner, and J. H. Wendorff, "Electrospun poly-l-lactide nanofibres as scaffolds for tissue engineering," *Biomedical Engineering*, vol. 49, no. 9, pp. 242-247, 2004.

[6] S. Agarwal, J. H. Wendorff, and A. Greiner, "Use of electrospinning technique for biomedical applications," *Polymer*, vol. 49, no. 26, pp. 5603-5621, 2008.

[7] N. J. Pinto, A. T. Johnson, and A. G. MacDiarmid, "Electrospun polyaniline/polyethylene oxide nanofiber field-effect transistor," *Applied Physics Letters*, vol. 83, no. 20, pp. 4244-4246, 2003.

[8] H. Liu, J. Kameoka, D. A. Czaplewski, and H. G. Craighead, "Polymeric Nanowire Chemical Sensor," Nano Letters, vol. 4, no. 4, pp. 671-675, 2004.

[9] X. Wang, C. Drew, S.-H. Lee, K. J. Senecal, J. Kumar, and L. A. Samuelson, "Electrospun Nanofibrous Membranes for Highly Sensitive Optical Sensors," Nano Letters, vol. 2, no. 11, pp. 1273-1275, 2002.

[10] T. Takahashi, M. Taniguchi, and T. Kawai, "Fabrication of DNA Nanofibers on a Planar Surface by Electrospinning," *Japanese Journal of Applied Physics*, vol. 44, no. 27, pp. L860-L862, 2005.

[11] W. E. Teo and S. Ramakrishna, "A review on electrospinning design and nanofibre assemblies," *Nanotechnology*, vol. 17, no. 14, pp. R89-R106, 2006.

[12] G. Taylor, "Disintegration of water drops in an electric field," *Proceedings of the Royal Society of London. Series A*, vol. 280, no. 1382, pp. 383-397, 1964.

[13] L. Larrondo and R. St. John Manley, "Electrostatic fiber spinning from polymer melts. I. Experimental observations on fiber formation and properties," *Journal of Polymer Science: Polymer Physics Edition*, vol. 19, no. 6, pp. 909-920, 1981.

[14] S. N. Reznik, A. L. Yarin, A. Theron, and E. Zussman, "Transient and steady shapes of droplets attached to a surface in a strong electric field," *Journal of Fluid Mechanics*, vol. 516 pp. 349-377, 2004.

[15] D. Li, Y. Wang, and Y. Xia, "Electrospinning nanofibers as uniaxially aligned arrays and layer-by-layer stacked films," *Advanced Materials*, vol. 16, no. 4, pp. 361-366, 2004.

[16] Z.-M. Huang, Y.-Z. Zhangb, M. Kotakic, and S. Ramakrishna, "A review on polymer

nanofibers by electrospinning and their applications in nanocomposites," *Composites Science and Technology*, vol. 63, no. 15, pp. 2223-2253, 2003.

[17] D. Li and Y. Xia, "Electrospinning of nanofibers: Reinventing the wheel?" *Advanced Materials*, vol. 16, no. 14, pp. 1151-1170, 2004.

[18] S. Y. Chew, J. Wen, E. K. F. Yim, and K. W. Leong, "Sustained release of proteins from electrospun biodegradable fibers," *Biomacromolecules*, vol. 6, no. 4, pp. 2017-2024, 2005.

[19] S. F. Fennessey and R. J. Farris, "Fabrication of aligned and molecularly oriented electrospun polyacrylonitrile nanofibers and the mechanical behavior of their twisted yarns," *Polymer*, vol. 45, no. 12, pp. 4217-4225, 2004.

[20] K.W. Kim, K.H. Lee, M.S. Khil, Y.S. Ho, and H.Y. Kim, "The effect of molecular weight and the linear velocity of drum surface on the properties of electrospun poly(ethylene terephthalate) nonwovens," *Fibers and Polymers*, vol. 5, no. 2, pp. 122-127, 2004.

[21] J. A. Matthews, G. E. Wnek, D. G. Simpson, and G. L. Bowlin, "Electrospinning of collagen nanofibers," *Biomacromolecules*, vol. 3, no. 2, pp. 232-238, 2002.

[22] R. Inai, M. Kotaki, and S. Ramakrishna, "Structure and properties of electrospun PLLA single nanofibres," *Nanotechnology*, vol. 16, no. 2, pp. 208-213, 2005.

[23] A. Theron, E. Zussman, and A.L. Yarin, "Electrostatic field-assisted alignment of electrospun nanofibers," *Nanotechnology*, vol. 12, no. 3, pp. 384-390, 2001.

[24] C.Y. Xu, R. Inai, M. Kotaki, and S. Ramakrishna, "Aligned biodegradable nanofibrous structure: a potential scaffold for blood vessel engineering," *Biomaterials*, vol. 25, no. 5, pp. 877-886, 2004.

[25] P. Katta, M. Alessandro, R. D. Ramsier, and G. G. Chase, "Continuous electrospinning of aligned polymer nanofibers onto a wire drum collector," *Nano Letters*, vol. 4, no. 11, pp. 2215-2218, 2004.

[26] N. Bhattaraia, D. Edmondsona, O. Veiseha, F. A. Matsenb, and M. Zhang, "Electrospun chitosan-based nanofibers and their cellular compatibility," *Biomaterials*, vol. 26, no. 31, pp. 6176-6184, 2005.

[27] H. Pan, L. Li, L. Hu, and X. Cui, "Continuous aligned polymer fibers produced by a modified electrospinning method," *Polymer*, vol. 47, no. 14, pp. 4901-4904, 2005.

[28] W. E. Teo, M. Kotaki, X. M. Mo, and S. Ramakrishna, "Porous tubular structures with controlled fibre orientation using a modified electrospinning method," *Nanotechnology*, vol. 16, no. 6, pp. 918-924, 2005.

[29] W. E. Teo and S. Ramakrishna, "Electrospun fibre bundle made of aligned nanofibres over two fixed points," *Nanotechnology*, vol. 16, no. 9, pp. 1878-1884, 2005.

[30] E. D. Boland, G. E. Wnek, D. G. Simpson, K. J. Pawlowski, and G. L. Bowlin, "Tailoring tissue engineering scaffolds using electrostatic processing techniques: A study of poly(glycolic acid) electrospinning," *Journal of macromolecular science*, vol. A38, no. 12, pp. 1231-1243, 2001.

[31] L. Buttafoco, N.G. Kolkman, P. Engbers-Buijtenhuijs, , A.A. Poot, P.J. Dijkstra, I. Vermes, and J. Feijen, "Electrospinning of collagen and elastin for tissue engineering applications,"

Biomaterials, vol. 27, no. 5, pp. 724-734, 2006.

[32] J. M. Deitzel, J. D. Kleinmeyer, J. K. Hirvonen, and N. C. Beck Tan, "Controlled deposition of of electrospun poly(ethylene oxide) fibers," *Polymer*, vol. 42, no. 19, pp. 8163-8170, 2001.

[33] G. H. Kim, "Electrospinning process using field-controllable electrodes," *Journal of Polymer Science: Part B: Polymer Physics*, vol. 44, no. 10, pp. 1426-1433, 2006.

[34] J. Stankus, J. Guan, W. Wagner, "Fabrication of biodegradable elastomeric scaffolds with sub-micron morphologies," *Journal of Biomedical Materials Research Part A*, vol. 70A, no. 4, pp. 603-614, 2004.

[35] D. Li, Y. Wang, and Y. Xia, "Electrospinning of polymeric and ceramic nanofibers as uniaxially aligned arrays," *Nano Letters*, vol. 3, no. 8, pp. 1167-1171, 2003.

[36] J. Kameoka, R. Orth, Y. Yang, D. Czaplewski, R. Mathers, G. W. Coates, and H. G. Craighead, "A scanning tip electrospinning source for deposition of oriented nanofibres," *Nanotechnology*, vol. 14, no. 10, pp. 1124-1129, 2003.

CHAPTER 3

NEAR-FIELD ELECTROSPINNING

3.1. Introduction and Background

Electrically driven liquid jets and the stability of electrically charged droplets have been studied for hundreds of years [1,2] while the practical apparatus of electrospinning, in which charged jet of polymer solution is deposited onto a collector under the influence of an electrical field, dated back in 1934 [3]. The feasibility to construct long and continuous polymeric [4, 5, 6], ceramic [7], and composite [8] nanofibers as well as nanotubes [9] with diameters less than 100 nm has been demonstrated using electrospinning. Typical applications include bio-scaffold [10], wound dressing [11], and filtrations [12] to name a few. Researchers have further explored the possibilities of using electrospun nanofibers in fabricating micro and nano device such as field-effect-transistors [13], gas [14] and optical sensors [15], and deposition of DNA on functional chips [16]. In these and other applications, the controllability of the electrospinning process is critical. Unfortunately, current setup of electrospinning is unstable in nature as it relies on the chaotic whipping of liquid jets to generate nanofibers.

Several groups in recent years have been developing orderly electrospinning processes using dynamic mechanical devices to improve the alignment and placement of electrospun nanofibers, including the use of a wheel-like reel, which has been shown to position and align individual polymer nanofibers into parallel arrays [17, 18, 19]. However, highly aligned nanofibers in a large and flat area are difficult to achieve using this method. Manipulation of electrical field has been exploited as well, including the use of an electrostatic lens element and collection target of opposite polarity, which has been implemented to dampen bending instability and control deposition [20]; aligned yarns of nylon-6 nanofibers, which have been collected by rapidly oscillating a grounded frame within the jet [21]; the use of a metal frame as the collector, which can also generate parallel arrays of polyamide nanofibers [22]; and the use of electrostatic forces guiding fibers across voids in the collector [23, 24]. The combination of dynamic mechanical devices and manipulation of electrical field can fabricate better aligned nanofiber patterns as parallel arrays and grids [25, 26]. However, these methods do not have good control on the pitch width and cannot make complex patterns such as circles. Buckling phenomena have also been studied in which electrically charged jets impinge onto collectors moving laterally at a constant velocity to produce buckling patterns with limited controllability [27].

Limited works toward the control of electrospinning have emerged. Furthermore, numerous investigations by means of analytical and experimental methodologies have been conducted to study the fundamental physics and chemistry of electrospinning for further improvement and control, such as the effects of polymer solution concentration, applied voltage, and electrode-to-collector distance [4, 28, 29, 30]. In this chapter, we will present the development of controllable electrospinning based on a new type of "near-field" electrospinning (NFES).

3.2. Principles of Operation

Figure 3.1 illustrates the schematic setup of NFES that merges several disparate concepts. First, the electrode-to-collector distance, h, is in the range of 500 μm to 3 mm to utilize the stable liquid jets region for controllable deposition. Second, a solid tungsten spinneret of 25 μm in tip diameter as illustrated in Figure 3.2A is used in NFES to achieve nanofibers with sub-100 nm

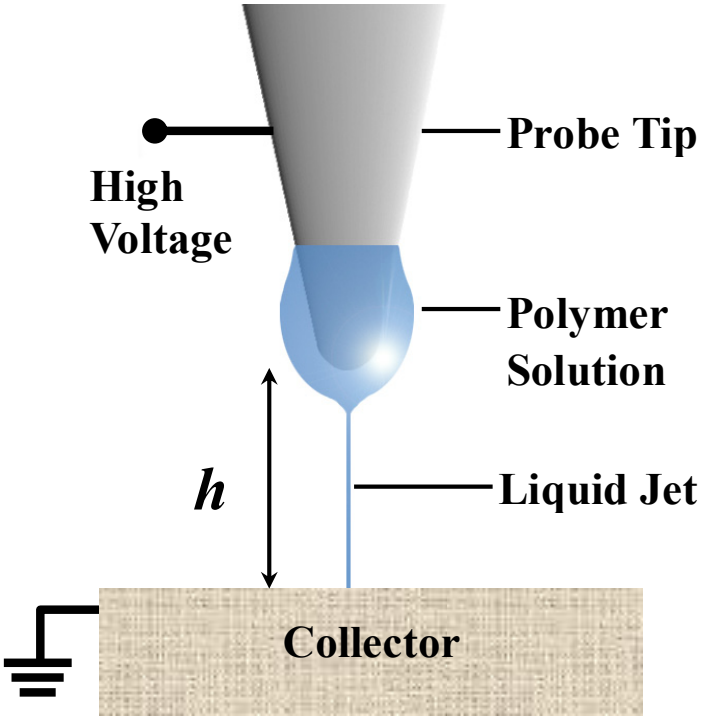

Figure 3.1. Schematic representation of NFES. The polymer solution is attached to the tip of the tungsten electrode in a manner analogous to that of a dip pen.

resolution. Third, the applied electrostatic voltage is reduced due to the short electrode-to-collector distance while the electrical field in the tip region maintains the strength in the range of 10^7 V/m as those used in conventional electrospinning to activate the process. Forth, discrete droplets of polymer solution are supplied in a manner analogous to that of a dip pen by immersing and pulling the tungsten electrode into and out of the polymer solution. Figure 3.2B shows that a droplet of 50 μm in diameter is extracted from the polymer solution under an optical microscope for NFES. A Taylor cone is observed under an optical microscope during the process of NFES as shown in Figure 3.3A. As the process proceeds, the polymer solution on the tungsten tip is consumed and its diameter shrinks, leading to smaller Taylor cone and thinner nanofibers as observed in Figure 3.3B.

NFES is not the only direct-write method for "serial" material deposition in nanofabrication. For example, dip pen (DPN) [31] which uses AFM tip to deliver collections of molecules to a solid substrate via capillary transport can deposit materials of better than 30 nm line-width with fine position control. This is an advantage over conventional electrospinning, unless one is trying to make large area, continuous and fast deposition. Inkjet printing [32], on the other hand, can make large area and fast deposition with discrete droplets with size in the μm range. The controllability of deposition location is again an advantage over conventional electrospinning unless one is trying to have continuous and sub-micron line-width resolution. In these regards, NFES complements DPN, inkjet and conventional electrospinning by providing the feasibility of controllable electrospinning for sub-100 nm nanofabrication.

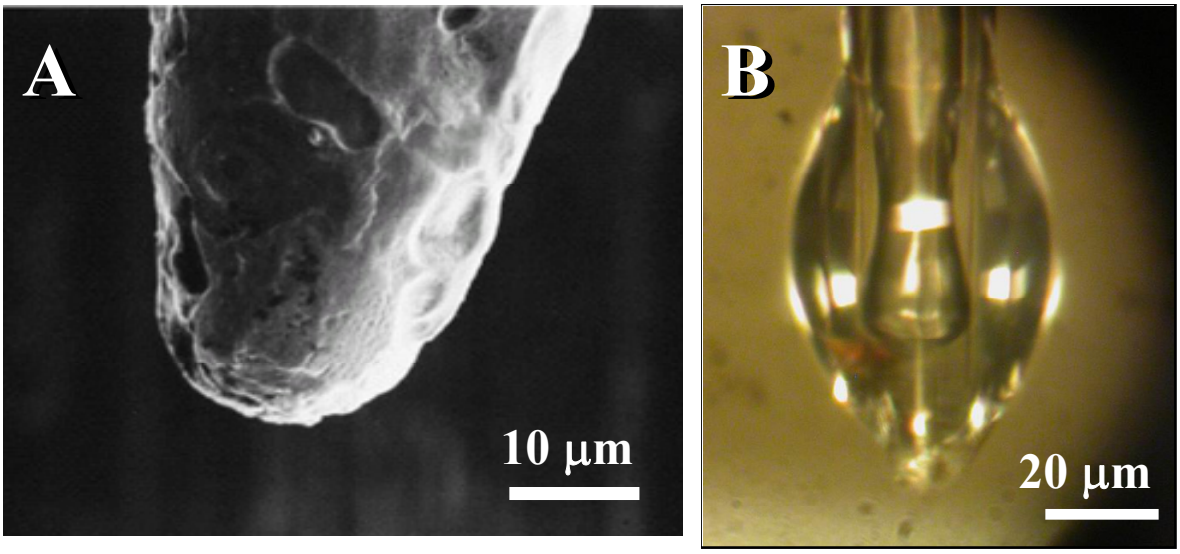

Figure 3.2. (A) SEM microphoto showing the tip region of the tungsten electrode used in the experiment with a tip diameter of 25 μm. (B) An optical photo showing a 50 μm in diameter polymer solution droplet is attached on the tip of the tungsten electrode.

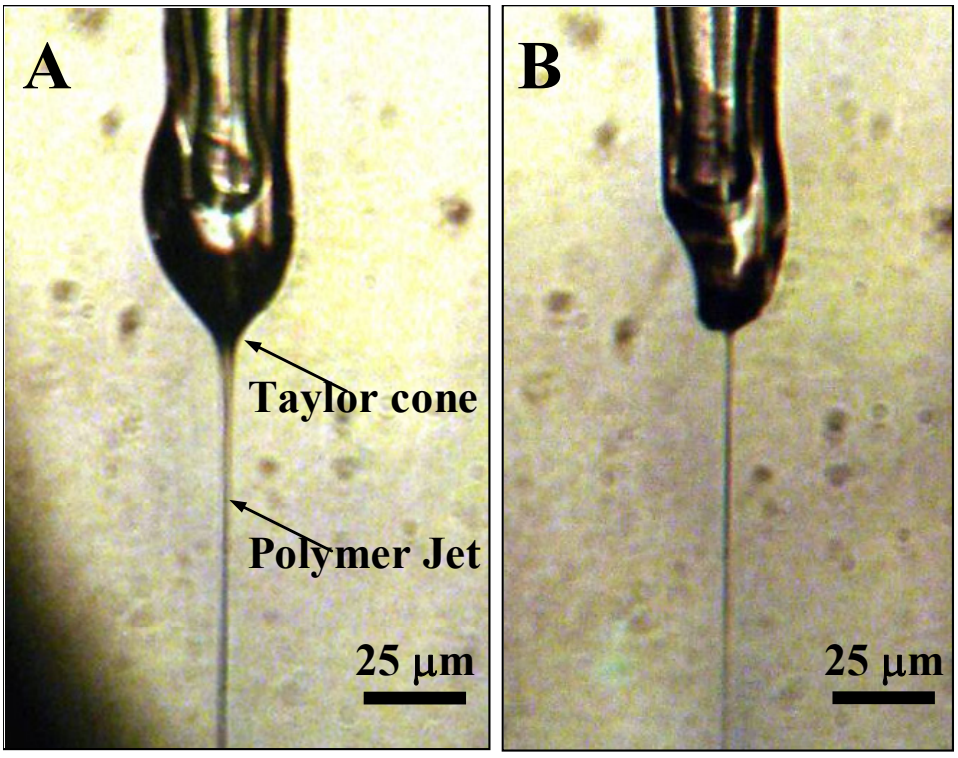

Figure 3.3. (A) A polymer jet is ejected from the apex of a Taylor cone under an applied electrical field and observed under an optical microscope. (B) The size of the polymer droplet decreases as the polymer jet continues to eject polymer solution.

3.3. Process and Experiment

Although there are various choices of nanofiber material and collector systems, we focus on the deposition of Polyethylene oxide (PEO, M_v =300,000), a polymer that has been studied extensively in electrospinning onto silicon-based collectors for possible system integration with MEMS (Microelectromechanical Systems) and microelectronics. All experiments are conducted under room temperature and one atmospheric pressure. During electrospinning, adequate electro-to-collector distance is required to allow solvent to evaporate and nanofibers to become thinner via the whipping and splitting processes [33]. NFES takes the advantage of stable liquid jets region immediately outside the spinneret for position controllable deposition by shortening the electrode-to-collector distance. At the same time, electrode with a fine tip is introduced to generate (1) intensified electrical field to activate electrospinning, and (2) small-diameter liquid jets in the stable region. In a typical NFES process of 5 seconds, a single nanofiber with length of several cm can be constructed. The droplet size, polymer solution concentration, applied voltage, and the electrode-to-collector distance collectively affect the morphology of the electrospun nanofibers. Overall, the near field electrospun solid nanofibers have similar morphology as the conventional electrospinning process.

3.3.1. Controllability

The controllability of nanofibers is demonstrated by moving the collector along a straight line to generate line-shape nanofibers. Figure 3.4 shows an example where parallel lines perpendicular to each other are constructed using an *x-y* stage (Nano Workcell, Adept Japan Inc.) to control the collector movement. In this experiment, the electrode-to-collector distance is 1 mm; applied voltage is 1000 volts; and PEO solution is 5% wt. The close view SEM microphoto in Figure 3.5 shows that the typical diameter of the nanofiber by NFES is 300 nm. More controllability is illustrated in Figure 3.6 when the collector is moving along a straight line with speed of 5, 10 and 15 cm/sec, respectively. In these cases, the nanofiber electrospinning speed is faster than the collector moving speed. The result is that "local spiraling" occurs as in Figure 3.6A and gradually diminishes as the collector is moving faster in Figure 3.6B and C. When the collector speed reaches 20 cm/sec as shown in Figure 3.6D, straight line-shape nanofibers can be constructed. In this case, we control the *x-y* stage to deposit two straight nanofibers 25 μm away from each other.

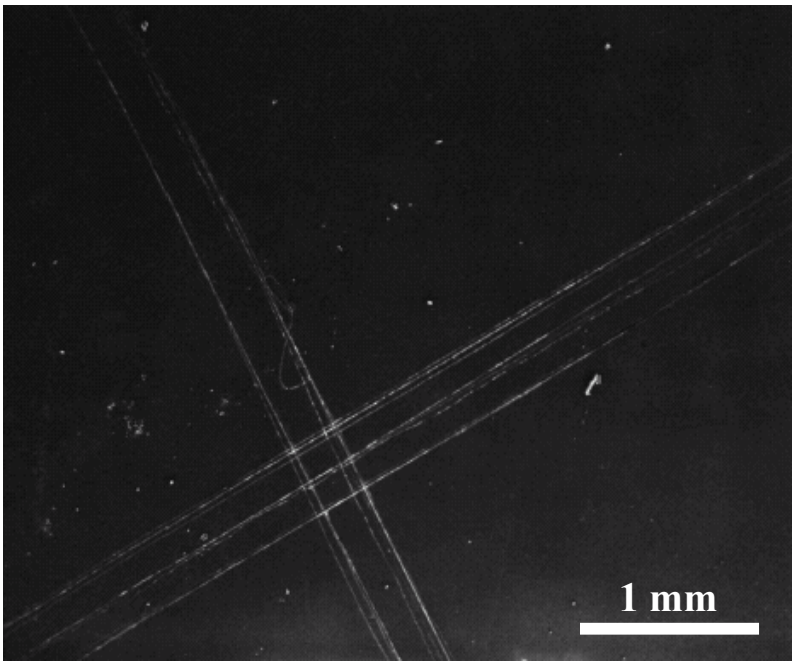

Figure 3.4. Two groups of parallel lines are constructed perpendicular to each other by NFES.

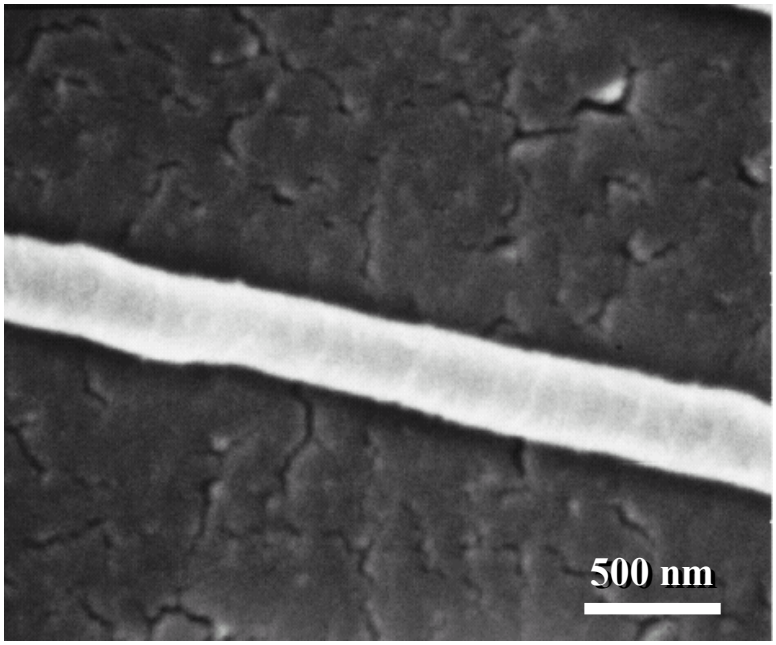

Figure 3.5. Enlarged SEM microphoto showing a nanofiber with diameter of 300 nm.

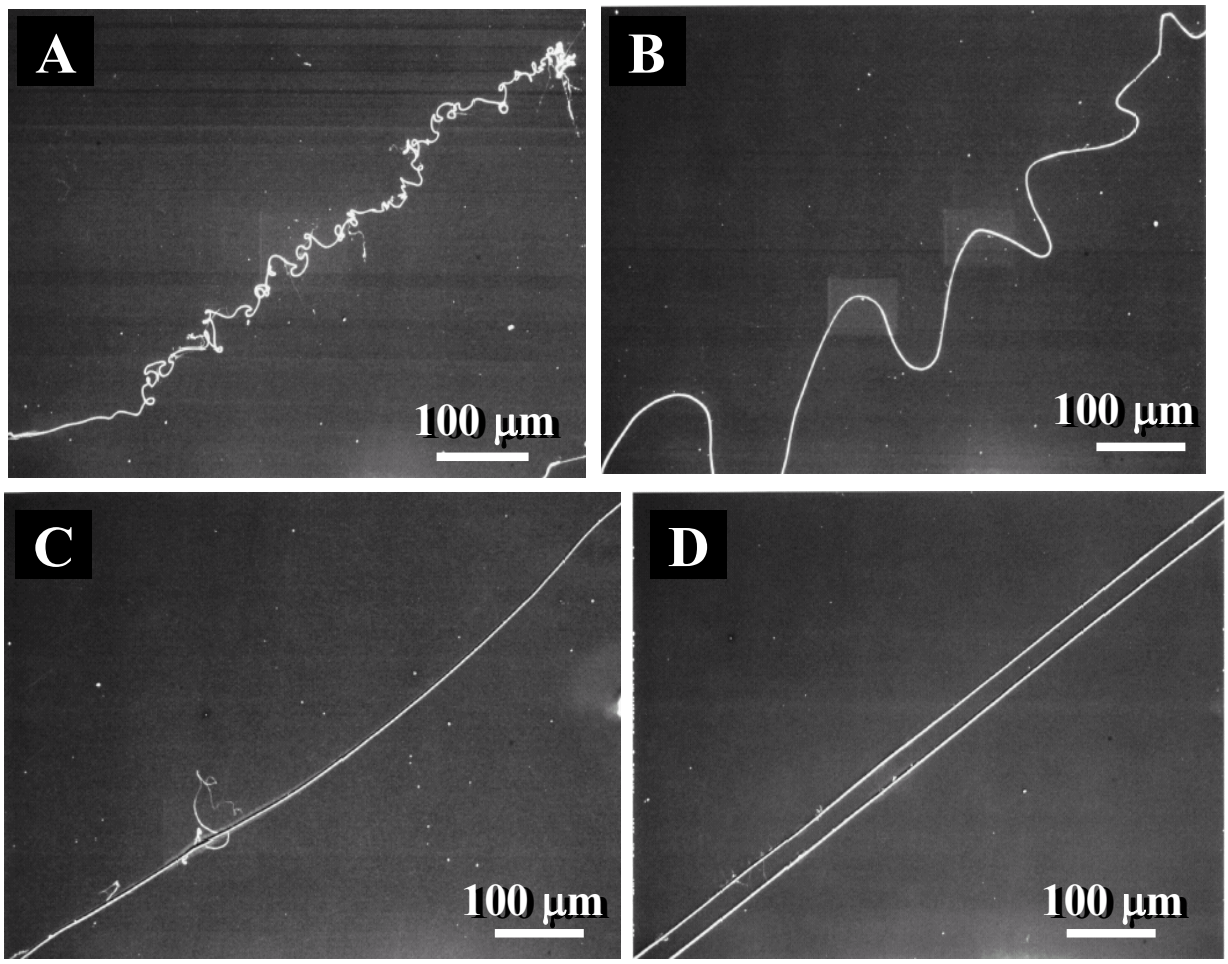

Figure 3.6. (A) NFES result when the collector has a moving speed of 5 cm/sec showing "local spiraling." (B) Collector moving speed at 10 cm/sec. (C) Collector moving speed at 15 cm/sec. (D) Collector moving speed is 20 cm/sec and straight lines can be constructed. The two nanofibers are separated 25 μm away from each other under the control of the *x*-*y* stage.

3.3.2. Deposition of Various Patterns

The location of the nanofiber formation under NFES is investigated by keeping the spinneret and collector with a fixed distance. It is observed that in a period of less than 1 second without moving the collector, the NFES deposition is concentrated within a short radial distance of 50 μm as seen in Figure 3.7. The local spiraling is the result of the self-expelling of nanofibers as they are electrically charged. This demonstrates the feasibility of location control of NFES on a conductive collector while conventional electrospinning will results in wide-spread and random deposition. Figure 3.8 shows a 2-second NFES deposition result on a stationary, 2 μm-thick insulating oxide-coated, silicon collector. Although the collector does not move, concentric and elliptical patterns of nanofibers are constructed as shown and cover an area with base length of more than 300 μm. The close view SEM photo in Figure 3.9 shows that the typical distance between adjacent nanofibers is about 1.5 μm that is relatively uniform over the whole pattern with no external control.

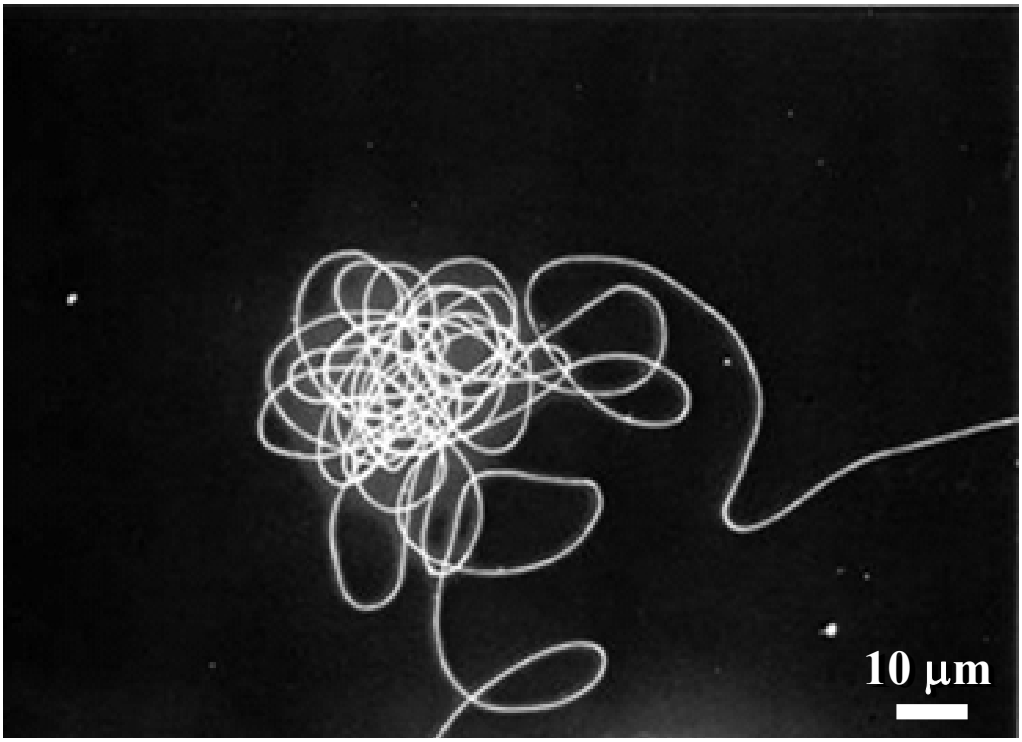

Figure 3.7. When the collector is stationary for 0.5 second while making a 90-degree turn, the local spiraling effect is observed as the result of self-expelling as nanofibers are electrically charged. The spread is in the range of 50 μm in diameter.

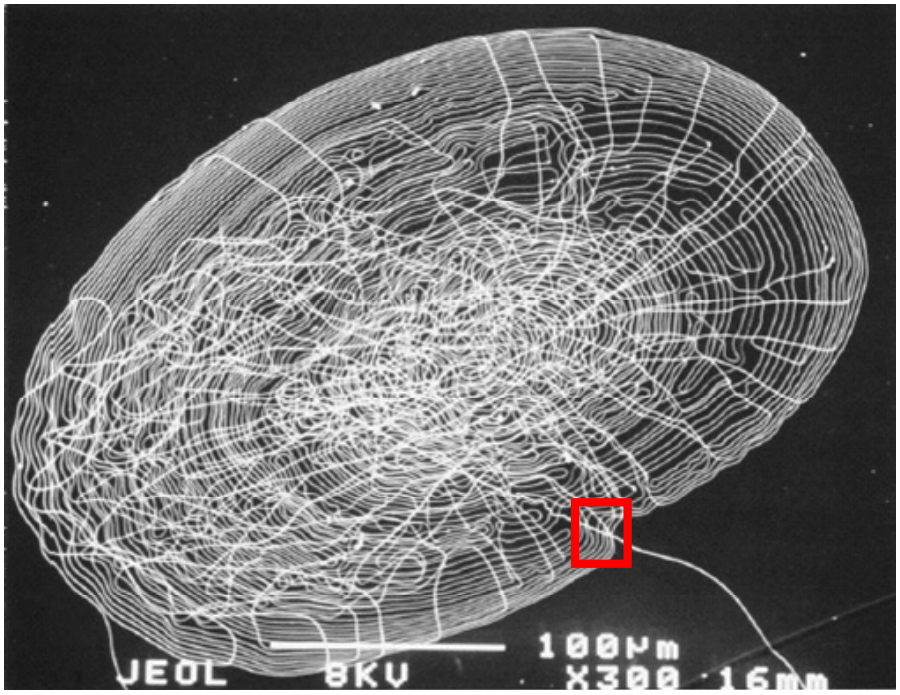

Figure 3.8. When the substrate is covered with an electrical isolation layer of silicon dioxide, the local spiraling is enhanced as the concentric/elliptical rings are formed in an area of about 300 μm in diameter.

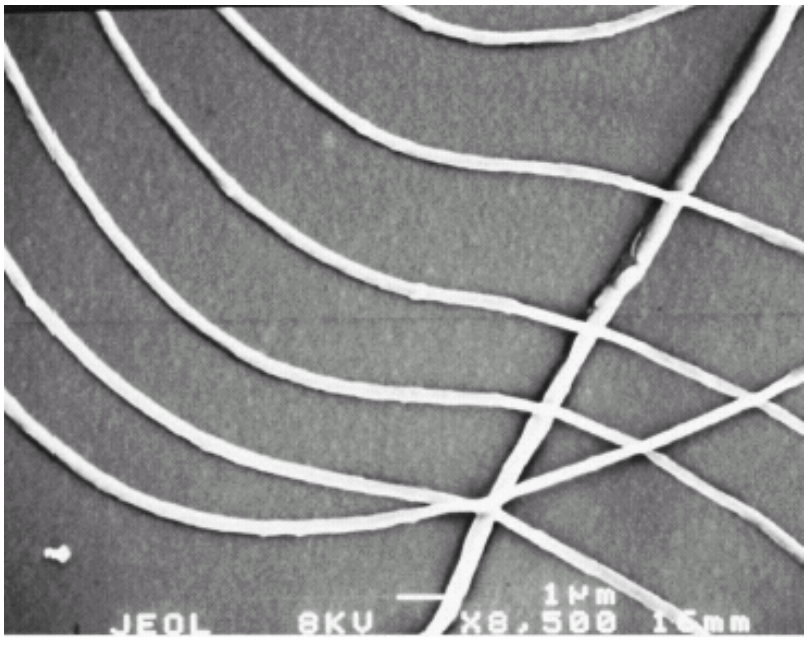

Figure 3.9. Close view of Figure 3.8 showing the distance between the adjacent nanofibers is about 1.5 μm.

Figures 3.10 and 3.11 further illustrate the controllability of NEFS under manual operations. Figure 3.10 shows that a "U" shape nanofiber is generated under one single NFES process. A straight line is plotted to construct the top line of the "U" shape structure. Afterwards, the collector stops to change to the downward direction and stops again before moving leftwards. It is shown during each stop of less than 0.5 second, the continuous deposition of nanofibers causes accumulation at the corners. We purposely slow down the collector moving speed to draw the middle and bottom portion of the "U" shape symbol and the "local spiraling" occurs as charged nanofiber expel each other when excessive nanofibers are to be deposited on the same location. Figure 3.11 shows an attempt to manually draw more complicated characters such as "Cal" in one single NFES process. Each character is about 1×2 mm^2 in size and it takes about 1 second to manually write one character. The writing speed is not fast enough to have clean shape under the manual control.

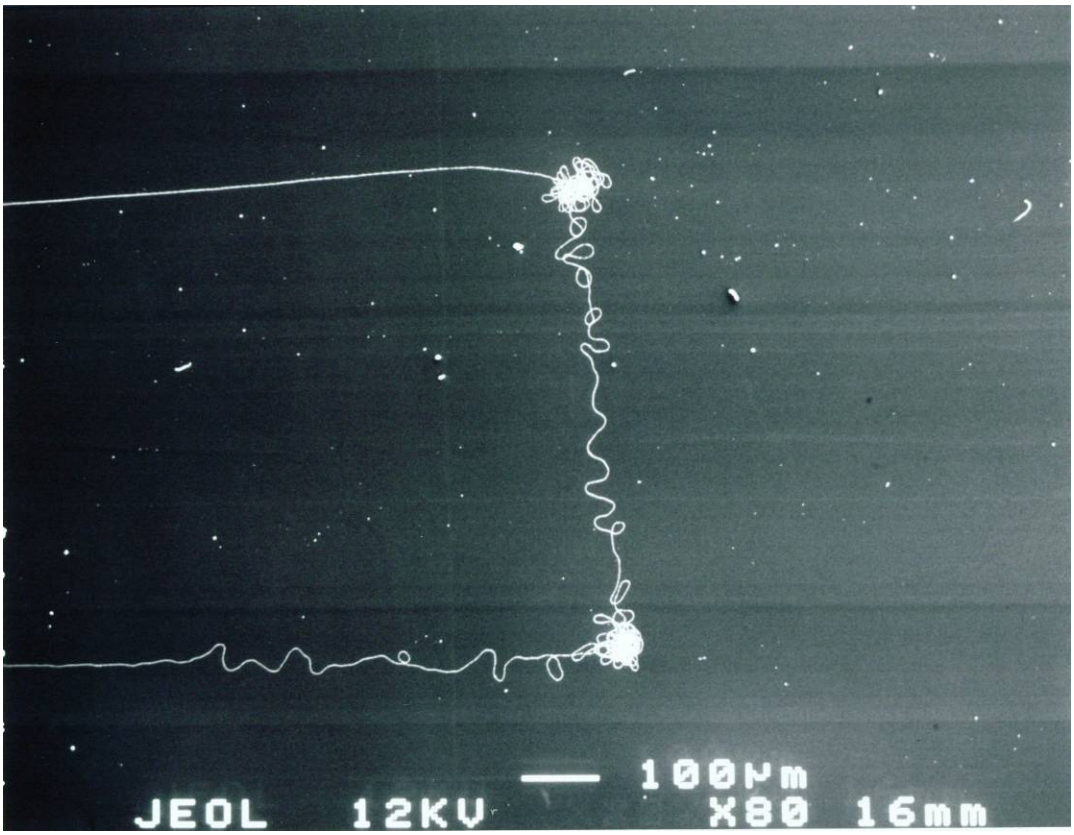

Figure 3.10. A "U" shape symbol is plotted manually by NFES. Excessive nanofiber depositions are observed at the two corners when the collector stopped shortly for the adjustment of the moving direction.

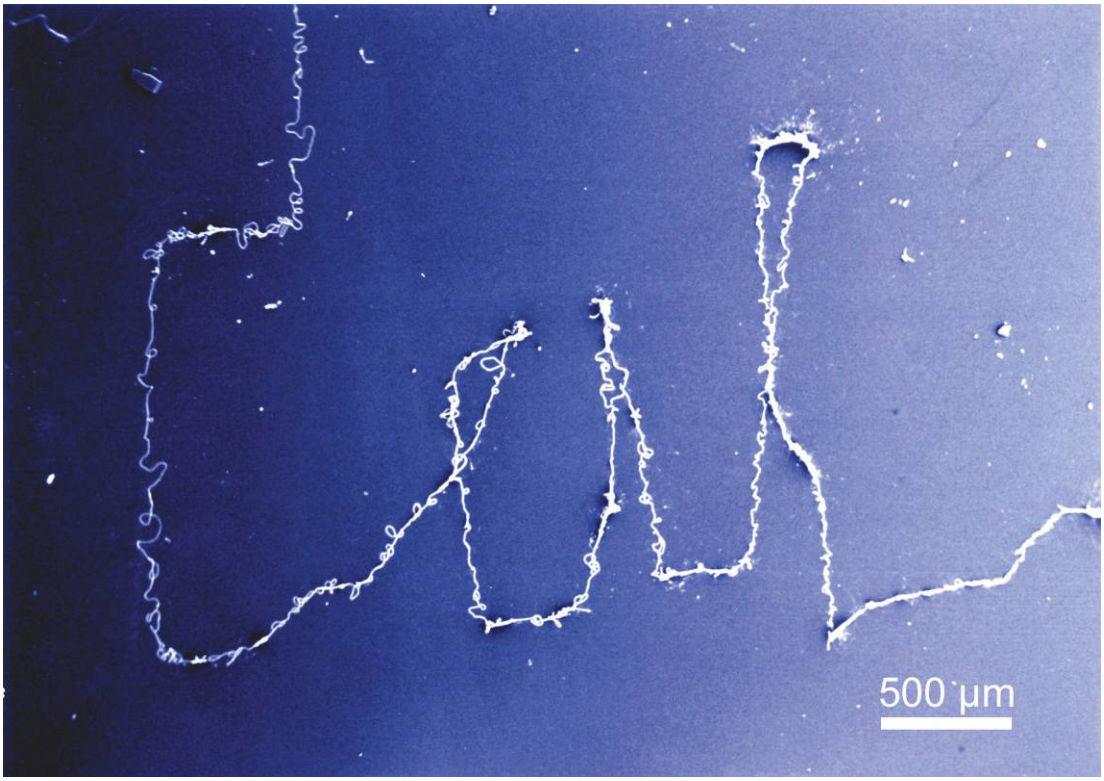

Figure 3.11. The three-character "Cal" is manually drawn in a period of 3 seconds.

We conclude that location and pattern control of NFES are achievable to deposit nanofiber without spiraling effects when the relative moving speed between the spinneret and collector is comparable to the electrospinning speed that is determined by various factors, including the viscosity, conductivity and surface tension of the polymer solution, applied electrical field, tip diameter of the spinneret, the size of the droplet, and ambient parameters including temperature, humidity and air velocity. Figure 3.12 shows experiments on the minimum required voltages versus electro-to-collector distances to activate NFES under various polymer concentrations and types of collectors when the polymer droplets have a nominal size of 50 µm in diameter. The minimum applied voltage increases when either the electrode-to-collector distance or the polymer solution concentration increases.

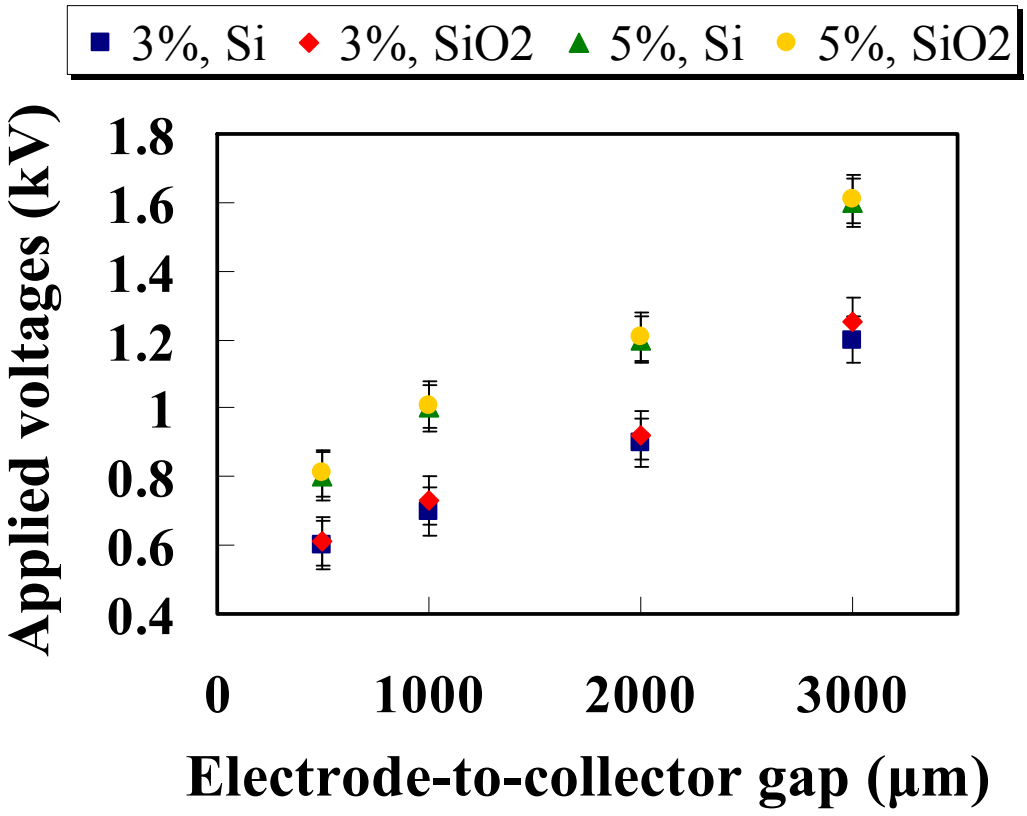

Figure 3.12. Experimental results on the minimum required voltages vs. electrode-to-collector distance to activate the NFES process under various polymer concentrations on either silicon or silicon oxide collectors.

An electrical field simulation was performed using COMSOL for both 500 µm-thick silicon wafer and 500 µm-thick silicon wafer coated with a 2-µm thick silicon dioxide. Simulation results (Figure 3.13 and 3.14) indicate that the magnitudes of the electrical field for the collectors with and without the oxide insulating layer are similar under the same applied bias as the thin oxide layer does not affect the electrical field strength significantly. The maximum electrical fields for both cases are 1.097×10^7 V/m and 1.089×10^7 V/m respectively and the parameters for the simulation are listed in Table 3.1.

Furthermore, it is observed that nanofibers collected on silicon collector are nominally bigger than those on oxide-coated collector under the same deposition condition since nanofibers travel a longer distance on average (Figure 3.8) and have more time for the solvent to evaporate. Statistical experimental results show that when the electrode-to-collector distance is 500 µm with 3% wt PEO, the diameters of nanofiber on the silicon and oxide-coated silicon collector are in the range of 150~300 nm, and 50~200 nm, respectively.

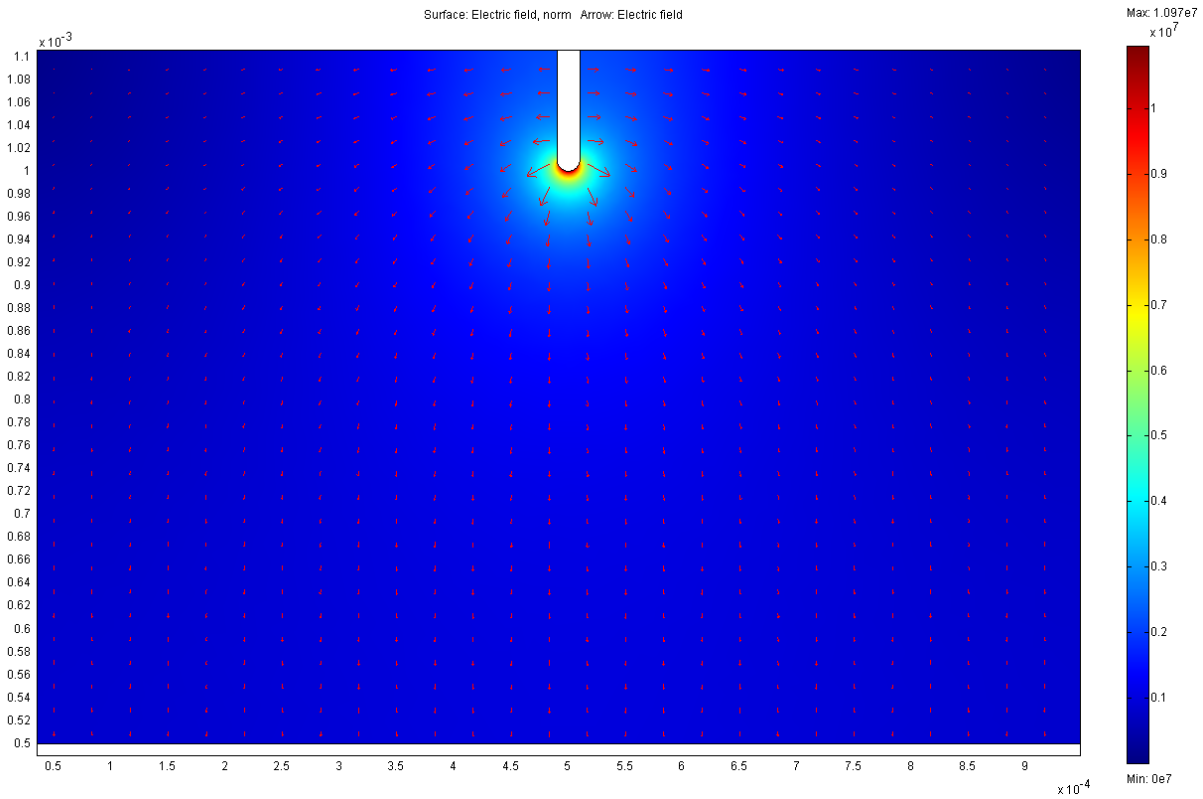

Figure 3.13. Simulation result of electric field for the collectors with the oxide insulating layer.

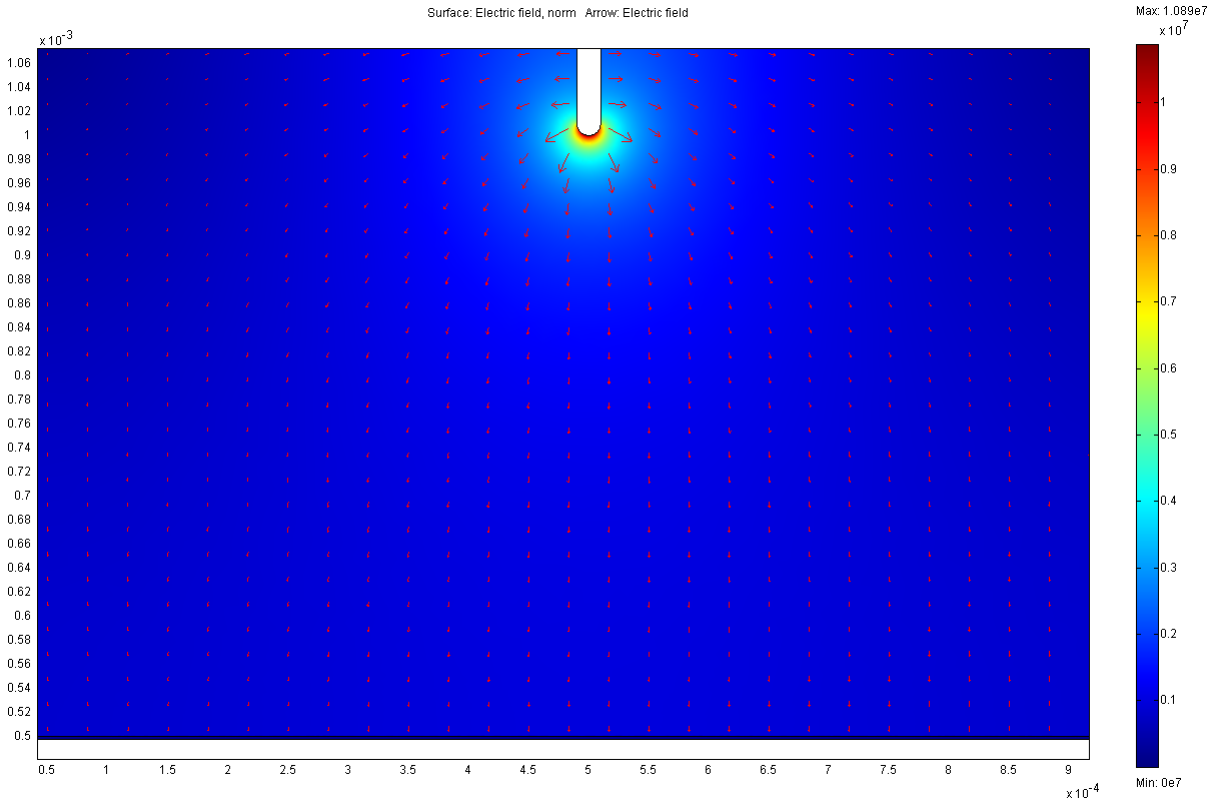

Figure 3.14. Simulation result of electric field for the collectors without the oxide insulating layer.

Table 3.1. Parameters for simulation

Parameter	**Value**
Tip radius	20 μm
Applied voltage	800 V
Electrode-to-collector distance	500 μm
Relative Permittivity of SiO_2	4
Relative Permittivity of Si	12
Thickness of SiO2	2 μm
Thickness of Si	500 μm

3.4. Summary

NFES is a simple yet powerful method for direct-write deposition of nanofibers with unprecedented controllability at resolutions comparable to those achieved with much more expensive and sophisticated lithography tools. It should be especially useful for the heterogeneous integration of nanoscale materials to devices prepared by conventional lithographic and manufacturing methods, such as microelectronics and MEMS structures. Furthermore, NFES could play a key role in building up larger-area, ordered non-woven nanofibers for various applications.

References

[1] F. R. S. Rayleigh, "On the equilibrium of liquid conducting masses charged with electricity," *London Edinburgh Dublin Philosophical Magazine and Journal*, vol. 44, pp. 184-186, 1882.

[2] J. Zeleny, "Instability of electrified liquid surfaces," *Physical Review*, vol. 10, pp. 1-6, 1917.

[3] A. Formhals, "Process and apparatus for preparing artificial threads," *US Patent*, 1,975,504, 1934.

[4] D. H. Reneker and I. Chun, "Nanometre diameter fibres of polymer, produced by electrospinning," *Nanotechnology*, vol. 7, no. 3, pp. 216-223, 1996.

[5] D. Li and Y. Xia, "Electrospinning of nanofibers: Reinventing the wheel?" *Advanced Materials*, vol. 16, no. 14, pp. 1151-1170, 2004.

[6] Y. Zhou, M. Freitag, J. Hone, C. Staii, A. T. Johnson, Jr., N. J. Pinto, and A. G. MacDiarmid, "Fabrication and electrical characterization of polyaniline-based nanofibers with diameter below 30 nm," *Applied Physics Letters*, vol. 83, no. 18, pp. 3800-3802, 2003.

[7] H. Dai, J. Gong, H. Kim, and D. Lee, "A novel method for preparing ultra-fine alumina-borate oxide fibres via an electrospinning technique," *Nanotechnology*, vol. 13, no. 5, pp. 674-677, 2002.

[8] M. M. Bergshoef and G. J. Vancso, "Transparent Nanocomposites with Ultrathin, Electrospun Nylon-4,6 Fiber Reinforcement," *Advanced Materials*, vol. 11, no. 16, pp. 1362-1365,1999.

[9] F. Ko, Y. Gogotsi, A. Ali, N. Naguib, H. Ye, G.L. Yang, C. Li, and P. Willis, "Electrospinning of Continuous Carbon Nanotube-Filled Nanofiber Yarns," *Advanced Materials*, vol. 15, no. 14, pp. 1161-1165, 2003.

[10] W.-J. Li, C. T. Laurencin, E. J. Caterson, R. S. Tuan, and F. K. Ko, "Electrospun nanofibrous structure: A novel scaffold for tissue engineering," *Journal of Biomedical Materials Research*, vol. 60, no. 4, pp. 613-621, 2002.

[11] B.-M. Min, G. Lee, S. H. Kim, Y. S. Nam, T. S. Lee, and W. H. Park, "Electrospinning of silk fibroin nanofibers and its effect on the adhesion and spreading of normal human keratinocytes and fibroblasts in vitro," *Biomaterials*, vol. 25, no. 7-8, pp. 1289-1297, 2004.

[12] P. Gibson, H. Schreuder-Gibson, and D. Riven, "Transport properties of porous membranes based on electrospun nanofibers," *Colloids and Surfaces A: Physicochemical and Engineering Aspects*, vol. 187-188, pp. 469-481, 2001.

[13] N. J. Pinto, A. T. Johnson, Jr., A. G. MacDiarmid, C. H. Mueller, N. Theofylaktos, D. C. Robinson, and F. A. Miranda, "Electrospun polyaniline/polyethylene oxide nanofiber field-effect transistor," *Applied Physics Letters*, vol. 83, no. 20, pp. 4244-4246, 2003.

[14] H. Liu, J. Kameoka, D. A. Czaplewski, and H. G. Craighead, "Polymeric Nanowire Chemical Sensor," Nano Letters, vol. 4, no. 4, pp. 671-675, 2004.

[15] X. Wang, C. Drew, S.-H. Lee, K. J. Senecal, J. Kumar, and L. A. Samuelson, "Electrospun Nanofibrous Membranes for Highly Sensitive Optical Sensors," Nano Letters, vol. 2, no. 11, pp. 1273-1275, 2002.

[16] T. Takahashi, M. Taniguchi, and T. Kawai, "Fabrication of DNA Nanofibers on a Planar Surface by Electrospinning," *Japanese Journal of Applied Physics*, vol. 44, no. 27, pp. L860-L862, 2005.

[17] J. A. Matthews, G. E. Wnek, D. G. Simpson, and G. L. Bowlin, "Electrospinning of collagen nanofibers," *Biomacromolecules*, vol. 3, no. 2, pp. 232-238, 2002.

[18] P. Katta, M. Alessandro, R. D. Ramsier, and G. G. Chase, "Continuous electrospinning of aligned polymer nanofibers onto a wire drum collector," *Nano Letters*, vol. 4, no. 11, pp. 2215-2218, 2004.

[19] L. Wannatong, A. Sirivat, and P. Supaphol, "Effects of solvents on electrospun polymeric fibers: preliminary study on polystyrene," *Polymer International*, vol. 53, no. 11, pp. 1851-1859, 2004.

[20] J. M. Deitzel, J. D. Kleinmeyer, J. K. Hirvonen, and N. C. Beck Tan, "Controlled deposition of of electrospun poly(ethylene oxide) fibers," *Polymer*, vol. 42, no. 19, pp. 8163-8170, 2001.

[21] H. Fong, W.-D. Liu, C.-S. Wang, and R. A. Vaia, "Generation of electrospun fibers of nylon 6 and nylon 6-montmorillonite nanocomposite," *Polymer*, vol. 43, no. 3, pp. 775-780, 2002.

[22] R. Dersch, T. Liu, A. K. Schaper, A. Greiner, and J. H. Wendorff, "Electrospun nanofibers: Internal structure and intrinsic orientation," *Journal of Polymer Science Part A: Polymer Chemistry*, vol. 41, no. 4, pp. 545-553, 2003.

[23] D. Li, Y. Wang, and Y. Xia, "Electrospinning of polymeric and ceramic nanofibers as uniaxially aligned arrays," *Nano Letters*, vol. 3, no. 8, pp. 1167-1171, 2003.

[24] D. Li, Y. Wang, and Y. Xia, "Electrospinning nanofibers as uniaxially aligned arrays and layer-by-layer stacked films," *Advanced Materials*, vol. 16, no. 4, pp. 361-366, 2004.

[25] A. Theron, E. Zussman, and A.L. Yarin, "Electrostatic field-assisted alignment of electrospun nanofibers," *Nanotechnology*, vol. 12, no. 3, pp. 384-390, 2001.

[26] E. Zussman, A. Theron, and A.L. Yarin, "Formation of nanofiber crossbars in electrospinning," *Applied Physics Letters*, vol. 82, no. 6, pp. 973-975, 2003.

[27] T. Han, D.H. Reneker, and A.L. Yarin, "Buckling of jets in electrospinning," *Polymer*, vol. 48, no. 20, pp. 6064-6076, 2007.

[28] A. Frenot and I. S. Chronakis, "Polymer nanofibers assembled by electrospinning," *Current Opinion in Colloid & Interface Science*, vol. 8, no. 5, pp. 64-75, 2003.

[29] Z.-M. Huang, Y.-Z Zhang, M. Kotaki and S. Ramakrishna, "A review on polymer nanofibers by electrospinning and their applications in nanocomposites," *Composite Science Technology*, vol. 63, pp. 2223-2253, 2003.

[30] W. K. Son, J. H. Youk, T. S. Lee, and W. H. Park, "The effects of solution properties and polyelectrolyte on electrospinning of ultrafine poly(ethylene oxide) fibers," *Polymer*, vol.

45, no. 9, pp. 2959-2966, 2004.

[31] R. D. Piner, J. Zhu, F. Xu, S. Hong, and C. A. Mirkin, "Dip-Pen Nanolithography," *Science*, vol. 283, no. 5402, pp. 661-663, 1999.

[32] H. Sirringhaus, T. Kawase, R. H. Friend, T. Shimoda, M. Inbasekaran, W. Wu, and E. P. Woo, "High-resolution inkjet printing of all-polymer transistor circuits," *Science*, vol. 290, no. 5499, pp. 2123-2126, 2000.

[33] D.H. Reneker, A.L. Yarin, H. Fong, and S. Koombhongse, "Bending instability of electrical charged liquid jets of polymer solutions in electrospinning," *Journal of Applied Physics*, vol. 87, no. 9, pp. 4531-4547, 2000.

CHAPTER 4

CONTINUOUS NEAR-FIELD ELECTROSPINNING

4.1. Introduction and Background

Conventional electrospinning processes producing randomly deposited nanofibers have been used in various applications including filtration [1], texturing [2], composite reinforcement [3, 4], and tissue scaffolds [5]. The disorderly fashion of such deposited nanofibers, however, has limited its full potential. For example, well-controlled architectures, rather than random configurations, could give rise to improvements in the aforementioned examples as well as other applications. Electrospinning using short needle-to-collector distance, including scanning tip electrospinning [6] and near-field electrospinning (NFES), have shown easier and more predictable location control for the deposition of nanofibers. However, the polymer droplet approach in these processes limits the total length of nanofiber deposition, and fiber thickness is inevitably nonuniform because the polymer droplet is consumed during the process.

Herein, the principle and methodology of continuous near-field electrospinning is proposed and demonstrated, which benefits from the continuity of conventional electrospinning and the superior location control of near-field electrospinning to produce orderly nanofiber patterns over large areas.

4.2. Principles of Operation

In the conventional electrospinning process, the applied electrical field generates sufficient electrostatic forces to deform the polymer meniscus into a conical shape called a Taylor cone [7]. A critical electrical field at which electrostatic forces overcome the surface tension forces is required to induce a polymer jet from the tip of Taylor cone. Typically the critical electrical field of conventional electrospinning process is on the order of 10^5 V/m [8]. In our experimental demonstration, 7% wt polyethylene oxide (PEO, M_v = 300,000) aqueous solution is used under room temperature and one atmosphere of pressure. The needle-to-collector distance is fixed at 500 μm and a syringe needle with 200 μm outer diameter and 100 μm inner diameter is utilized as the spinneret to continuously supply polymer solution.

Figure 4.1 shows that when the applied voltage on the syringe needle reaches a critical value of 1.5 kV for jet initiation and the cone has a semi-vertical angle of around 49°. The corresponding critical electrical field (3×10^6 V/m) is one order of magnitude larger than that of conventional electrospinning because the surface tension of the droplet increases as syringe needle diameter decreases. The polymer jet below the tip of the cone is about 25 μm in diameter, similar to that of the conventional electrospinning process in which the needle-to-collector distance is about 5~50 cm. However, since the needle-to-collector distance is only 500 μm in the near-field setup, the solvent in the polymer jet does not have enough time to fully evaporate. As a result, as-spun fibers are 3~6 μm in diameter and remain in liquid form shortly after deposition as shown in Figure 4.2. Oftentimes, consequent fibers will merge with those that have just deposited onto the collector.

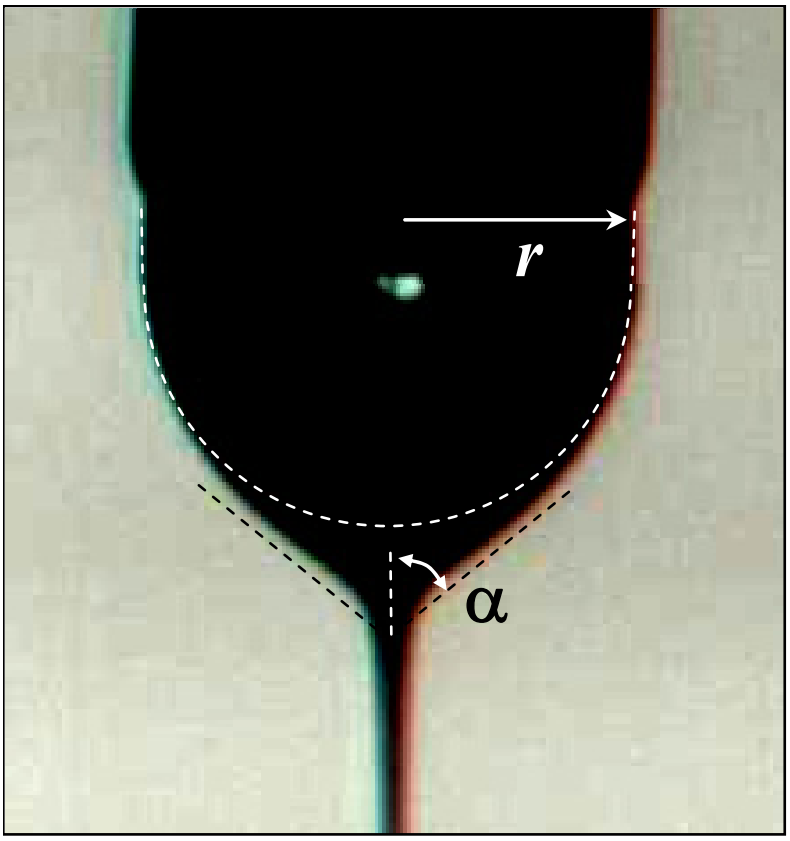

Figure 4.1. Optical image showing the syringe needle (r = 100 μm), droplet and cone (α = 49°) of conventional electrospinning in near-field setup. The white dashed curve represents the fluid surface just before jet initiation and the cone part is the fluid surface right at jet initiation. A polymer jet starts to eject from the droplet while 1.5 kV is applied on the syringe needle and the needle-to-collector distance is 500 μm.

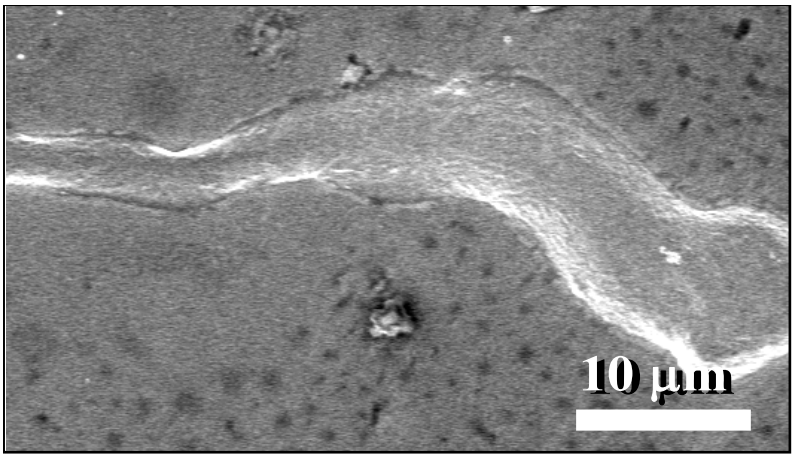

Figure 4.2. SEM photomicrograph showing the as-spun fibers from Figure 4.1.

In order to have electrospun nanofibers with diameter in the sub-100 nm range, the applied electrical field for conventional electrospinning can be increased to cause greater stretching of the polymer solution. However, the controllability of nanofiber deposition is severely affected by bending instability [9]. The key strategy for producing sub-100 nm nanofibers via NFES, on the other hand, is to reduce the size of the polymer jet emerging from the cone by reducing the applied electrical field below the critical value.

Theoretically, this can be accomplished by simultaneously reducing the applied voltage and polymer solution supply rate after the on-set of electrospinning is achieved (Figure 4.1). Practically, this is very difficult to control as a high supply rate would result in excess polymer plummeting to the collector, disrupting the delicate electrospinning process, while a low supply rate would cause the pendant droplet to shrink quickly and terminate the electrospinning process. To circumvent the limitations of these approaches, we have developed a simple and reliable technique to achieve continuous NFES by means of an initial mechanical drawing process that aids electrical force in overcoming surface tension to initiate the ejection of a polymer jet.

This process starts by applying a sub-critical voltage to deform the polymer meniscus without inducing electrospinning. Mechanical drawing is applied by using a tungsten probe with 1 μm tip diameter to poke inside the meniscus. The probe is then rapidly pulled away from the polymer droplet to activate the continuous electrospinning process as illustrated in Figure 4.3A, B and C. The initial location of the probe tip is not crucial since the polymer jet will automatically move downwards and align to the applied electrical field as shown in Figure 4.3C and D.

Instead of mechanical drawing, the sub-critical voltage is the key control parameter in deciding the size of deposited nanofibers as evidenced in Figure 4.3B where the fiber jet is relatively thick during the mechanical drawing process while Figure 4.3C and D show thinner fiber jet after the mechanical probe is removed.

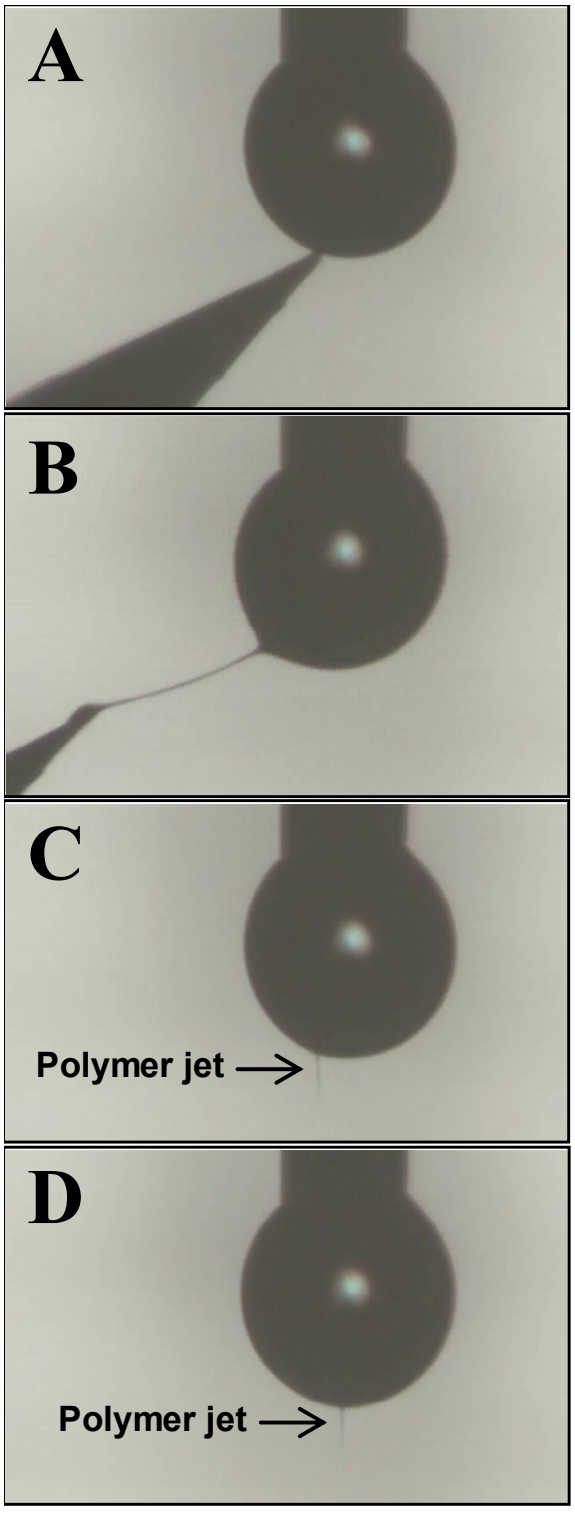

Figure 4.3. (A) Optical image showing a tungsten probe tip poking inside the polymer meniscus. (B) Optical image showing mechanical drawing of a fiber from polymer droplet. (C) Optical image showing the electrospinning process is initiated. (D) Optical image showing the polymer jet automatically moves downwards due to the applied electrical field.

In this case as shown in Figure 4.4, the applied voltage is 600 V, corresponding to an electrical field of 1.2 $\times 10^6$ V/m, and the polymer jet diameter immediately outside of the cone is about 3 m, and the deposited nanofibers on the collector have diameters of about 50 nm as shown in Figure 4.5. The semi-vertical angle of the cone is 75°. A polymer feed rate of about 0.1 μL/hr can maintain the droplet shape for continuous and uniform deposition of nanofibers. With the aid of this initial mechanical drawing process, continuous supply of polymer solution is maintained for NFES while the size of polymer jet emerging from the cone is drastically reduced to achieve sub-100 nm deposition of nanofibers. Moreover, this approach avoids the cumbersome issue of consistently extruding a polymer droplet of the same size through a syringe needle of small diameter.

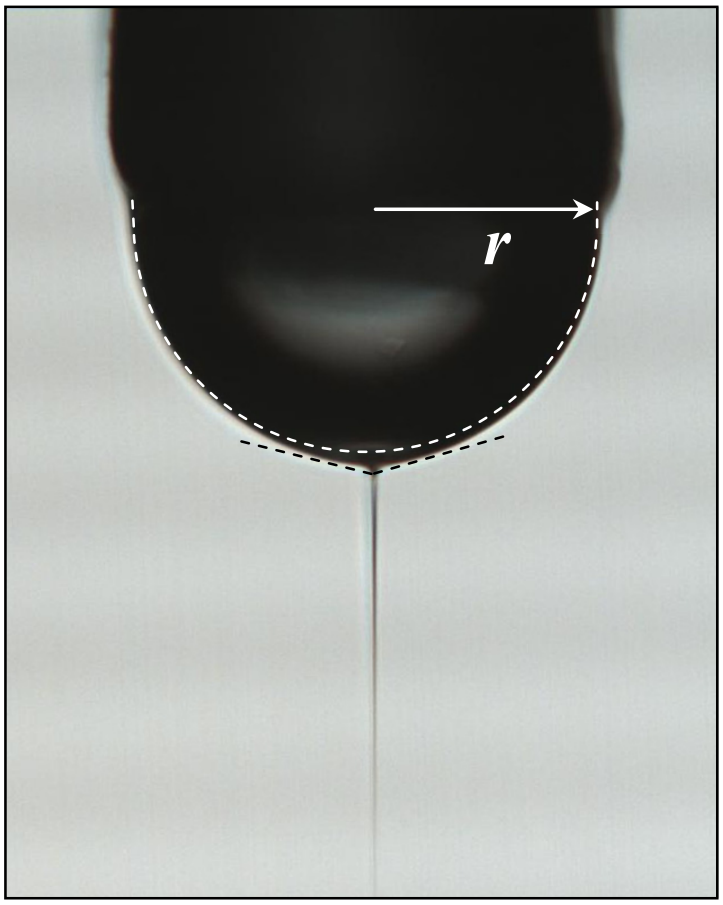

Figure 4.4. Optical image showing the syringe needle (r = 100 μm), droplet and cone (α = 75°) of continuous NFES. The process is initiated with the aid of a probe tip at a voltage of 600 V while the needle-to-collector distance is 500 μm.

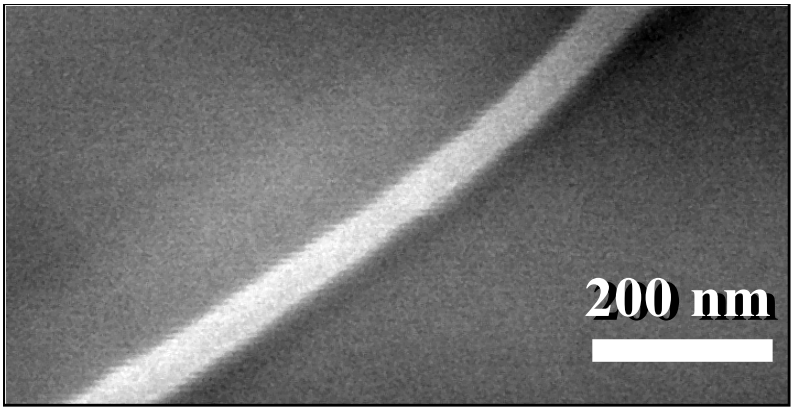

Figure 4.5. SEM photomicrograph showing the as-spun fibers from Figure 4.4.

4.3. Controllability and Continuity

To demonstrate the controllability and continuity of this process, a variety of orderly patterns are deposited onto silicon collectors using a programmable *x-y* stage (XPS controller driver, Newport Inc.). Experimentally, the syringe needle is fixed while the stage translates at a speed of 120 mm/s. Figure 4.6 shows the smooth writing of "Cal" in an area of 1×0.5 mm^2 where the diameter of the fiber is 150 nm. The smoothness of the pattern was achieved by setting the translational speed of the stage as close as possible to the deposition rate. A slow translational speed would cause the nanofiber to form spiraling patterns as shown in the region preceding the script 'C' in Figure 4.6, while a high translational speed would not afford the nanofiber enough time to anchor itself at all points on the intended pattern. A circular design, for instance, would appear as a polygonal nanofiber pattern.

Additionally, the size of the pattern of Figure 4.6 does not represent the smallest design that can be drawn using continuous NFES. Since the speed of the *x-y* stage must match the electrospinning deposition rate for smoothness, this criterion must be met regardless of the intricacy of the pattern; however, smaller arc trajectories demand extremely large radial acceleration, and the extent to which this acceleration can be executed depends on the capabilities of the *x-y* stage.

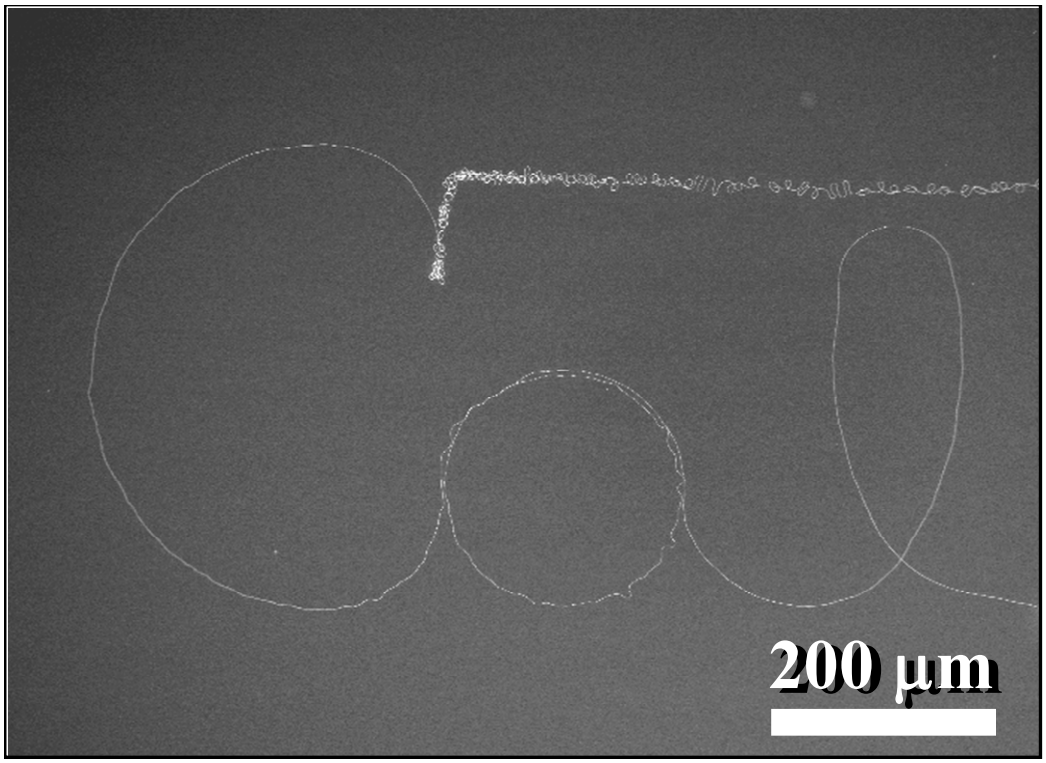

Figure 4.6. The three-character "Cal" is drawn on a silicon chip by a programmable *x-y* stage.

Figure 4.7 illustrates experimental results of the continuous NFES of a single nanofiber deposited on a silicon chip in a designed trajectory over a 4 × 4 cm^2 large area. The process can continue running as long as polymer solution is supplied from the syringe needle. In this case, the deposition period is 15 minutes for a total length of 108 m and the nanofiber has a diameter of 709 ± 131 nm. The diameter and standard deviation are calculated based on 100 data points measured directly from SEM. The optical image in Figure 4.8 shows that the nanofiber is deposited on the silicon chip with a fiber pitch of 49.88 ± 3.98 μm (from 50 data points) while the designed trajectory has a fiber pitch of 50 μm. We believe this uneven spacing is mainly due to the oscillation of the cone on the polymer droplet, which is caused by the interference of the fiber charges with the electrical field, mechanical buckling during impact between polymer jet and collector [10], and external perturbations [9]. Further investigation is required in order to minimize such errors on nanofiber deposition. A triangular pattern is also deposited using the same process, shown in Figure 4.9.

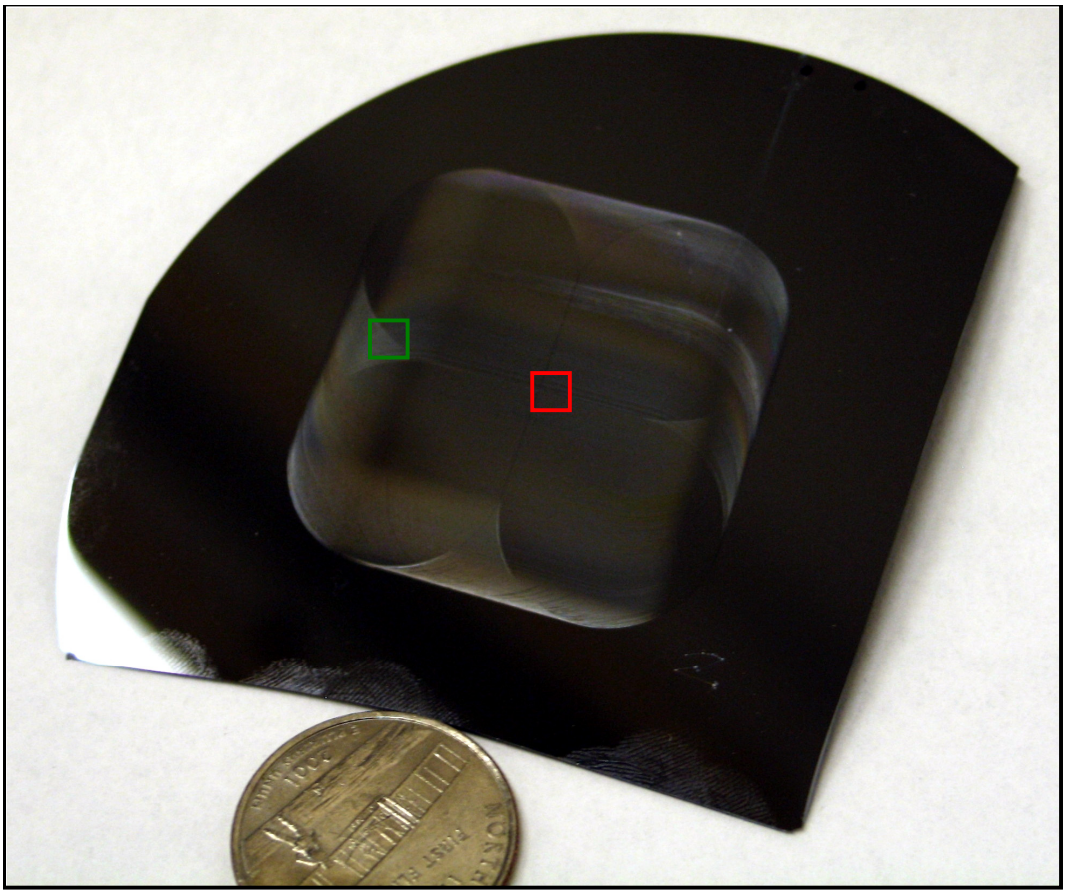

Figure 4.7. A single nanofiber deposited on a silicon chip in a designed trajectory covers a 4 × 4 cm^2 area in 15 minutes via continuous NFES. In the foreground is a US quarter.

Figure 4.8. Optical image of a grid pattern with controlled 50-μm spacing from an area highlighted by the red box in Figure 4.7.

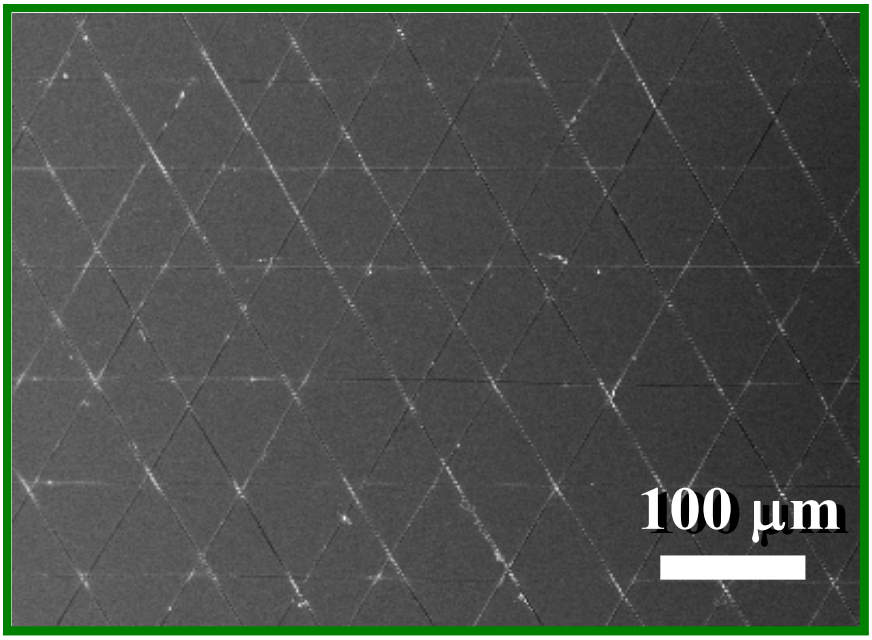

Figure 4.9. SEM photomicrograph of a crosshatch pattern from an area highlighted by the green box in Figure 4.7.

4.4. Process Characterization

Similar to the conventional electrospinning process, the diameter of nanofibers could be adjusted by controlling various operating parameters. The following characterization of fiber diameters and standard deviation are calculated based on 50 data points measured directly from SEM in each experiment.

When the PEO concentration is 7% wt and the needle-to-collector distance is fixed at 500 μm, the average fiber diameter can be varied in the range of 38 ± 4 to 2314 ± 622 nm under different applied voltages as shown in Figure 4.10. The proportional relationship between the fiber diameter and applied voltage confirms the previous observation that the cone size and polymer jet diameter both increase with applied electrical field. Therefore, higher voltage results in thicker fibers in continuous NFES, which is contrary to the trends observed in conventional electrospinning [11, 12, 13]. In the conventional electrospinning process, higher bias voltages imply stronger Columbic repulsion force in the polymer jet to further stretch the nanofibers during the whipping process. In the continuous NFES process, this effect is diminished due to short needle-to-collector distance such that the initial polymer jet diameter dominates the final nanofiber diameter rather than bending instability.

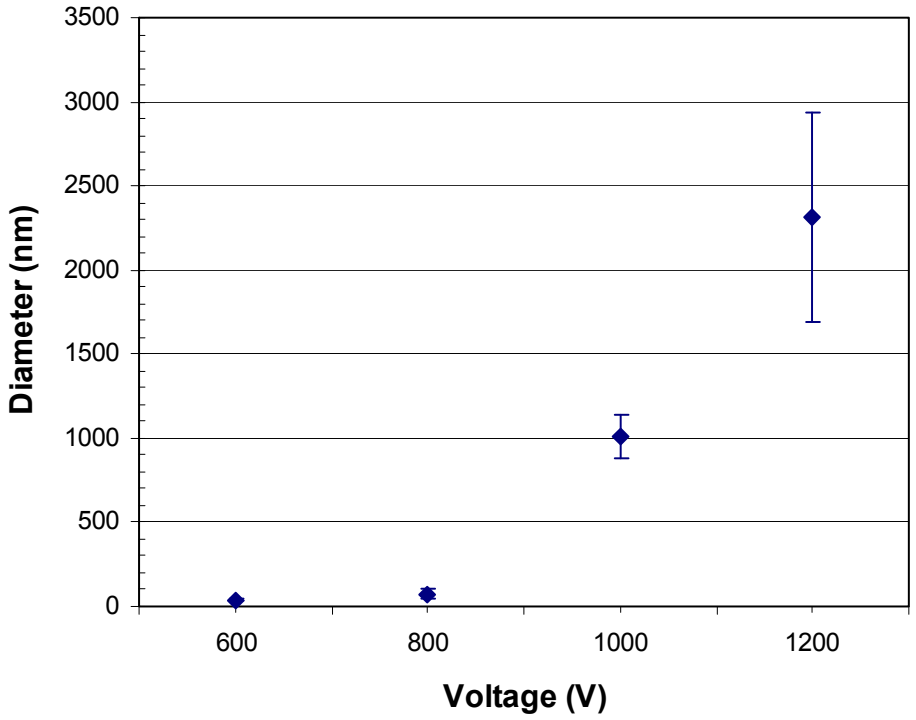

Figure 4.10. Plots showing the dependence of nanofiber diameters on applied voltage. Other parameters are maintained as the following: PEO concentration (7% wt); Needle-to-collector distance (500 μm). Experiments are under room temperature and one atmosphere pressure.

The polymer concentration also affects the morphology of the electrospun nanofibers. If the PEO solution concentration is lower than approximately 3% wt, the continuous NFES process can not be activated due to its insufficient viscoelasticity. At such low polymer concentrations, the elongational viscosity is insufficient to suppress capillary breakup. When the polymer concentration is increased nanofibers are obtained due to an increase in viscosity, thus counteracting the stretching via electrical force. As shown in Figure 4.11, the average fiber diameter can range from 37 ± 3 to 119 ± 6 nm by increasing the polymer concentration when the needle-to-collector distance is fixed at 1000 μm under a bias voltage of 500 V.

The needle-to-collector distance is another key factor that affects the diameters of deposited nanofibers. As shown in Figure 4.12, larger needle-to-collector distance results in thinner fibers due to a longer period of stretching as polymer jets travel towards the collector. The average fiber diameter ranges from 49 ± 7 to 74 ± 9 nm when the applied voltage is 800 V and the concentration of PEO solution is 7% wt.

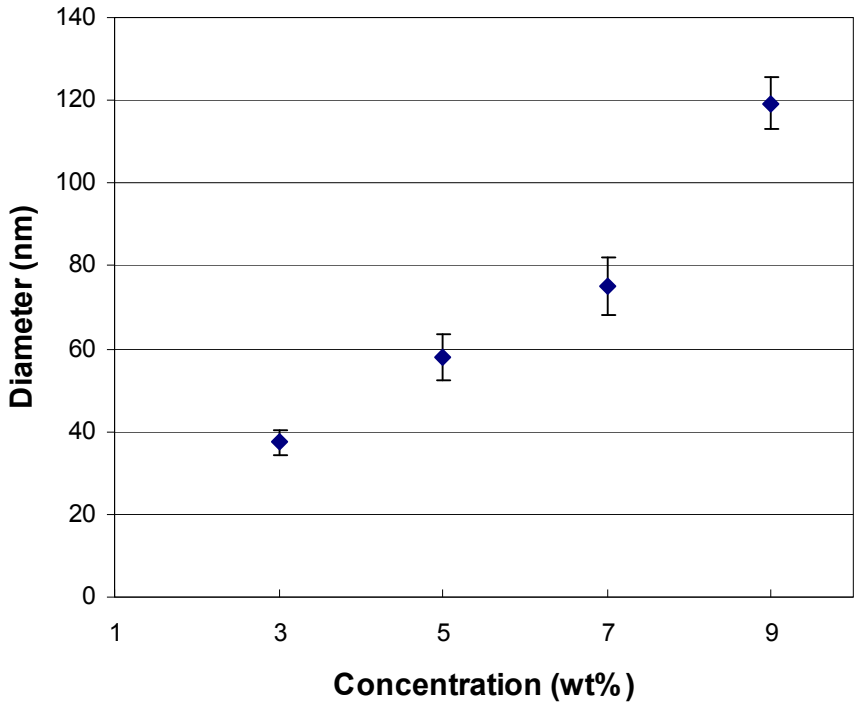

Figure 4.11. Plots showing the dependence of nanofiber diameters on polymer concentration. Other parameters are maintained as the following: Applied voltage (500 V); Needle-to-collector distance (1000 μm). Experiments are under room temperature and one atmosphere pressure.

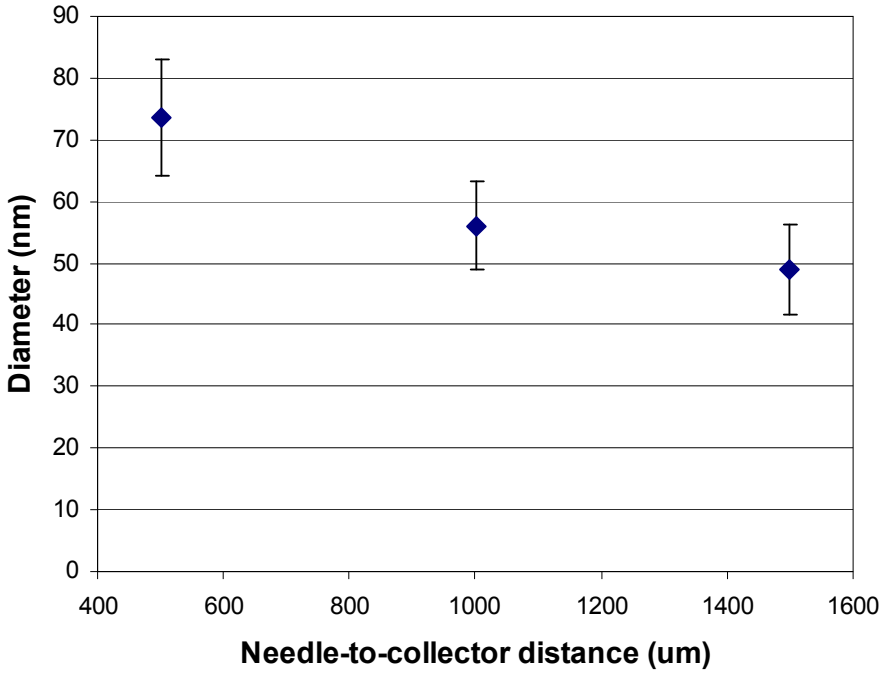

Figure 4.12. Plots showing the dependence of nanofiber diameters on needle-to-collector distance. Other parameters are maintained as the following: PEO concentration (7% wt); Applied voltage (800 V). Experiments are under room temperature and one atmosphere pressure.

4.4. Summary

The concept and demonstration of continuous NFES make possible new applications that were impossible by conventional electrospinning. We believe that the ability of depositing polymeric materials at specific locations with specific patterns can open up opportunities for heterogeneous integration of a variety of materials and continuous NFES is the necessary technology for cost-effective manufacturing. There are many other areas to be explored with the utilization of continuous NFES. For example, continuous NFES has the potential to create orderly patterns through automated processes to enable bioengineers to create scaffolds in vitro that are highly representative of real extracellular matrices. Such scaffolds could potentially extend current tissue engineering techniques to develop previously unachievable organs types and increase the viability of these tissues.

References

[1] P. Gibson, H. Schreuder-Gibson, and D. Riven, "Transport properties of porous membranes based on electrospun nanofibers," *Colloids and Surfaces A: Physicochemical and Engineering Aspects*, vol. 187-188, pp. 469-481, 2001.

[2] K. J. Pawlowski, H. L. Belvin, D. L. Raney, J. Su, J. S. Harrison, and E. J. Siochi, "Electrospinning of a micro-air vehicle wing skin," *Polymer*, vol. 44, no. 4, pp. 1309-1314, 2003.

[3] Y. Dzenis and Y. Wen, "Continuous Carbon Nanofibers For Nanofiber Composites," *Materials Research Society Symposia Proceedings*, vol. 702, pp. 173-178, 2002.

[4] H. Ye, H. Lam, N. Titchenal, Y. Gogotsi, and F. Ko, "Reinforcement and rupture behavior of carbon nanotubes–polymer nanofibers," *Applied Physics Letters*, vol. 85, no. 10, pp. 1775-1777, 2004.

[5] I.-S. Yeo, J.-E. Oh, L. Jeong, T. S. Lee, S. J. Lee, W. H. Park, and B.-M. Min, "Collagen-based biomimetic nanofibrous scaffolds: preparation and characterization of collagen/silk fibroin bicomponent nanofibrous structures," *Biomacromolecules*, vol. 9, no. 4, pp. 1106-1116, 2008.

[6] J. Kameoka, R. Orth, Y. Yang, D. Czaplewski, R. Mathers, G. W. Coates, and H. G. Craighead, "A scanning tip electrospinning source for deposition of oriented nanofibres," *Nanotechnology*, vol. 14, no. 10, pp. 1124-1129, 2003.

[7] G. Taylor, "Disintegration of water drops in an electric field," *Proceedings of the Royal Society of London. Series A*, vol. 280, no. 1382, pp. 383-397, 1964.

[8] D. H. Reneker and I. Chun, "Nanometre diameter fibres of polymer, produced by electrospinning," *Nanotechnology*, vol. 7, no. 3, pp. 216-223, 1996.

[9] D.H. Reneker, A.L. Yarin, H. Fong, and S. Koombhongse, "Bending instability of electrical charged liquid jets of polymer solutions in electrospinning," *Journal of Applied Physics*, vol. 87, no. 9, pp. 4531-4547, 2000.

[10] T. Han, D.H. Reneker, and A.L. Yarin, "Buckling of jets in electrospinning," *Polymer*, vol. 48, no. 20, pp. 6064-6076, 2007.

[11] J. S. Lee, K. H. Choi, H. Do Ghim, S. S. Kim, D. H. Chun, H. Y. Kim, and W. S. Lyoo, "Role of molecular weight of atactic poly(vinyl alcohol) (PVA) in the structure and properties of PVA nanofabric prepared by electrospinning," *Journal of Applied Polymer Science*, vol. 93, no. 4, pp. 1638-1646, 2004.

[12] C. J. Buchko, L. C. Chen, Y. Shen, and D. C. Martin, "Processing and microstructural characterization of porous biocompatible protein polymer thin films," *Polymer*, vol. 40, no. 26, pp. 7397-7407, 1999.

[13] S. Megelski, J. S. Stephens, D. B. Chase, and J. F. Rabolt, "Micro- and nanostructured surface morphology on electrospun polymer fibers," *Macromolecules*, vol. 35, no. 22, pp. 8456-8466, 2002.

CHAPTER 5

DIRECT-WRITE PIEZOELECTRIC NANOGENERATOR

5.1. Introduction and Background

Mechanical energy scavenging from ambient environments is an attractive renewable source of power for various applications. Examples range from large-scale power generators which convert mechanical actuation found in nature, such as waterfalls, wind, and ocean waves, into electricity [1,2] to small-scale energy harvesters which scavenge energy from mechanical vibration sources in building, automotives, appliances, and human movements [3,4]. In pursuing these mechanical energy harvesters, especially for small-scale applications, one fundamental issue is the design and selection of structural materials for efficient conversion of mechanical energy into electricity.

Recent work in the field of nanomaterials has provided new opportunities and directions in engineering effective materials and structures for energy harvesters. Prior research [5, 6, 7, 8] on energy scavenging using zinc oxide (ZnO) nanowires has illustrated the feasibility of utilizing inorganic nanomaterials with semiconducting and piezoelectric properties for nanogenerators. Further advancements for nanogenerators include the utilization of non-semiconducting and organic nanomaterials, direct-integration with other structures and processes, and improvements in energy conversion efficiency. In this chapter, we report direct-write, piezoelectric polymeric nanogenerators based on organic nanofibers with high energy conversion efficiency to address some of the aforementioned challenges.

These nanofibers are made of polyvinylidene fluoride (PVDF) with high flexibility, minimizing resistance to external mechanical movements in low-frequency, large-deflection energy scavenging applications.

5.2. Polyvinyliene fluoride

Polyvinylidene fluoride (PVDF) is a semi-crystalline polymer performing good chemical resistance, mechanical strength and flexibility and is well known for its ferroelectric and piezoelectric properties. PVDF has four major crystalline phases: α, β, γ and δ, which are distinguished by the conformation of the C-C bonding along the chain backbone. Among these, α-phase is the most energetic stable phase and thus most common. It is usually observed in commercial PVDF powders and as-manufactured films. Chemical structure of theα-phase is illustrated in Figure 5.1A. In this phase, the chains stack with the respective polarizations in alternating directions (trans gauche+ trans gauche- conformation, tg+tg-), such that the energy level is at the minimum. This phase, however, does not exhibit piezoelectricity. The β-phase is known to be responsible for the piezoelectric response of PVDF. In the β-phase, the conformation is all-trans (tttt), such that the dipoles are oriented in the same direction (Figure 5.1B). This causes the piezoelectric properties of the material.

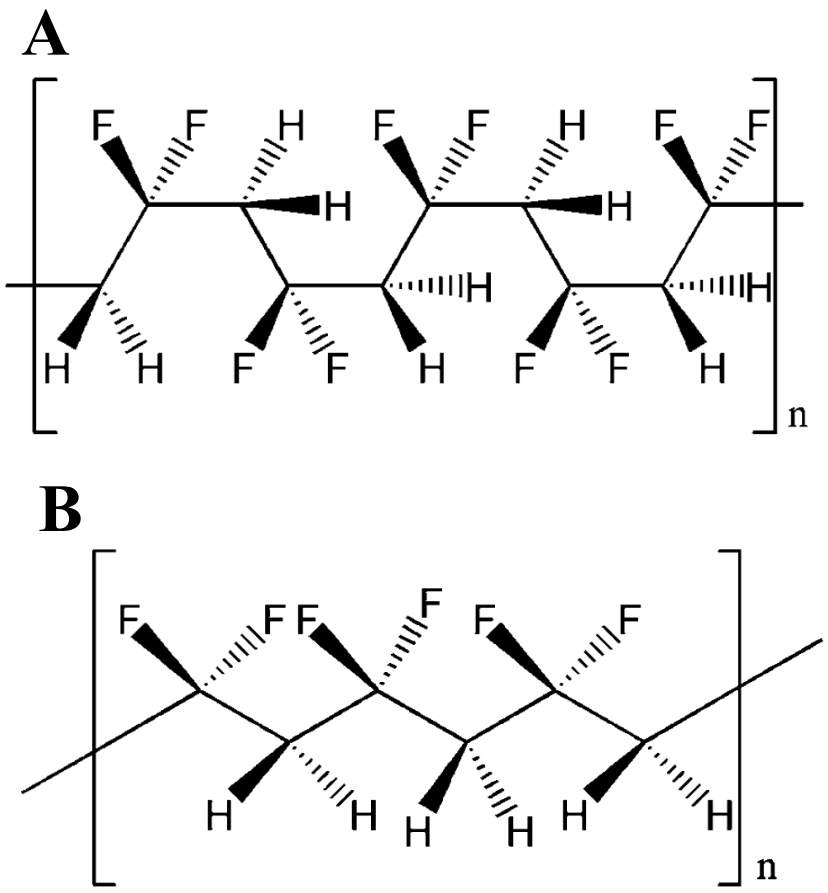

Figure 5.1. Chemical structure of PVDF in its (A) α-phase and (B) β-phase. Dipoles are oriented randomly in α-phase and organized in the β-phase, causing the material to exhibit piezoelectricity.

Many research groups have studied the formation of the *β*-phase structure of PVDF by different processing methods: crystallization under high pressure [9], poling under a high electrical field [10], polymer stretching [11, 12], annealing [13], or blending [14]. Lately, it has been reported that *β*-phase can be formed during an electrospinning process [15, 16, 17, 18, 19, 20, 21, 22, 23, 24]. The suggested mechanism is that the strong electrical field in an electrospinning process forces the dipoles to organize in the same direction, as illustrated in Figure 5.2. This introduces the essential concept of a PVDF nanogenerator.

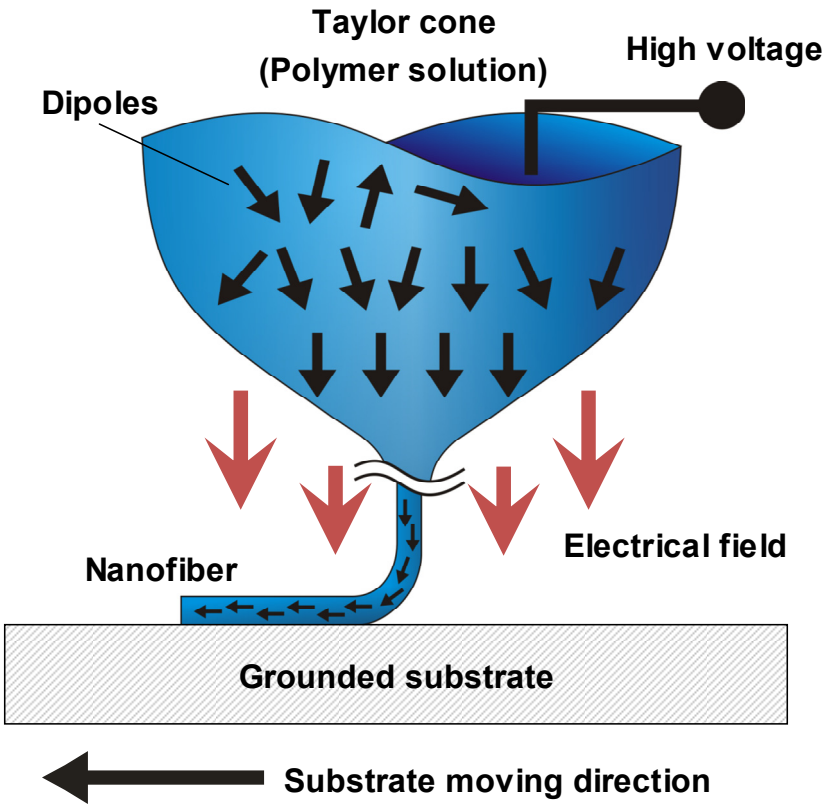

Figure 5.2. Schematic of the *in-situ* poling process during electrospinning.

5.3. Theoretical Studies for Realization of Electrospun PVDF Nanofibers

5.3.1. Review on Electrospinning of PVDF

As introduced in previous section, a number of studies have investigated the fabrication of PVDF nanofibers via conventional electrospinning, including processing, characterization of fiber morphology and crystalline structures process [15, 16, 17, 18, 19, 20, 21, 22, 23, 24]. Although NFES differs from conventional electrospinning in many aspects, a good understanding about electrospinning of PVDF could still be valuable. For instance, an essential point is the possibility of β-phase formation during electrospinning. This section provides a review on present studies on electrospinning of PVDF to gain better insights in process fundamentals and especially influence factors on the resulting fiber characteristics.

The first extensive study on electrospinning of PVDF was presented by Nasir *et al.* [18]. Their work investigated the influence of electrospinning parameters, e.g. polymer concentration, applied voltage, feeding rate, and electrode-to-collector distance, on the characteristics of the resulting nanofibers, e.g. diameter, morphology, and crystalline structure. In their study, PVDF solutions were prepared in N,N-Dimethylacetamide (DMAc) at different concentrations ranging from 5-26% wt. The solution was used in a conventional electrospinning set up with voltage ranging from 7.5-15 kV, tip-to-collector distance ranging from 8-15 cm, and flow rate ranging from 1-11 μm/min. Results from the process followed the typical electrospinning behaviors. For example, fiber formation was promoted by higher polymer concentration, or solution viscosity. The fiber diameter increased with increasing concentration and applied voltage. The distance from tip to collector had no significant effect on the resulting fibers and their diameter, once the fibers were successfully deposited. The feeding rate of the polymer solution showed an effect up to a rate of 5 μl/min and fiber diameter decreased as the flow rate increased to 5μl/min and remained constant at higher flow rates.

In a subsequent study, Nasir *et al.* [19] studied the effect of ionic fluorinated surfactants on β-phase formation of electrospun PVDF nanofibers. PVDF nanofibers were electrospun from solutions of PVDF in DMF/acetone mixtures with addition of ionic fluorosurfactants – both anionic and cationic. It was observed that the addition of ionic fluorinated surfactants was useful for the formation of bead-free, homogeneous fibers. In addition, it was found that ionic fluorosurfactants enhanced the formation of β-phase crystalline structure of PVDF. A possible mechanism was suggested based on the interaction between the positive charge in the ionic surfactant and fluorine atom in PVDF chain, as illustrated in Figure 5.3.

Ren and Dzenis [20] also reported fabrication of PVDF nanofibers via electrospinning. In their experiments, solutions of PVDF with different molecular weight in DMF and DMSO were tested. The produced fibers were characterized with XRD and FTIR. It was found that the α-phase of the raw material was converted to the β-phase during electrospinning. This verified the concept that electrospinning was a simple yet effective method to yield β-phase PVDF. A summary of processing conditions for piezoelectric PVDF is given in Table 5.1.

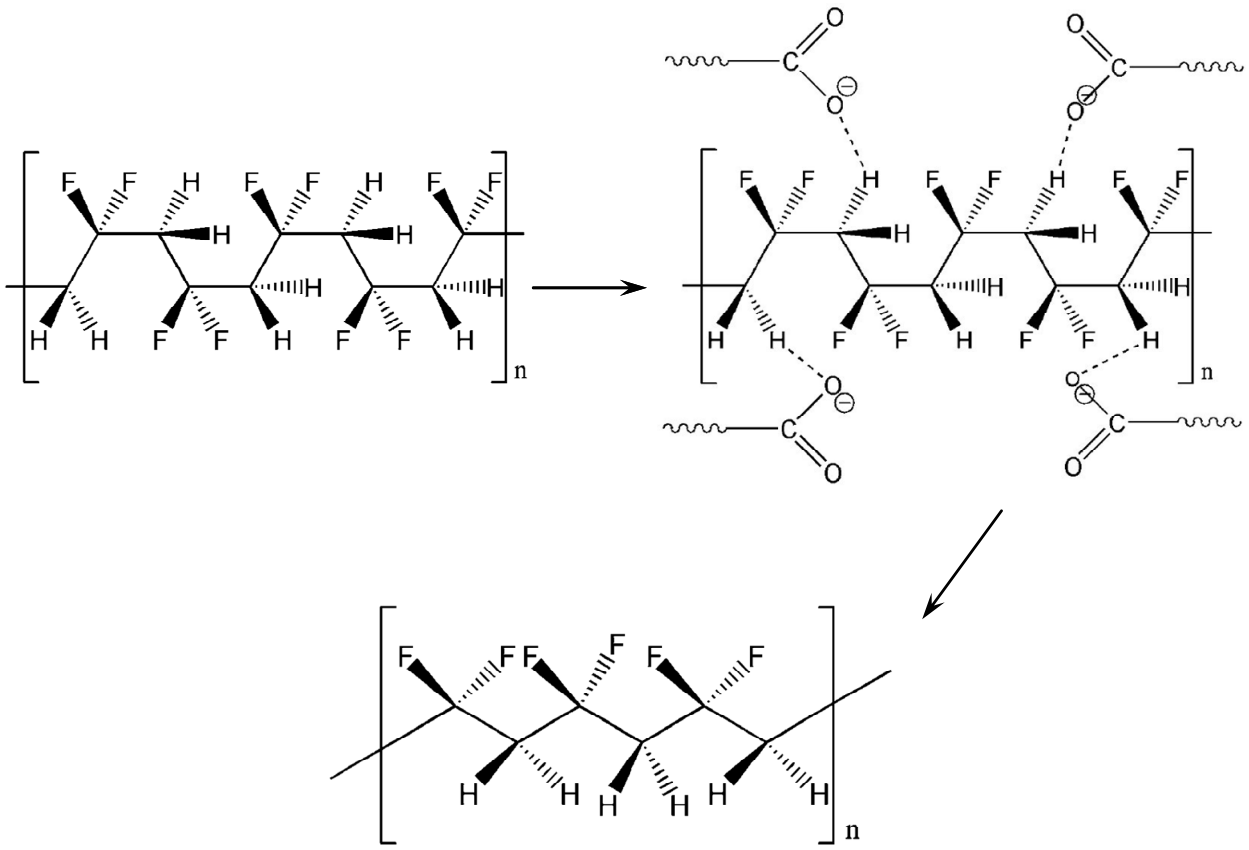

Figure 5.3. Mechanism of the transformation from α-phase to β-phase of PVDF in the presence of an anionic surfactant [19].

Table 5.1. Operating parameters for electrospinning of PVDF solutions

Parameter	Value
Solvents	DMF, DMAc, DMSO, mixture with acetone
Concentration	5 ~ 25% wt
Additives	TBAC, fluorosurfactants
Applied voltage	6 ~ 25 kV
Tip-to-collector distance	5 ~ 25 cm
Flow rate	1 ~ 11 μl/min

5.3.2. Study of Solution Properties in NFES Process

In conventional electrospinning, a number of parameters can influence the resulting fiber morphology. These parameters can be categorized in three groups: (1) solution properties including viscosity, elasticity, conductivity, and surface tension; (2) governing parameters including electric potential at the electrodes, flow rate of the polymer solution, and distance between the electrode and the collector; and (3) ambient parameters including solution temperature, surrounding temperature and humidity, and air velocity [25]. In NFES, fiber deposition occurs almost immediately right after the jet is ejected from the tip, such that environmental factors such as temperature or air drag only play a minor role. Solution characteristics become the most important factors and they are discussed in this section.

Figure 5.4 illustrates a schematic diagram of a polymer jet in a NFES process. A positive voltage is applied on the polymer solution while the collector is grounded. The applied voltage induces an electric field E. The collector is moving with a velocity v. The electric field exerts an electric force on the charged polymer solution, so that a polymer jet is ejected from the tip and moves toward the collector. The fluid parameters of the polymer jet are: conductivity κ, dielectric constant ε, density ρ, dynamic viscosity μ, and surface tension γ. It is assumed that the collector's speed is well matched, such that the polymer jet is deposited as a solid straight fiber on the surface of the collector.

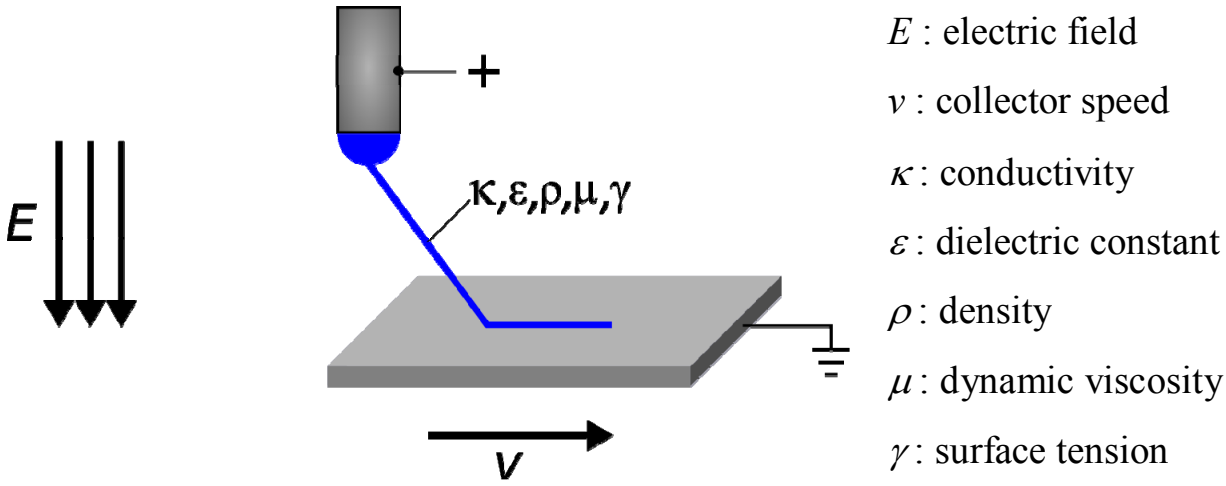

Figure 5.4. Schematic description of a polymer jet in a NFES process.

Polymer solution must have proper viscosity and surface tension for a successful electrospinning process and conductivity helps improving the fiber qualities. For the case of PVDF solution in DMF/acetone mixture, Figure 5.5 summarizes the factors that affect its viscosity and surface tension, including PVDF concentration, amount of acetone in the solvent, and addition of surfactant. Higher polymer concentration can result in higher viscosity and higher surface tension because stronger intermolecular interactions in the solution. The addition of surfactant reduces mainly the surface tension and it also reduces the viscosity. Using solvent mixture of DMF and acetone helps decreasing mainly the viscosity of the solutions thanks to the low viscosity and low density of acetone. However, a negative property of acetone is its high volatility, causing incessant changing in viscosity and surface during electrospinning. High amount of acetone additive could cause fast dry out of polymer solution and terminate the process. Furthermore, many studies reported process improvements by adding salt to the solutions because of increasing conductivity [18, 19, 21, 26]. Therefore, polymer solution with ionic surfactant for higher conductively is preferred. A stable electrospinning process is usually empirically optimized for each individual polymer and solvent system for the following solution parameters:

1. Determination of PVDF concentration
2. Determination of solvent recipe: mixing ratio of DMF and acetone
3. Choice of surfactant and its concentration
4. Other additives, if needed
5. Preparing method

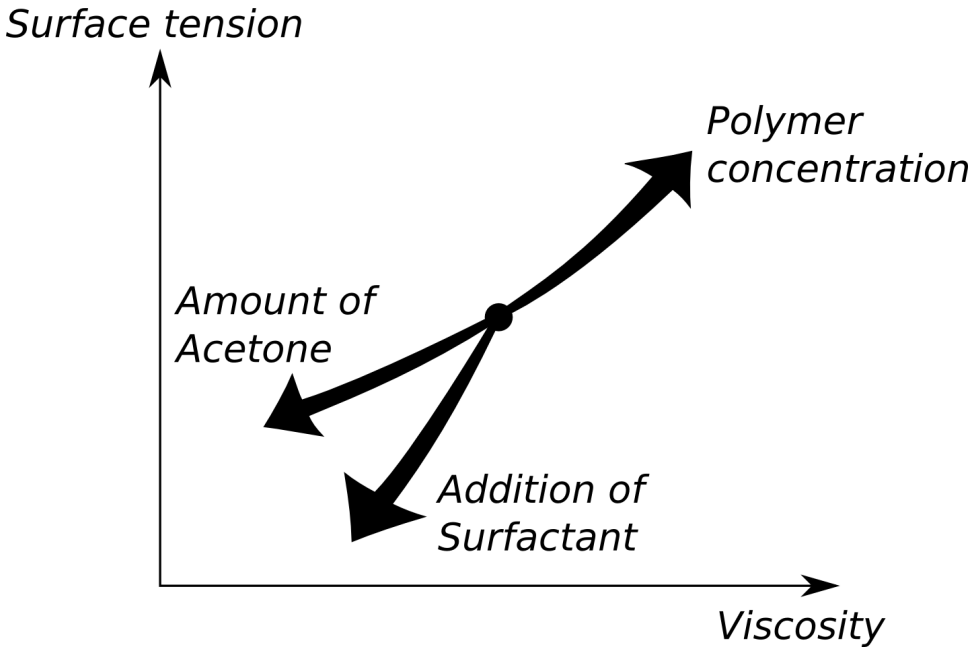

Figure 5.5. Influences of the polymer solution parameters on its viscosity and surface tension.

5.4. Electrospinning of PVDF Nanofibers

5.4.1. Solution Preparation

Different PVDF solutions were prepared in a three-step method by dissolving PVDF powder in a solvent mixture of DMF and acetone with an addition of different fluorochemical surfactants. NFES experiments showed that a highly homogenous solution was required before the solution could be successfully electrospun into fibers. This could be achieved in a time-saving manner by the three-step method. The solutions prepared by this method exhibited good homogeneity that promoted continuous formation of the electrospun fibers.

Furthermore, carbon nanotubes (CNT) have been popular nanoparticles to be embedded in nanofibers to increase the conductivity as well as to store the charges. Because CNT could form agglomerates such that a much longer mixing time and a final sonication were required to achieve a well dispersion of CNT in the PVDF solution. It has been observed that, after sufficient mixing, CNT particles were mixed in the solutions without any further stabilization. The following descriptions are the details of these preparation steps.

PVDF solutions in DMF/acetone without CNT:

1. PVDF in powder form is dispersed with calculated amount of acetone for 30 minutes using a magnetic stirrer. Because acetone is highly volatile, a small amount of acetone evaporates during the process. Therefore, the suspension is re-weighed afterward and acetone is added to maintain its designated weight percentage.
2. A suitable amount of DMF is added to the PVDF-acetone suspension. At the same time Zonyl®UR is also added to the mixture. The mixture is stirred for at least one hour to reach a good homogeneity.
3. Because of the surfactant, an intensive foaming occurs during the stirring process. The solution is allowed to stand still for another one hour to allow the foam to escape.

PVDF solution with CNT: the procedure is similar to the above process with additional steps.

1a. CNT is dispersed in DMF with proper percentage and PVDF is dispersed in acetone at the same time. The CNT-DMF suspension is sonicated for at least one hour to break possible agglomerates.

2a. PVDF solution and CNT-DMF is mixed and surfactant is added.

3a. The solution needs to stand still for one hours before the electrospinning process.

These polymer solutions are prepared and stored at room temperature in a well ventilated laboratory environment. To minimize the evaporation effects, containers are sealed with Parafilm. Table 5.2 lists the detail efforts and records in different polymer solutions in this work. Typically, a solution amount of about 10 – 15 g (10g solvent) is prepared to ensure a proper weighing. It is noted that the concentration of all substances is calculated in weight ratio (% wt) (amount of respective substance per amount of solvent).

Table 5.2. Experimental data of PVDF solutions. Highlighted are varied parameters.

Solution No.	Determined weight ratio (PVDF/solvent)	PVDF amount [g]	Solvent (DMF : acetone)			Fluorosurfactant		Carbonanotube (if desired)		Total amount [g]
			Ratio	DMF [g]	Acetone [g]	Weight ratio	Amount [g]	Weight ratio	Amount [g]	
01	15 % wt	1.5	8 : 2	8	2	3 % wt	0.3	(0.01 % wt)	(0.01)	11.8
02	15 % wt	1.5	6 : 4	6	4	3 % wt	0.3	(0.01 % wt)	(0.01)	11.8
03	17 % wt	1.7	6 : 4	6	4	3 % wt	0.3	(0.01 % wt)	(0.01)	12.0
04	18 % wt	1.8	6 : 4	6	4	3 % wt	0.3	(0.01 % wt)	(0.01)	12.1
05	19 % wt	1.9	6 : 4	6	4	3 % wt	0.3	(0.01% wt)	(0.01)	12.2
06	20 % wt	2.0	6 : 4	6	4	3 % wt	0.3	(0.01 % wt)	(0.01)	12.3
07	20 % wt	2.0	5 : 5	5	5	3 % wt	0.3	(0.01 % wt)	(0.01)	12.3
08	20 % wt	2.0	5 : 5	5	5	5 % wt	0.5	(0.01 % wt)	(0.01)	12.5
09	20 % wt	2.0	5 : 5	5	5	7 % wt	0.7	(0.01 % wt)	(0.01)	12.7
10	20 % wt	2.0	5 : 5	5	5	8 % wt	0.8	(0.01 % wt)	(0.01)	12.8
11	20 % wt	2.0	5 : 5	5	5	9 % wt	0.9	(0.01 % wt)	(0.01)	12.9
12	20 % wt	2.0	5 : 5	5	5	10 % wt	1.0	(0.01 % wt)	(0.01)	13.0
13	21 % wt	2.1	5 : 5	5	5	10 % wt	1.0	(0.01 % wt)	(0.01)	13.1
14	22 % wt	2.2	5 : 5	5	5	10 % wt	1.0	(0.01 % wt)	(0.01)	13.2

5.4.2. Effect of Surfactants

It is observed that solutions of PVDF in DMF exhibited a high surface tension, making continuous NFES impossible. To reduce the surface tension, three kinds of fluorochemical surfactants were examined: Zonyl®FSN-100, a nonionic fluorosurfactant; Zonyl®FSP and ®FSJ, both are anionic fluorosurfactant in aqueous solutions; and Zonyl®UR, an anionic phosphate fluorosurfactant that contents no solvent. According to [20], addition of Zonyl®FSN-100 could help eliminating the beading phenomenon for the electrospun nanofibers. However, in NFES, solutions with Zonyl®FSN-100 didn't work. This could be explained by its non-ionic character that didn't increase the conductivity of the solutions. As a result, jet formation is difficult.

Zonyl®FSP and Zonyl®FSJ are anionic fluorosurfactants. However, these surfactants consists of water in their as-delivered form which can cause the gel-formation of PVDF which is unsuitable for NFES. Zonyl®UR is an anionic phosphate fluorosurfactant without solvent or water. The surface tension was significantly reduced with Zonyl®UR such that PVDF solutions were successful in the NFES process. Moreover, because the surfactant is anionic, the dissolved ions worked as an additional salt in the solutions which helped the conductivity of the solution and the electrospinning process.

5.4.3. Characterization of the Solutions

As reported in Table 5.2, solutions with various parameters were prepared to find the optimal recipe. The most important factor is the polymer concentration. Solutions with 15% wt PVDF have been found to have low viscosity and could not produce continuous nanofibers. At very high concentration at 22% wt, PVDF was close to its equilibrium solubility and a homogenous solution was difficult to achieve. At concentration of 20% wt, good homogeneity and viscosity were achieved for NFES.

Furthermore, different concentrations of Zonyl®UR were examined. It was found that the better process in terms of continuity have been recorded with higher concentrations of surfactants due to reduced surface tension. However, from 8-10% wt, no significant changes were observed. Therefore, the suitable concentration of Zonyl®UR was set at 10% wt. It has been reported that good amount of fluorochemical surfactant could facilitate β-phase formation of PVDF nanofibers [19].

Three mixing ratios of DMF to acetone have been examined, including 8:2 based on the experiences of previous NFES experiments, 6:4 and 5:5. Because of higher concentration of PVDF than that in previous experiments (20% wt compared to 15% wt), an increasing amount of acetone was required to promote the evaporation of the solution. The ratio of 5:5 was found to have the best electrospinning results.

5.4.4. Continuous NFES of PVDF

With the new solution recipe containing Zonyl®UR, PVDF solutions were successfully conducted in NFES on a silicon wafer in a continuous manner. The continuous NFES

deposition was activated by using a tungsten probe to poke inside the polymer meniscus and break the surface tension. The mechanically drawn nanofiber was rapidly pulled away from the polymer droplet, as described in chapter 4. The experimental setup is shown in Figure 5.6.

Figure 5.7 shows experimental results under various parameters. For the lowest PVDF concentration of 15% wt, discontinuous short fibers were deposited (Figure 5.7A). Polymer solutions with higher PVDF concentration resulted in longer fibers (Figure 5.7B and C for 20% and 22%, respectively). The addition of Zonyl®UR showed a visible effect on the fiber morphology. Figure 5.7D shows the best fiber result with the optimized recipe: 22% wt PVDF and 10% wt Zonyl®UR in 5:5 DMF: acetone. Straight and well-aligned fibers were deposited. The fibers were collected at a collector which was running at a speed of about 10 cm/s.

A close-up look on the deposited nanofibers revealed non-uniformity in diameter (Figure 5.8) and beads or necks have been observed occasionally. One major reason could be the manual control of the collector movements. In general, uniformity of nanofibers depends strongly on the complex combination of material properties and processing parameters, which need to be further optimized.

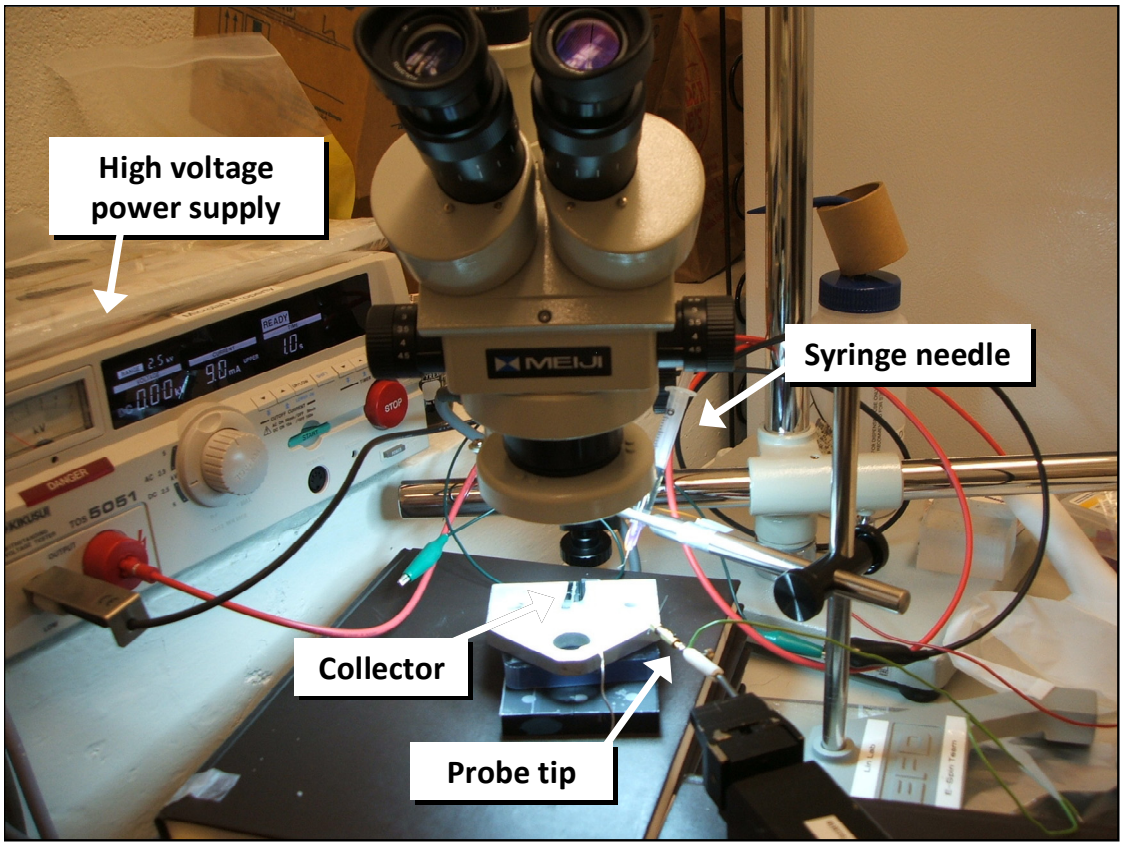

Figure 5.6. Experimental setup of continuous NFES for PVDF nanofibers.

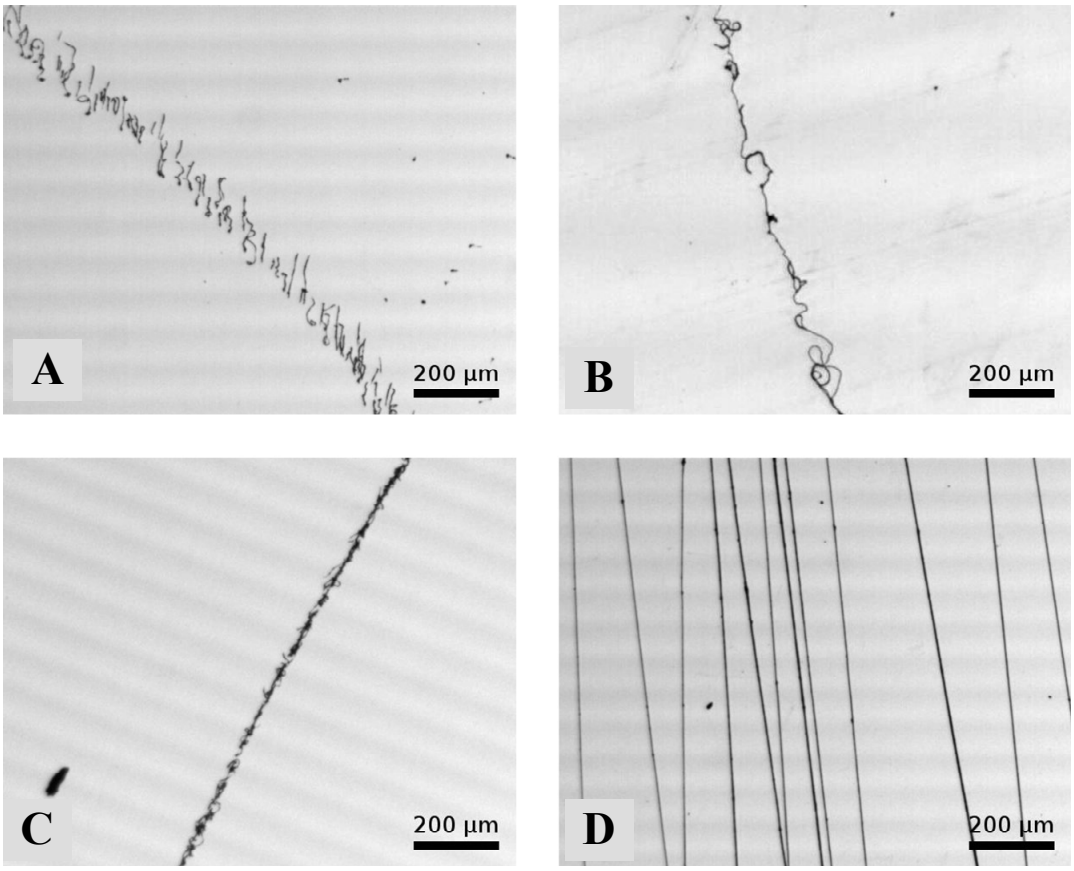

Figure 5.7. Optical images of electrospun PVDF fibers from solutions with different parameters. (A) 15% wt PVDF, (B) 20% wt PVDF, (C) 22% wt PVDF with 3% wt Zonyl®UR, and (D) with 10% wt Zonyl®UR.

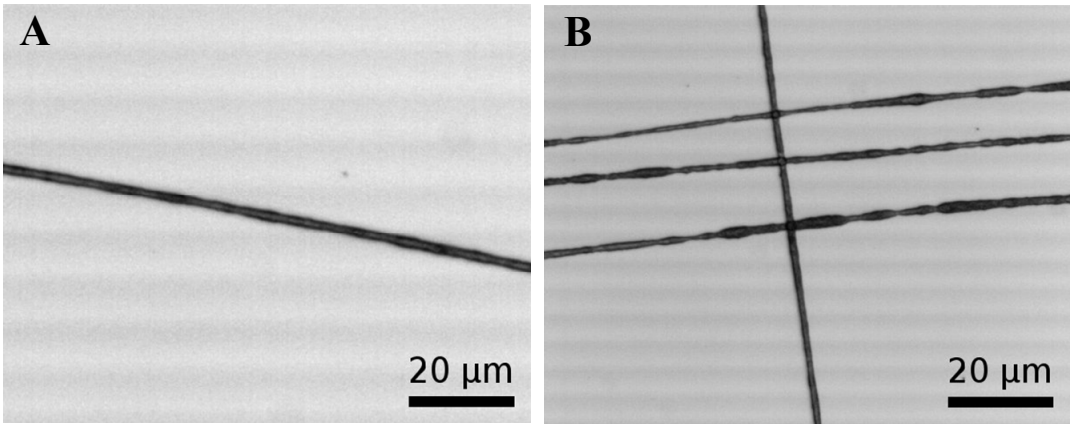

Figure 5.8. Close-up images for (A) a single PVDF fiber, and (B) a pattern of crossing fibers showing non-uniformity in fiber diameter.

5.5. Detailed Discussions on Process Parameters

5.5.1. Solution Viscosity and Surface Tension

Similar to any conventional electrospinning process, solution viscosity and surface tension have a great effect on the fiber morphology. These characters are determined through polymer concentration, choice of solvent and surfactant, and polymer concentration is the most important factor. In NFES, polymer concentration should be increased such that the solvent can evaporate in the short distance before reaching the collector. Sufficiently high viscosity also helps the polymer jet to remain stable during the NFES process.

As described in section 5.4.3, both viscosity and surface tension of a polymer solution will increase when the polymer concentration increases. It was observed in NFES, similar to conventional electrospinning, that higher viscosity promoted better fiber formation. With a concentration of 15% wt PVDF, the viscosity was not high enough such that fibers were often broken, resulting in short, discontinuous fibers (Figure 5.9A). For concentration in the range of 20-22% wt, continuous fibers could be deposited (Figure 5.9B). The looped fiber could be improved by increasing the collector speed to be discussed in the next section. Higher concentration resulted in poor mixing of polymer.

The addition of Zonyl®UR at 3% wt showed a positive effect on fiber formation under continuous NFES as shown in Figure 5.10A. With 10% wt of Zonyl®UR, continuous and straight fibers could be successfully deposited in orderly pattern as seen in Figure 5.10B.

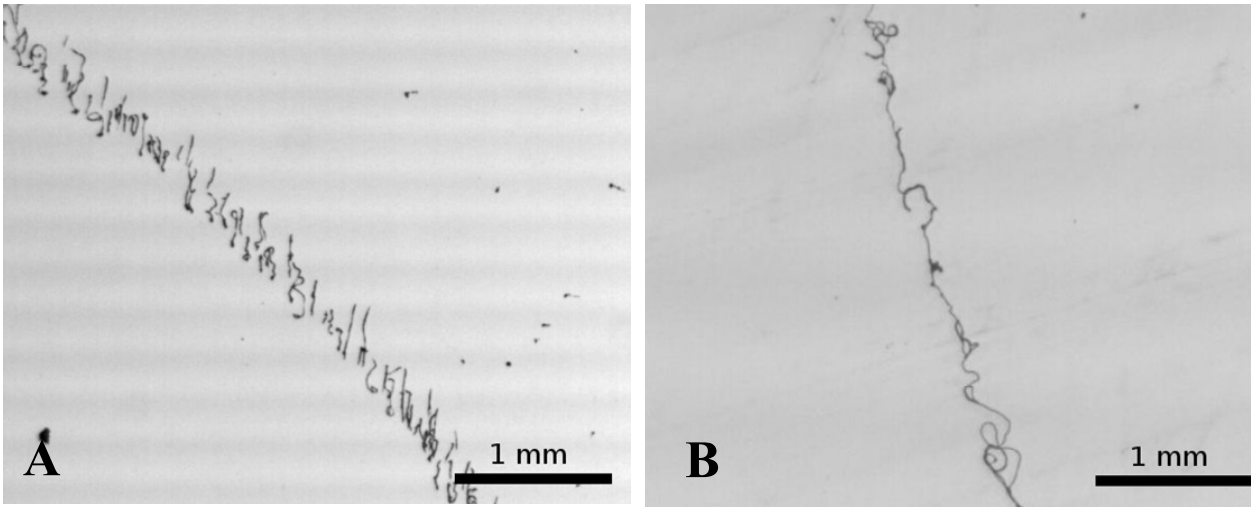

Figure 5.9. Effect of polymer concentration on fiber formation: Optical images of PVDF fiber by NFES from (A) a 15% wt solution and (B) 20% wt solution.

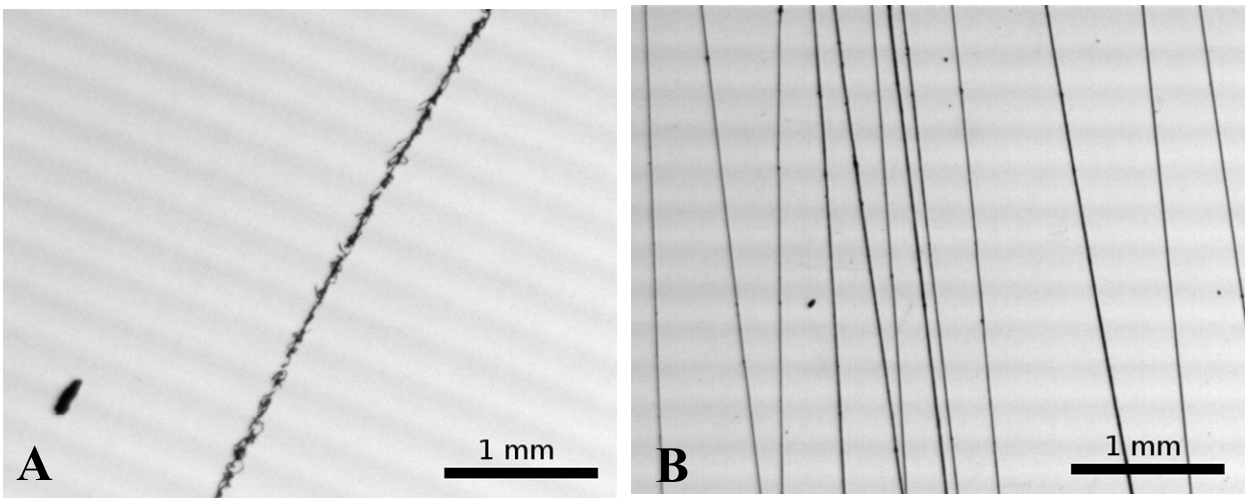

Figure 5.10. Effect of fluorosurfactant on fiber formation: Optical images of PVDF fiber by NFES from a 20% wt PVDF solution with (A) 3% wt and (B) 10% wt Zonyl®UR.

5.5.2. Moving Speed of the Collector

Differing from a conventional electrospinning where a collector could be a stationary plate, a continuously moving collector is essential in NFES. The short distance between the dispenser tip and the collector results in short evaporation period in the air and agglutination of wet fibers on the collector. If the collector doesn't move, the deposited wet fibers would agglutinate to a bundle and this could quickly connect the tip to the electrode and the process would have to be aborted due to short-circuit. By continuously moving the collector, solvents can evaporate and the wet fibers become solid to avoid agglutination. The moving speed must be high enough to prevent clustering and beading of fibers to produce straight-line shapes, as demonstratively shown in Figure 5.11.

The movement of the collector also induces a stretching force on the deposited fibers. The collector speed therefore has an effect on the fiber diameter. Assuming that the fibers adhere well on the collector surface, increasing the collector speed yields smaller fiber diameter. However it was often observed that the fibers could be detached from collector because of weak adhesion.

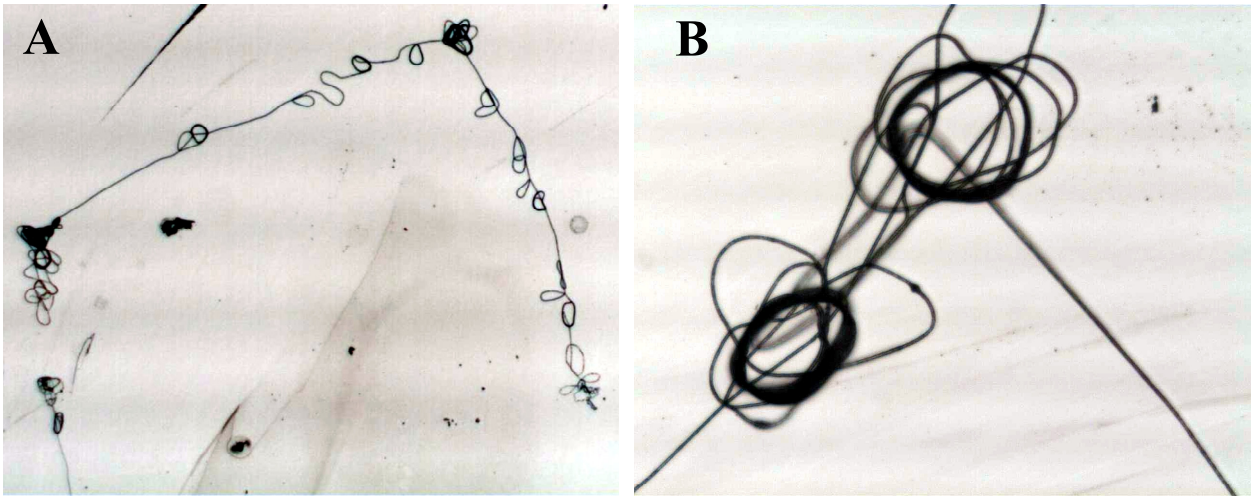

Figure 5.11. Optical images of NFES PVDF fiber from a 20% wt solution under 1 kV applied voltage to illustrate the effect of collector's moving speed on fiber straightness. (A) At low speed, about 5 m/s, spiraling occurs. (B) Enlarged view.

5.5.3. Applied Voltage

Electrical force generated through the applied voltage is the stretching forces on the liquid jet. Therefore, the applied voltage affects the deposited fiber properties. Many studies on conventional electrospinning have demonstrated that the effect of applied voltage is ambiguous. This contradictory phenomenon is reviewed and discussed in [25, 27, 28]. Particularly in the case of electrospinning of PVDF, different phenomena have been observed. While Nasir *et al.* [18] reported an increase in fiber diameter with increasing voltage, Andrew *et al.* [15] and Gao *et al.* [17] observed that higher voltage yielded thinner fibers. It is obvious that the effect of the applied voltage on the resulting fibers varies individually for each polymer-solvent system as well as other electrospinning parameters.

In this study, the suitable voltage for NFES PVDF in DMF/acetone could only be varied in a small range from 1 kV to about 1.5 kV, no clear trend for fiber diameter could be observed. However, it was found that at a higher voltage, the NFES was more continuous with more bead formation along the fibers. It was also observed that higher voltage was required at the beginning to drive the solution out of the tip. Once a stable fiber deposition started, the voltage could be slowly reduced to 1 kV to obtain thinner fibers.

5.5.4. Electrode-to-Collector Distance

The short electrode-to-collector distance is the symbol of NFES. The magnitude of this distance relies on the stable region of the polymer jet in an electrical field. One could expect that a small change in the distance could lead to dramatic change in the NFES process. It was observed that above a distance of 1 mm, the process lost its characteristics of NFES and switched to conventional electrospinning and the polymer jet began to whip. Small distance (less than

500 μm) could lead to short circuit. Experiments showed that at a distance of 500 μm, NFES was successfully executed and aligned straight fibers were obtained.

5.5.5. Diameter of the Dispenser Tip

The diameter of the tip needs to be selected appropriately with the surface tension and the viscosity of the polymer solution. The ideal condition is that during the idle state, a droplet of the polymer solution could form at the end of the tip by its own weight without dropping down. The inner diameter of the dispenser affects the diameter of fibers as it directly controls the diameter of the Taylor cone. Smaller tip diameter would lead to thinner fibers. However, if the diameter of the tip is too small, continuous NFES may fail. In NFES experiments with PVDF solutions, it was observed that the tip size of 30-gauge (equivalent to about 150 μm inner diameter) could yield better processing and longer fibers than the tip of size 32-gauge (inner diameter about 100 μm). Tip sizes larger than 30-gauge would cause polymer solution to drop out easily and result in short circuit to stop the NFES process.

5.6. Experimental Realization of PVDF Nanogenerator

5.6.1. Materials

5.6.1.1. Polymer Solution

The polymer solutions were made from polyvinylidene fluoride (PVDF) powders (*Mw* = 534 000) *(Sigma-Aldrich)*, N,N-Dimethylformamide (DMF) *(Sigma-Aldrich)*, acetone *(Sigma-Aldric)*, Zonyl®UR *(DuPont)*, and single-walled carbon nanotubes (SWCNTs) *(Unidym)*. All reagents were not further purified or modified prior to generation of the solutions. The SWCNTs (mix of both metallic and semiconducting CNTs) had diameters of 0.8 – 1.2 nm and lengths of 100 – 1000 nm. Zonyl®UR is an anionic phosphate fluorosurfactant that was provided without solvents.

5.6.1.2. Poled PVDF Thin Film

Poled PVDF thin films *(Precision Acoustics)* [29] were used for benchmark experimental testing. The films had dimensions of 5 × 5cm^2 with thicknesses of 28, 52, and 110 μm with sputtered metal electrodes on the top and bottom surfaces. These films were cut into smaller pieces (4 – 8 mm wide and 9 – 15 mm long) and subsequently attached onto plastic substrates for experiments with glue.

5.6.1.3. Plastic Substrate

The plastic testing substrates were made of TOPAS® 8007 Cyclic Olefin Copolymer via injection molding with a thickness of *c.* 0.75 mm, width of 25 – 30 mm, and length of 60 – 70 mm. 3M™ cleanroom high temperature ESD tape 1258 (0.07 mm thick) was applied on the top surface of the plastic substrate for enhanced electrostatic discharge performance. Finally, 3M™ aluminum conductive tape (0.05 mm thick) was cut and affixed to the tops of the ESD tape to serve as collectors for the NFES process and as electrodes for piezoelectricity measurements.

5.6.2. Fabrication of PVDF Nanogenerator

PVDF solutions were filled into plastic syringes with tips of 200 μm in diameter. All metallic electrodes on the deposition substrate were grounded and kept at a fixed vertical separation distance of 0.5 – 2 mm from the needle tip. Before the onset of electrospinning, a bias voltage of 0.7 – 1.5 kV was applied. A probe tip was used to mechanically draw a single fiber from the droplet to initiate continuous NFES. Experimentally, the syringe needle was stationary while the plastic substrate was moved using an *x*-*y* stage at a speed of 120 mm/s for the controlled deposition of PVDF nanofibers (Figure 5.12). Multiple nanofiber deposition can be achieved by repeating the direct-write process. With the knowledge of nanofiber polarities and the design of electrodes on the plastic substrate, these PVDF nanofibers can be connected in serial or parallel. An actual device is shown in Figure 5.13.

The diameter of deposited fibers ranged from 700 nm to 3 μm and yield was low because the plastic substrate was not conductive. Deposition of fibers were disturbed and terminated from time to time. The deposited fibers were not always uniform as seen in Figure 5.14 and this could be attributed to the manual operation of the collector without a constant speed control. Nevertheless, continuous NFES was convenient to fabricate a large number of nanogenerators and good ones were selected for detail characterizations.

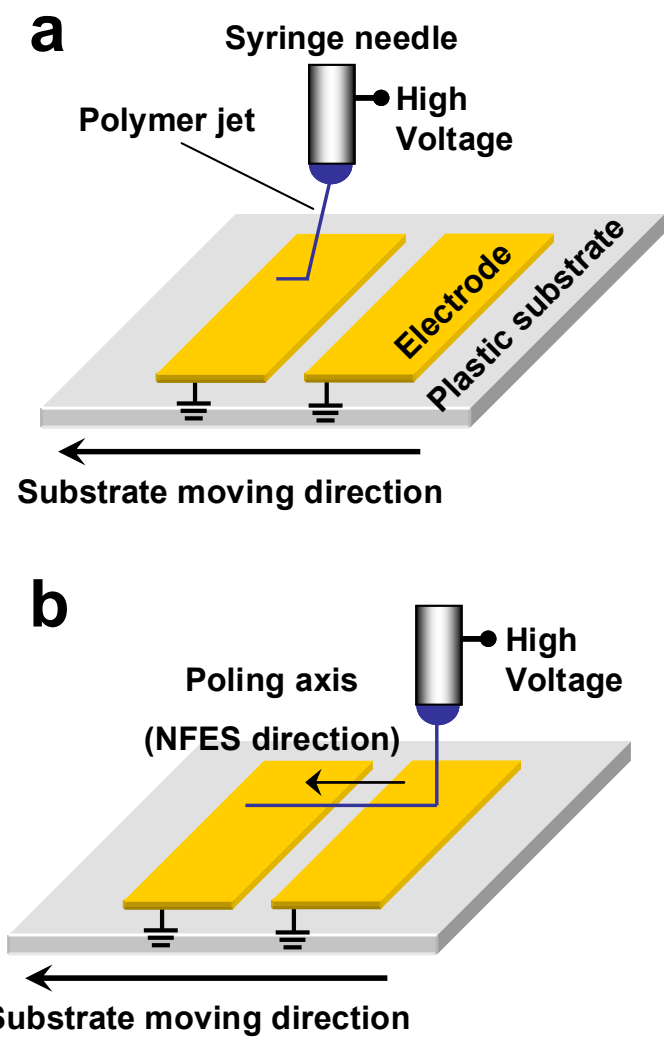

Figure 5.12. Fabrication of PVDF nanogenerator on a plastic substrate with pre-fabricated metallic electrodes using NFES.

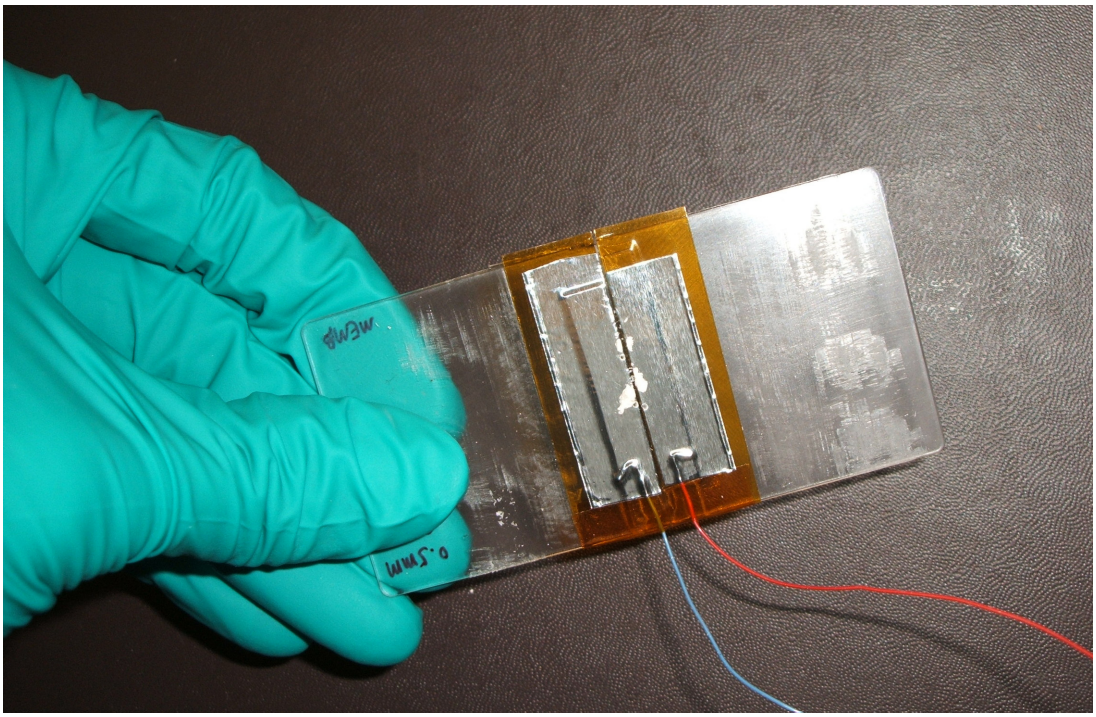

Figure 5.13. Photo of PVDF nanogenerator on a plastic substrate.

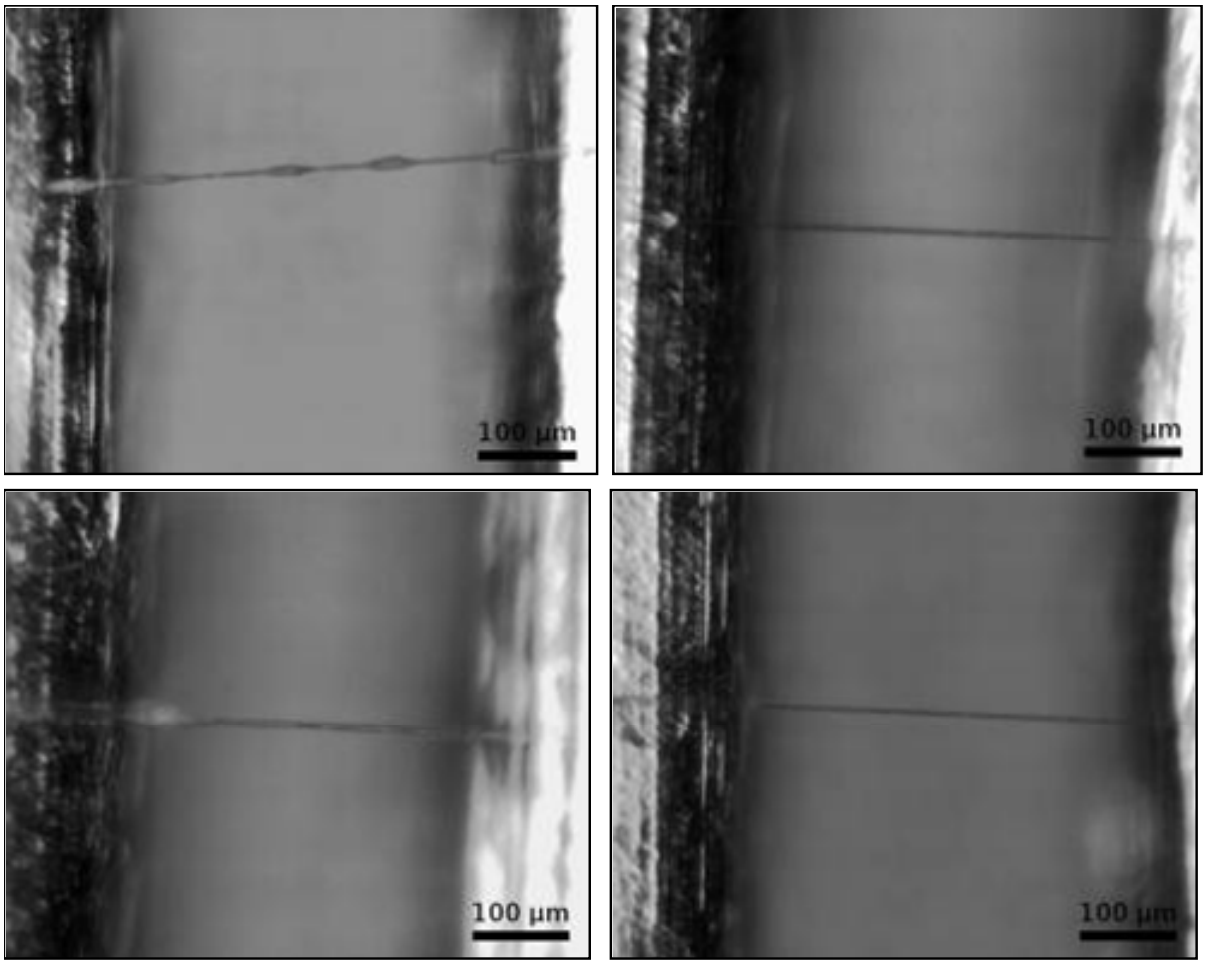

Figure 5.14. Optical images of single PVDF fibers across a gap of 500 µm as a nanogenerators. Some fibers are uniform while beads or necks are observed in some samples.

With continuous NFES, it was possible to produce aligned arrays of fibers as shown in Figure 5.15. For nanogenerator application, it was important to have the same poling direction for fibres, i.e. same electrospinning direction or electrical outputs of individual fibers would cancel out each other. Manual manipulation of collector results in misalignment of fiber depositions as shown in Figure 5.15: (a) formation of beads and different distance between two fibers; (b) formation of beads and non-uniform fiber diameter; and (c) two fibers are merged together.

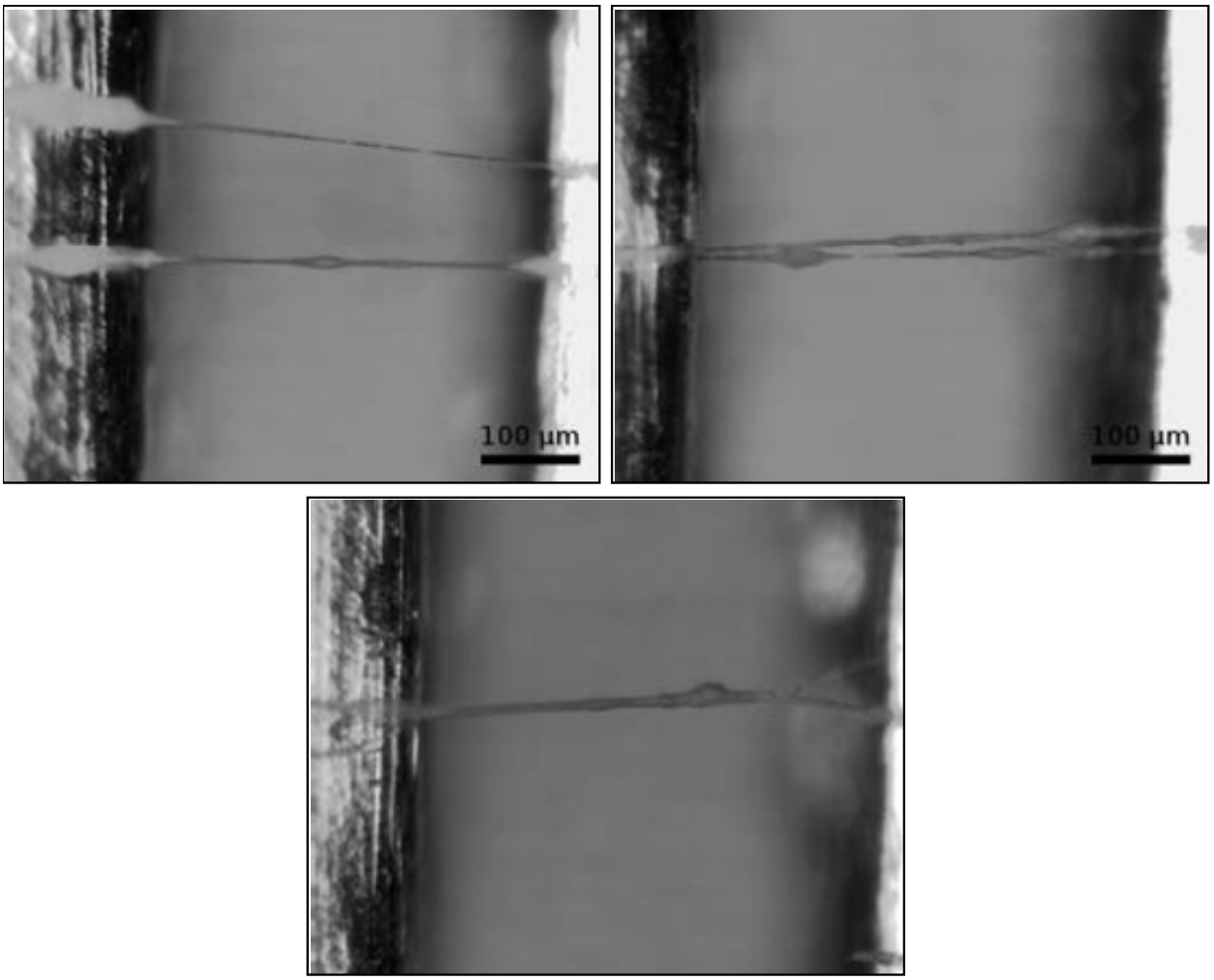

Figure 5.15. Optical images of PVDF fiber arrays across a gap of 500 µm: (a) formation of beads and different distance between two fibers; (b) formation of beads and non-uniform fiber diameter; and (c) two fibers are merged together.

5.6.3. Stretch of Nanofiber

Uniaxial stress is applied to the PVDF nanofibers by bending the plastic substrate, creating piezoelectric potentials that are uniformly distributed along the nanofiber with a polarity determined by the poling axis, i.e. NFES direction (Figure. 5.12B). The piezoelectric constant, g_{33}, of PVDF is negative which results in the generation of voltage with opposite polarity with respect to the poling axis direction of the PVDF nanofibers during the stretching process. Experimentally, the PVDF nanofibers were stretched to measure the output voltage and current between two electrodes (Figure. 5.16). Figure 5.17 shows the actual experimental setup. The loading force on the plastic substrate was exerted by an electrically-powered rotating machine as illustrated in Figure 5.18. The rotating frequency and direction can be controlled by built-in switches. In most experiments, the rotating direction of the machine is not changed during the whole testing. Therefore, the plastic substrate restores to its original state at a speed which is controlled by the substrate rigidity, rather than the machine rotating frequency. The rotating direction of the machine within one testing is changed only in the experiments where the release strain rate is the control factor.

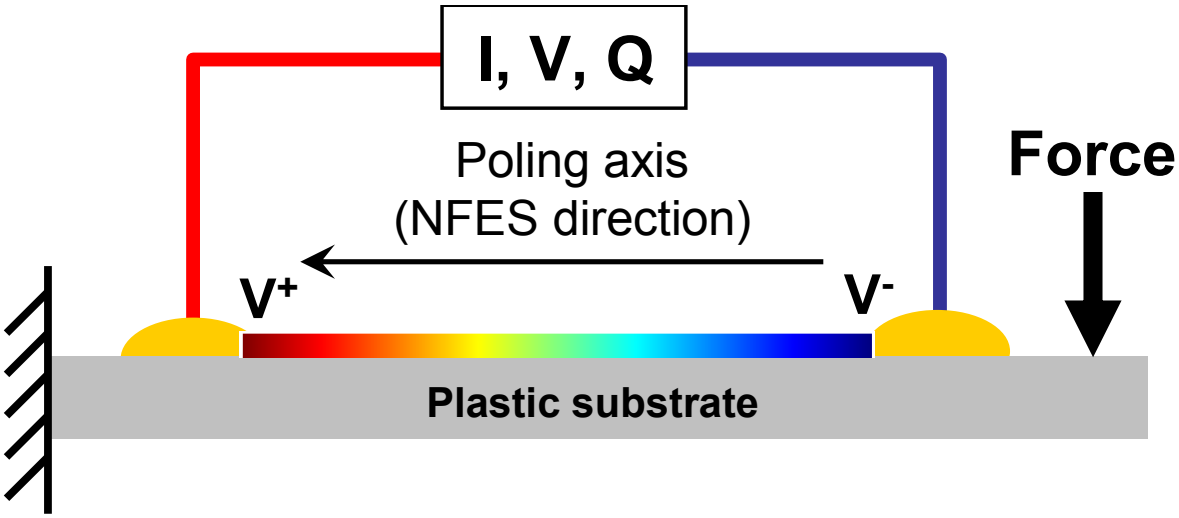

Figure 5.16. Experimental setup of the nanogenerator with controlled polarity from the NFES process. Electrical signals including voltage, current and charge are characterized when the nanogenerator is mechanically stretched by bending the substrate.

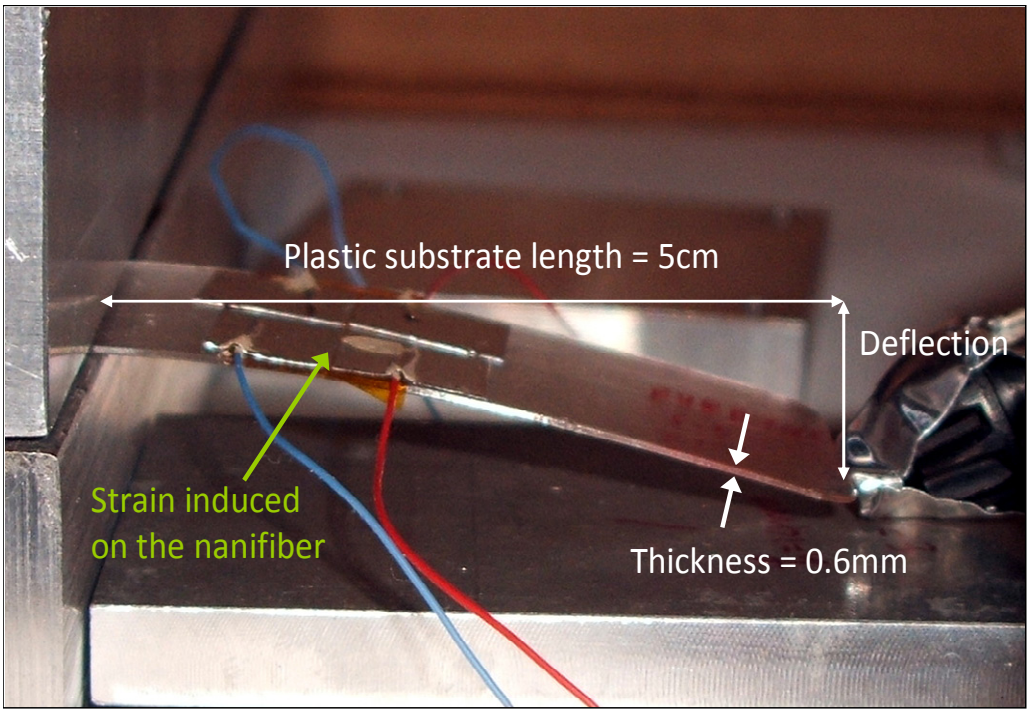

Figure 5.17. Photo of experimental strain loading setup.

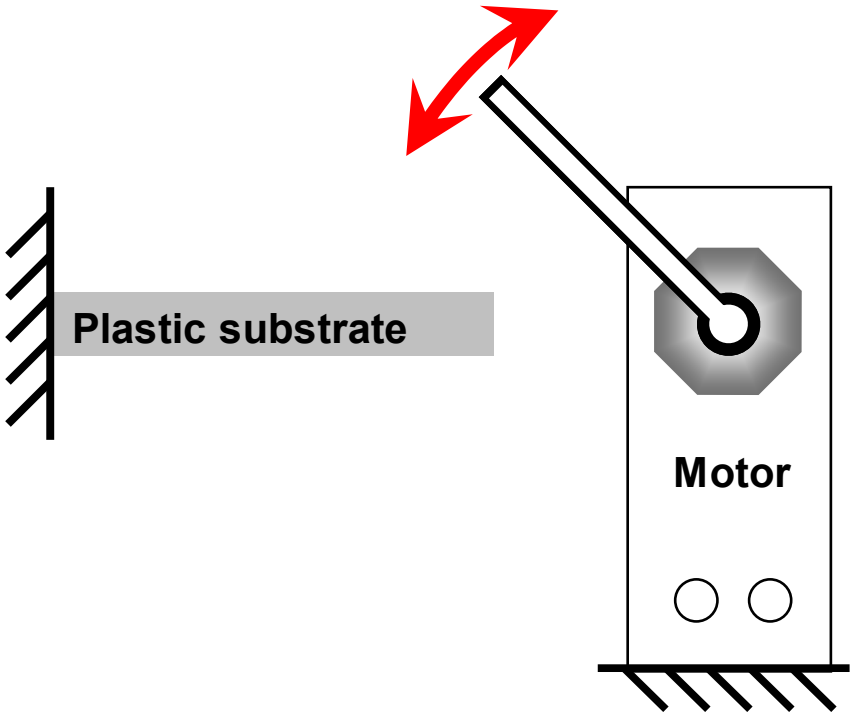

Figure 5.18. Illustration of strain loading mechanism.

5.6.4. Measurements

5.6.4.1. Scanning Electron Microscopy (SEM)

The morphology of the PVDF nanofibers was examined using a LEO 1550 SEM. A thin layer (50 – 100 Å) of gold-palladium was depositing on the sample surface using Hummer Sputtering System before SEM to enhance visualization. All electrical measurements were performed prior to the SEM to avoid unwanted effect such as electron charging and short circuiting of the nanofibers by the metal coatings.

5.6.4.2. Strain Measurement

A foil strain gauge (0.015 mm thick) *(Omega)* was glued onto the surface of the control plastic substrate to measure the axial strains. The strain ε occurring on the curved surface may be expressed with the following equation:

$$\varepsilon = \frac{t}{2r}$$

where t is the thickness of the substrate, and r is the bending radius of the substrate (Figure. 5.19). Since the bending radius of the substrate in our experiment (>400 mm) and the thickness of the plastic substrate (*c.* 0.75 mm) were both much larger than the thickness of the PVDF nanofiber (500 nm – 6.5 μm), the strain of PVDF nanofiber was approximately equal to the strain of the outer surface of plastic substrate. The PVDF thin films (28 – 110 μm thick) could have had thicknesses close to that of the plastic substrate (0.75 mm). Therefore, the real strain applied on the thin film would have been larger than the measured strain on the top surface of the plastic substrate.

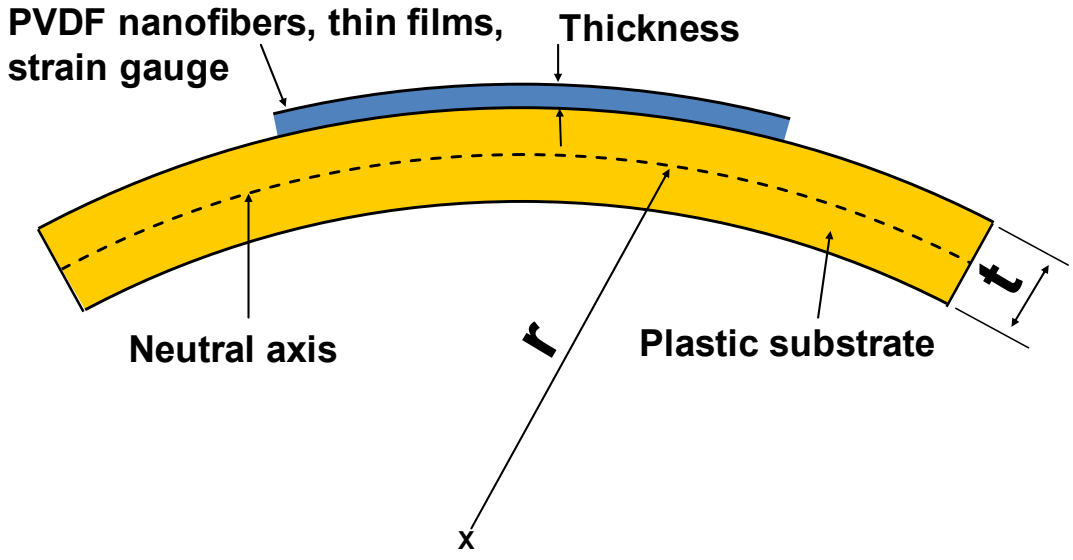

Figure 5.19. Strain on the curved surface.

5.6.4.3. Electrical Measurement

All electrical measurements were performed using a Gamry Reference 600 high precision electrometer (I_{bias} < 5 pA) inside a Faraday cage without connecting any external power sources to the PVDF nanogenerator. Before the electrical measurements, the two ends of the PVDF nanofiber were grounded to dissipate residual charges from the electrospinning process. The output voltages were measured with a load resistance of 10 MΩ while the output currents were measured by directly connecting the nanogenerator to the measurement system.

It was noted that the *RC* time constant of the nanogenerator must be much larger than that of the measurement system or a large percentage of piezoelectric charges could leak out before being measured [30]. In our experiments, the *RC* time constants of the nanogenerator, voltage measurement, and current measurement systems were *c.* 2.4 sec (R_{NG} = 150 GΩ, C_{NG} = 160 pF), 1.0×10^{-3} sec (R_L = 10 MΩ, C_L = 100 pF), 2.2×10^{-3} sec (R_L = 10 MΩ, C_L = 220 pF), respectively.

The piezoelectric charges were measured by a circuit (Figure 5.20) using the Texas Instruments OPA129 Precision Amplifier ($R_{in} = 10^{13}\Omega$, I_{bias}< 100fA). The extremely small input bias current of the op-amp ensured that the charges generated by the piezoelectric response were not shadowed in our measurement system. The charge generated by the nanogenerator was transferred onto the feedback capacitance C_F, which was known and fixed. Therefore, the calibration factor was fixed irrespective to the capacitance of the nanofiber generator. The *RC* time constant of the readout circuit R_FC_F is 10^{-4} sec, which was also smaller than that of nanogenerator.

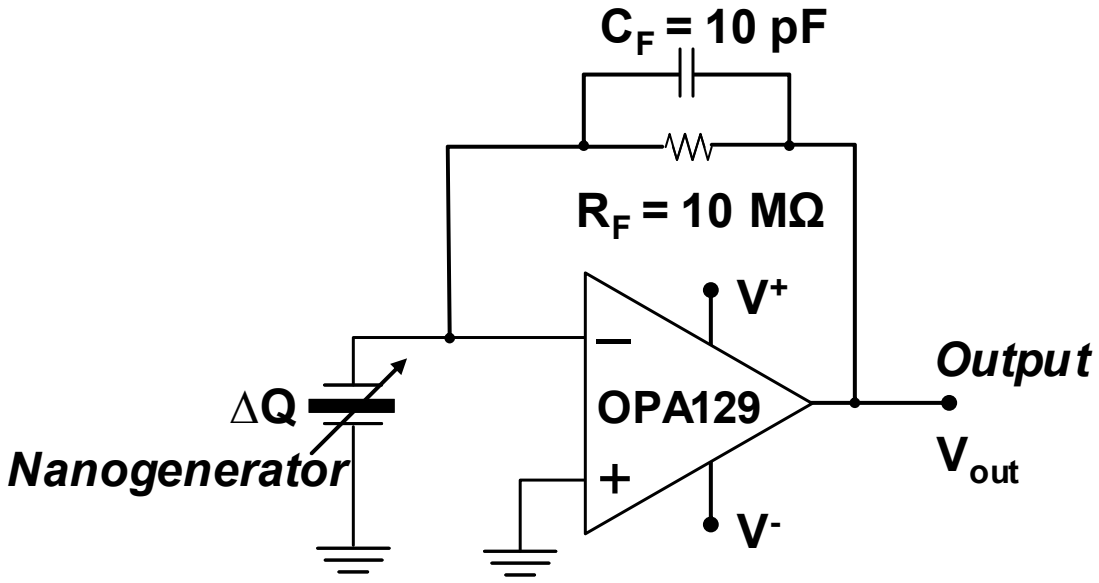

Figure 5.20. Circuit of charge amplifier.

The impedance measurement of nanogenerator was performed using the Electrochemical Impedance Spectroscopy (EIS) module of Gamry Reference 600. EIS measured the impedance by applying a sinusoidal voltage with different frequency between 10^{-2} and 10^{5} Hz to the sample and measuring the current. The equivalent circuit of our nanogenerator was fit to the measured data using the Marquardt-Levenberg algorithm as shown in Figure. 5.21. The resistance R_G and the capacitance C_G of the nanogenerator system were therefore extracted from data fit.

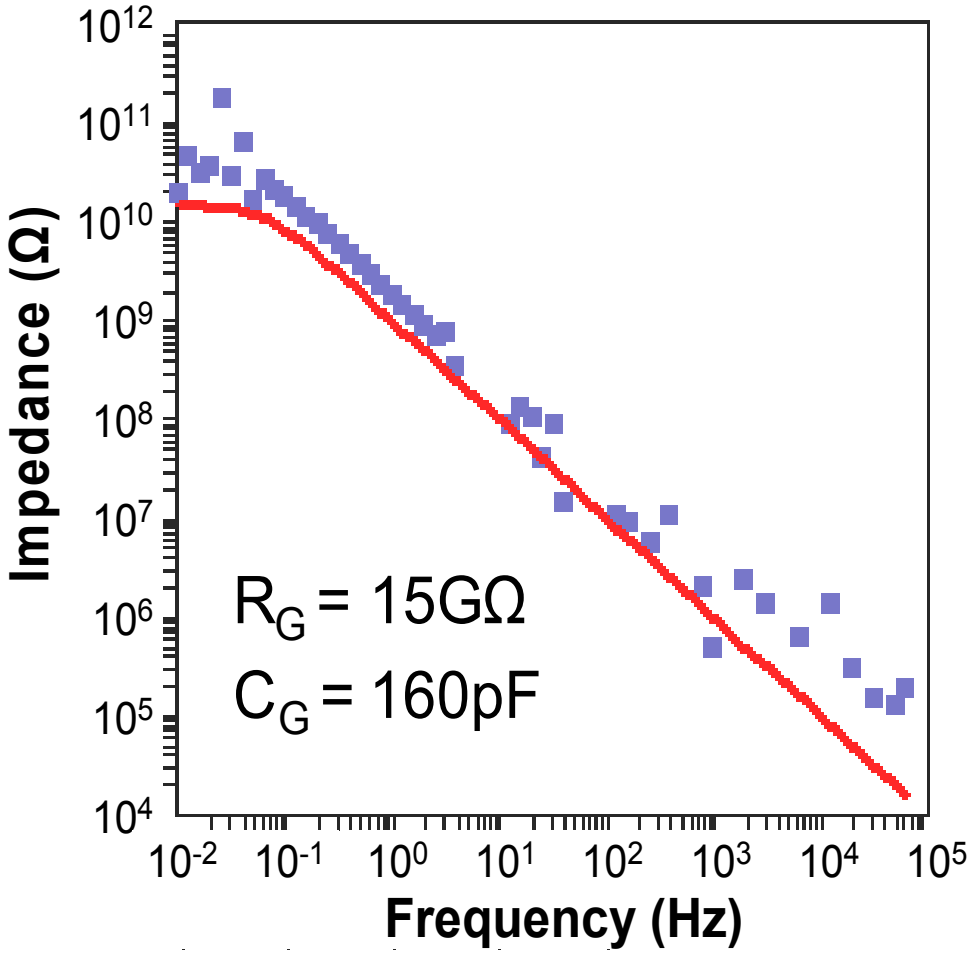

Figure 5.21. Impedance measurement (blue dots) and data-fitted analytical model (red solid line) of the PVDF nanogenerator.

5.6.5. Results and Discussions

5.6.5.1. Experimental Results

The as-spun PVDF nanofibers have diameters ranging from 500 nm to 6.5 μm with variable lengths defined by the separation distance (100 – 600 μm) between two metallic electrodes (Figure 5.22). When an axial stress is applied by bending the plastic deposition substrate, a piezoelectric potential is generated. The piezoelectric constant, g_{33}, of PVDF is negative such that stretching PVDF nanofibers along the poling axis generates a voltage with the polarity opposite to the electric field direction (the poling axis) during the electrospinning process. Therefore, a positive voltage output is expected by connecting the positive port of the multimeter to the distal end of the electrospun nanofiber. When the substrate is stretched and released repeatedly, voltage and current outputs can be recorded, respectively (Figure 5.23A, B). The typical electrical outputs of more than 50 tested nanogenerators were 5 – 30 mV and 0.5 – 3 nA.

As the strain is released from the nanogenerator, corresponding negative peaks can be observed in both the output voltage and current measurements. This phenomenon can be explained by examining the equivalent circuit model of the nanogenerator in Figure 5.24. The PVDF nanogenerator is modeled as a charge source in parallel with a capacitor C_G and a resistor R_G with estimated values of 160 pF and 15 GΩ, respectively (as measured in Figure 5.21). The equivalent circuit of a piezoelectric PVDF nanogenerator connected to readout circuit with an equivalent load resistor, R_L and capacitor, C_L. The positive output current is defined as the current flow from node a (distal end of the electrospun nanofiber) to the readout circuit. Mechanical strain can induce piezoelectric bound charges (polarization) which results in a potential difference at the two ends of the nanogenerator. Since the nanogenerator has a large internal resistance, there is little charge leakage/loss in the nanogenerator during the short period of the stretch-hold-release experiments (Figure 5.25).

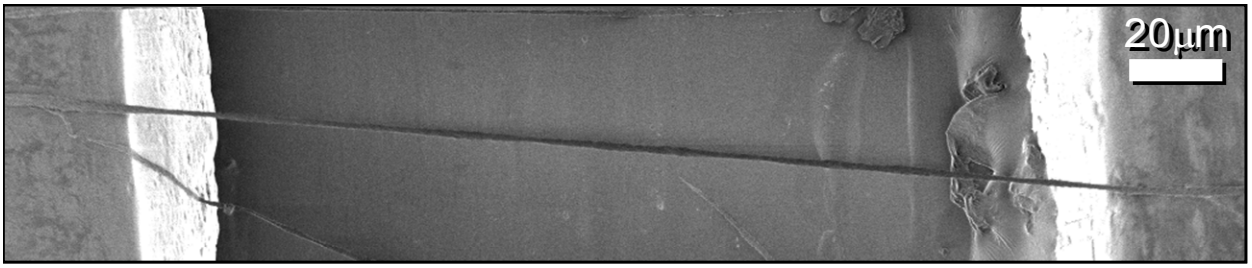

Figure 5.22. Scanning electron microscope (SEM) image of a nanogenerator comprised of a single PVDF nanofiber, two contact electrodes, and a plastic substrate.

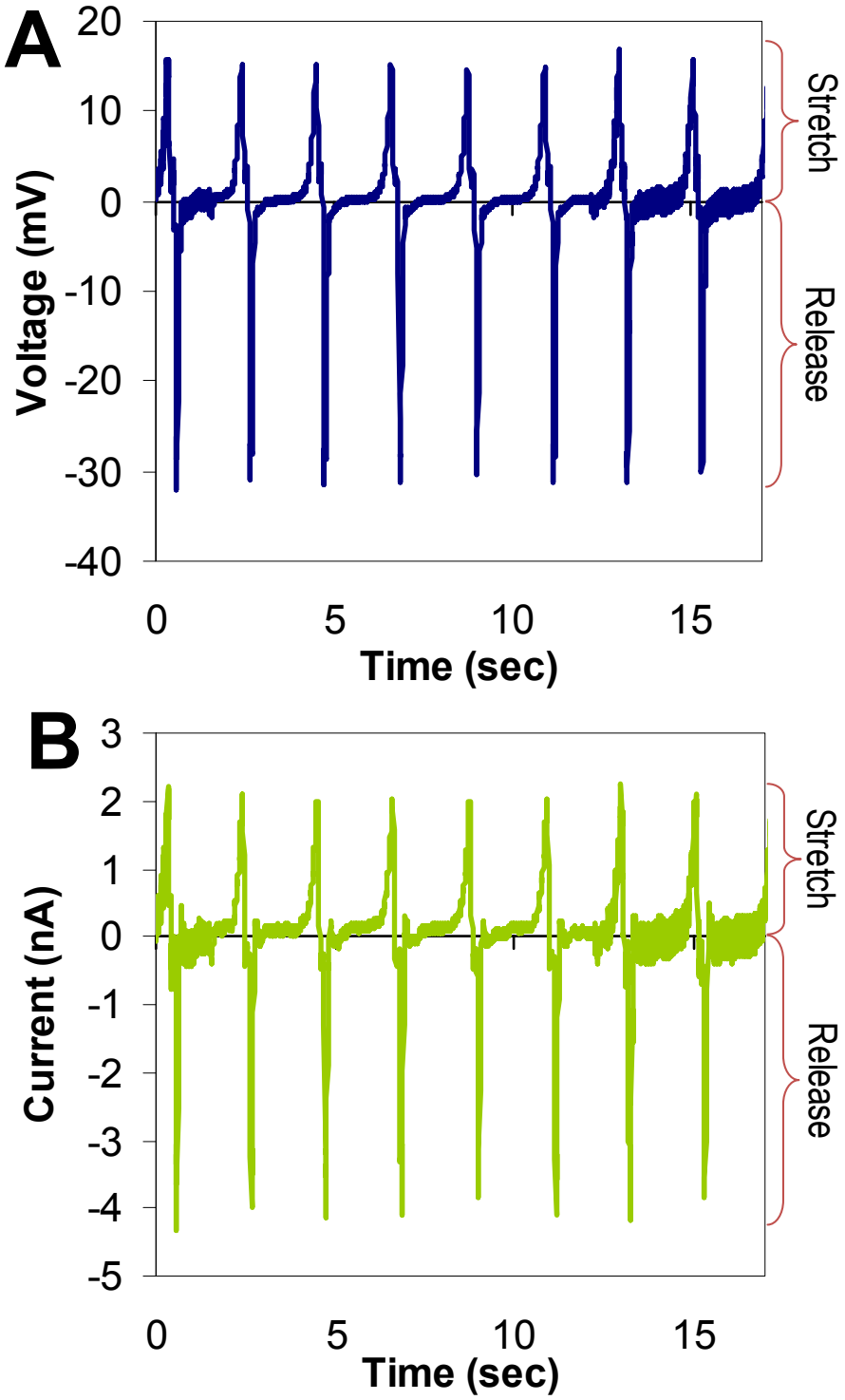

Figure 5.23. (A) Output voltage measured with respect to time under an applied strain at 2Hz. (B) Output current measured with respect to time under applied strain at 2Hz.

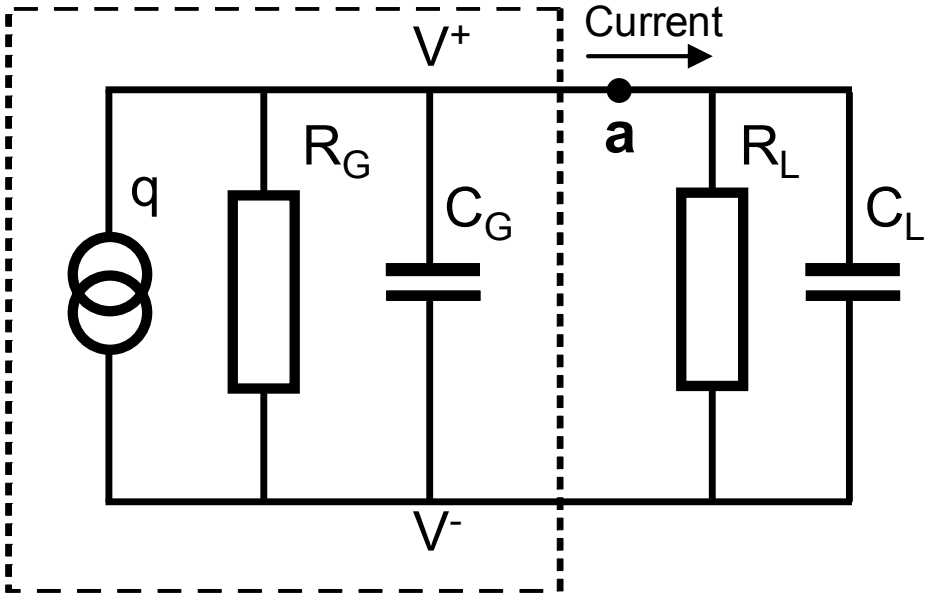

Figure 5.24. The equivalent circuit of a piezoelectric PVDF nanogenerator.

During the stretch process, the piezoelectric bound charges induced a built-in potential in the nanogenerator. In response, the external free charges (yellow line in Figure 5.25) are driven to the nanogenerator to neutralize this potential at a speed set by both the external circuitry and the built-in potential. During this process, the net charge (red line in Figure 5.25) increases with the piezoelectric bound charges at a rate that is faster than the flow of the external free charges. At a constant strain (the strain is on hold), both the net charges and the built-in potential gradually diminish to zero as the piezoelectric bound charges are balanced by the free charges. When the strain is released, the piezoelectric potential diminishes and the free charges that have accumulated at both ends of the nanofiber generate an opposing potential. The free charges gradually flow back in a direction opposite to the accumulation process and the current reduces to zero (green line in Figure 5.25) at a rate set by the external circuitry.

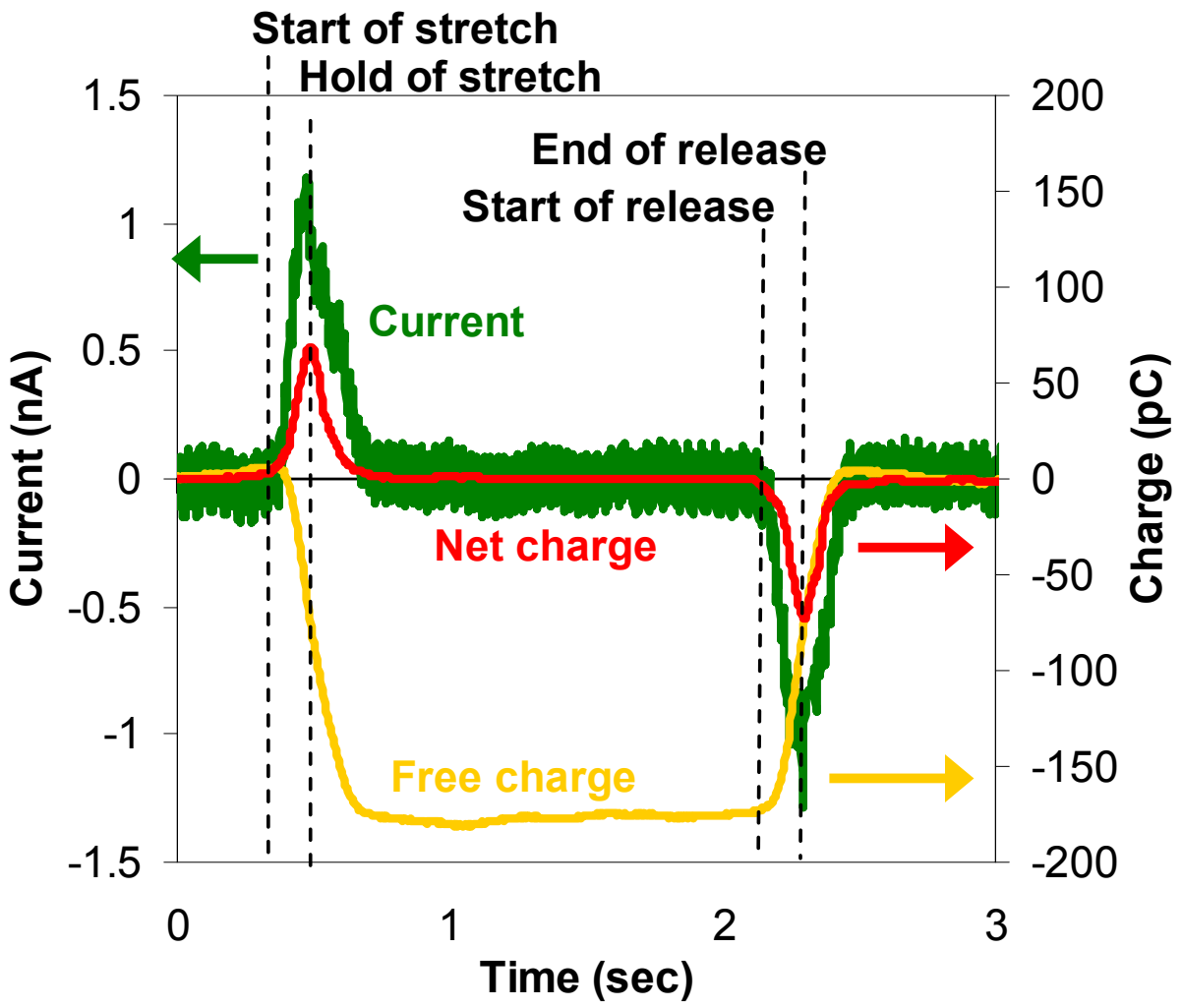

Figure 5.25. Charge movements during the stretch and release of the PVDF nanogenerator. The green line represents the measured output current during the stretch and release stages. The yellow line, which is generated from the integral of measured output current, represents the external free charges (electrons) transported from external wires to the nanogenerator. The red line represents measured net charges (holes) of the PVDF nanogenerator.

The electrical outputs are also affected by the strain rate. For a strain of 0.085% applied over 0.04 and 0.10 seconds, output currents of 2.74 and 1.16 nA were experimentally measured , respectively, with charges similar in both experiments (Figure. 5.26). Specifically, the small discrepancy in piezoelectric charges between186 pC for fast strain rate experiments and 175 pC for slow strain rate experiments results from the *RC* time constant of the nanogenerator (*c*. 2.4 second) which allows a small portion of piezoelectric charge to leak through. In the fast strain rate (*c*. 0.17 second) and slow strain rate (*c*. 0.33 second) experiments, there are estimated *c*. 6.8% and *c*. 12.8% of the piezoelectric charges leaking through the nanogenerator, respectively. This

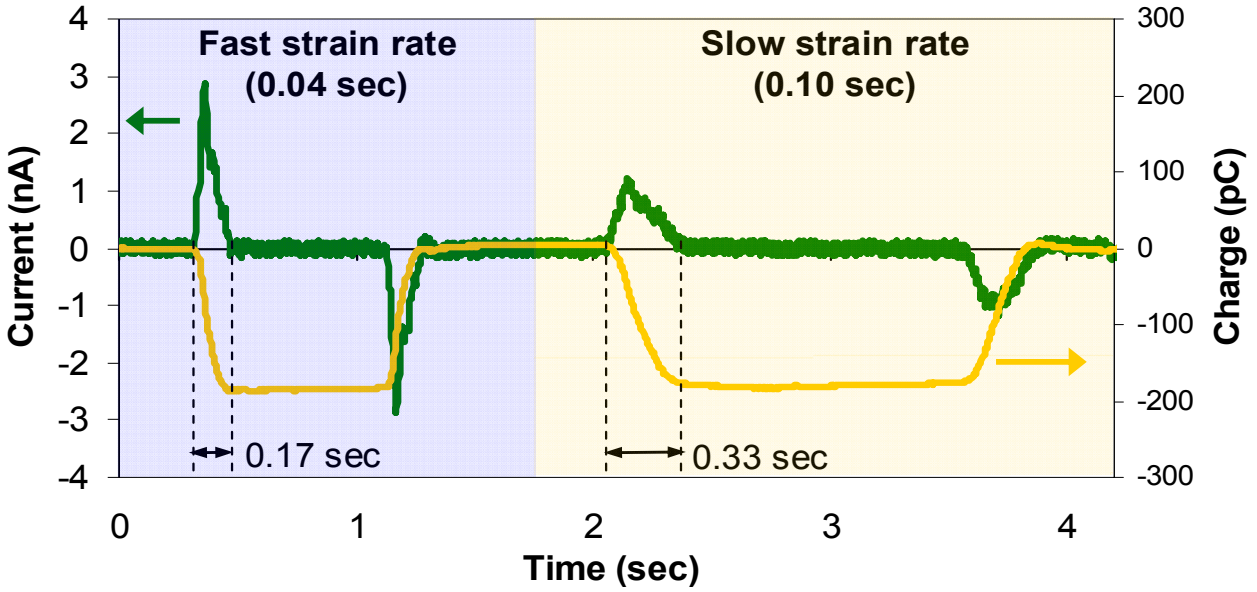

Figure 5.26. Output current (green line) of a PVDF nanogenerator subject to different strain rates under the same applied total strain. The current output increases with strain rate. However, the total charges generated (yellow line, from integral of the output current) are approximately the same under different strain rates.

corresponds to *c*. 93.2% and *c*. 87.2% of the piezoelectric charges that are neutralized by the free charges through the external circuitry, from the same peak value of *c*. 200 pC in both cases. The results are consistent with fundamental piezoelectric theory $i = \dot{q} = d_{33} EA\dot{\varepsilon}$ [31], where i is the generated current, q is the generated charge, d_{33} is the piezoelectric charge constant, E is the Young's modulus, A is the cross-sectional area, and $\dot{\varepsilon}$ is the applied strain rate.

Figure 5.27 shows the responses of the nanogenerator under various cycling frequencies ranging from 2 to 4 Hz for the same applied external strain. The output current during the stretch cycle increases with the frequency, while it remains approximately constant during the release cycle; a phenomenon that can be attributed to the applied strain rate. In the experimental setup, the loading machine controls the stretching profile and therefore the increases in both the strain rate and cycling frequency for a given applied strain. The release process is the release of the cantilever beam substrate from the strained position, which restores the nanogenerator to its original state. The speed with which it reaches this state is controlled by the substrate rigidity, resulting in a higher strain rate that dominates electrical outputs more than the cycling frequency. It is also noted that the output impedance of the nanogenerator varies with frequency and as the cycling frequency increases from 2 to 4 Hz, the impedance drops from 900 MΩ to 300 MΩ (Figure 5.21). This leads to better impedance matching with the measurement system and results in higher electrical outputs. Output voltages with respect to time from the stretch-release frequency cycling experiments (Figure 5.28) exhibited high consistency with the current output results.

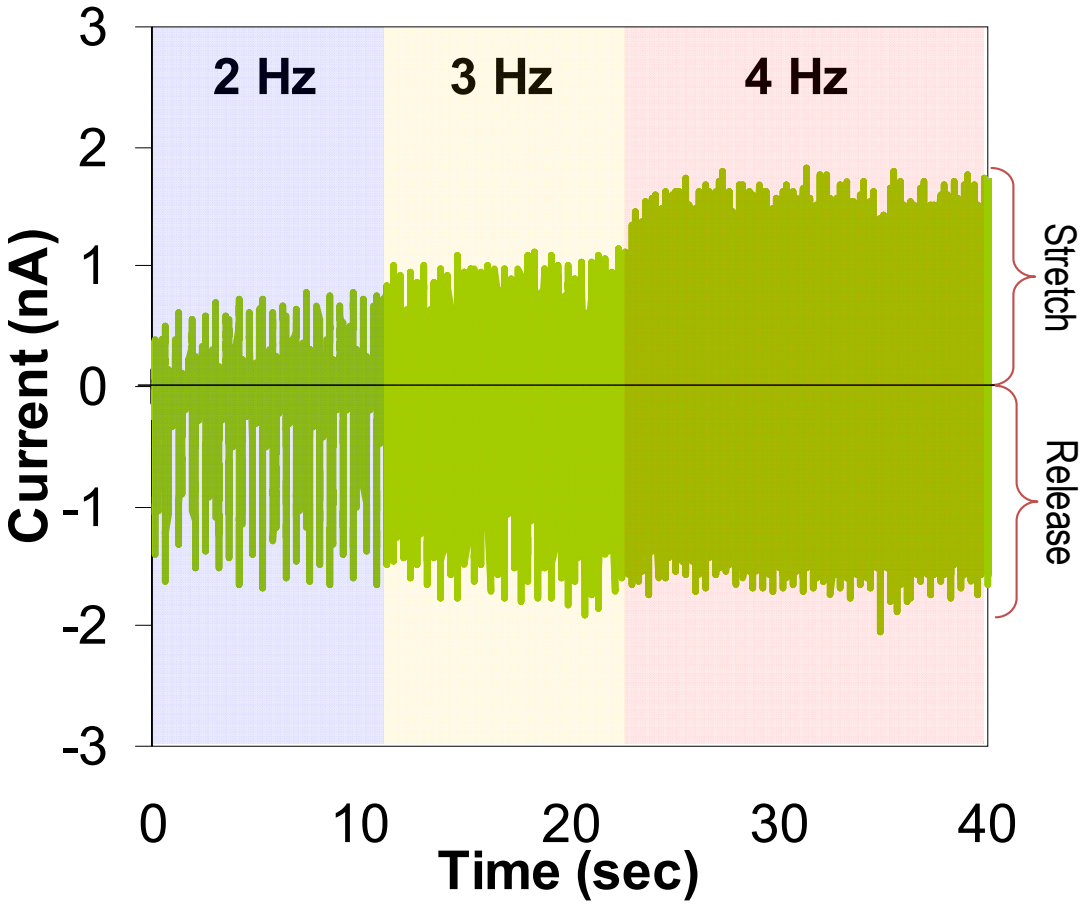

Figure 5.27. Output current of a PVDF nanogenerator subject to different stretch-release cycling frequencies of 2 to 4Hz.

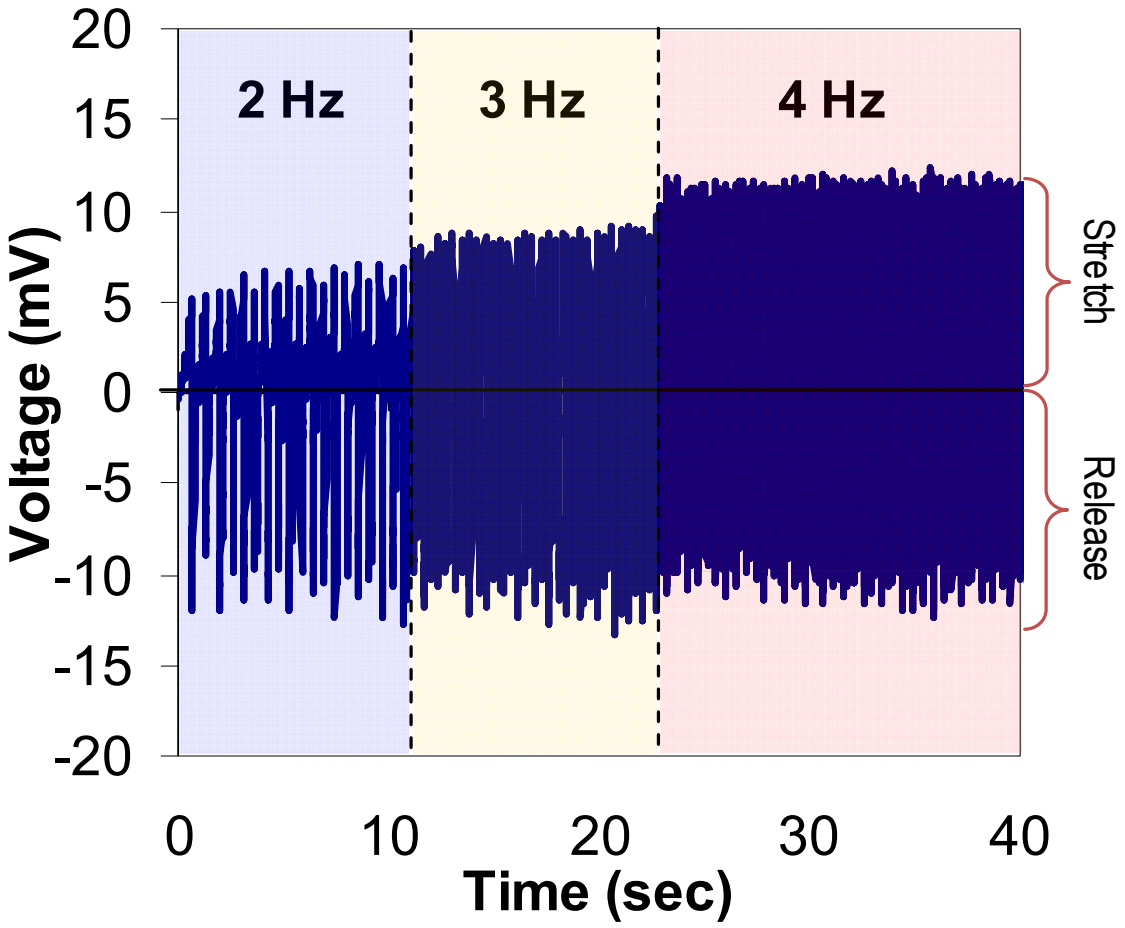

Figure 5.28. Output current of a PVDF nanogenerator subject to different stretch-release cycling frequencies of 2 to 4Hz.

The long-term stability of the PVDF piezoelectric nanogenerator is examined through operation over an extended period of time and exposing it to the ambient environment sans protective packaging. For these experiments, the electrical outputs were relatively stable without noticeable degradation for a stretch-release cycle frequency of 0.5 Hz and an operation time of 100 minutes (Figure 5.29). Output voltages under long-term operation of 0.5Hz for 100 minutes (Figure 5.30) also illustrated similar performance with the current outputs.

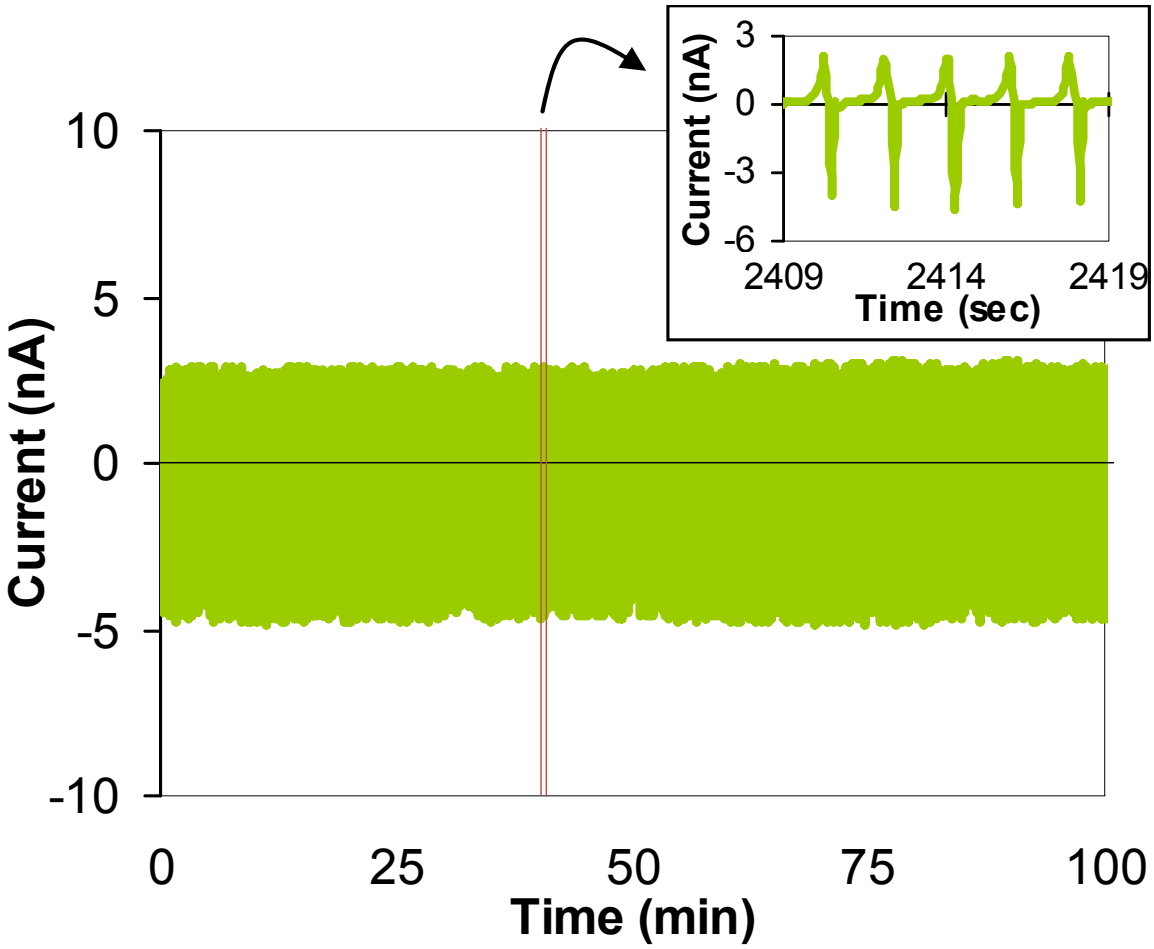

Figure 5.29. Output current of a PVDF nanogenerator under 0.5 Hz of continuous stretch-release for 100 minutes, demonstrating the stability of the nanogenerator. The inset shows the detailed profiles of the electrical outputs.

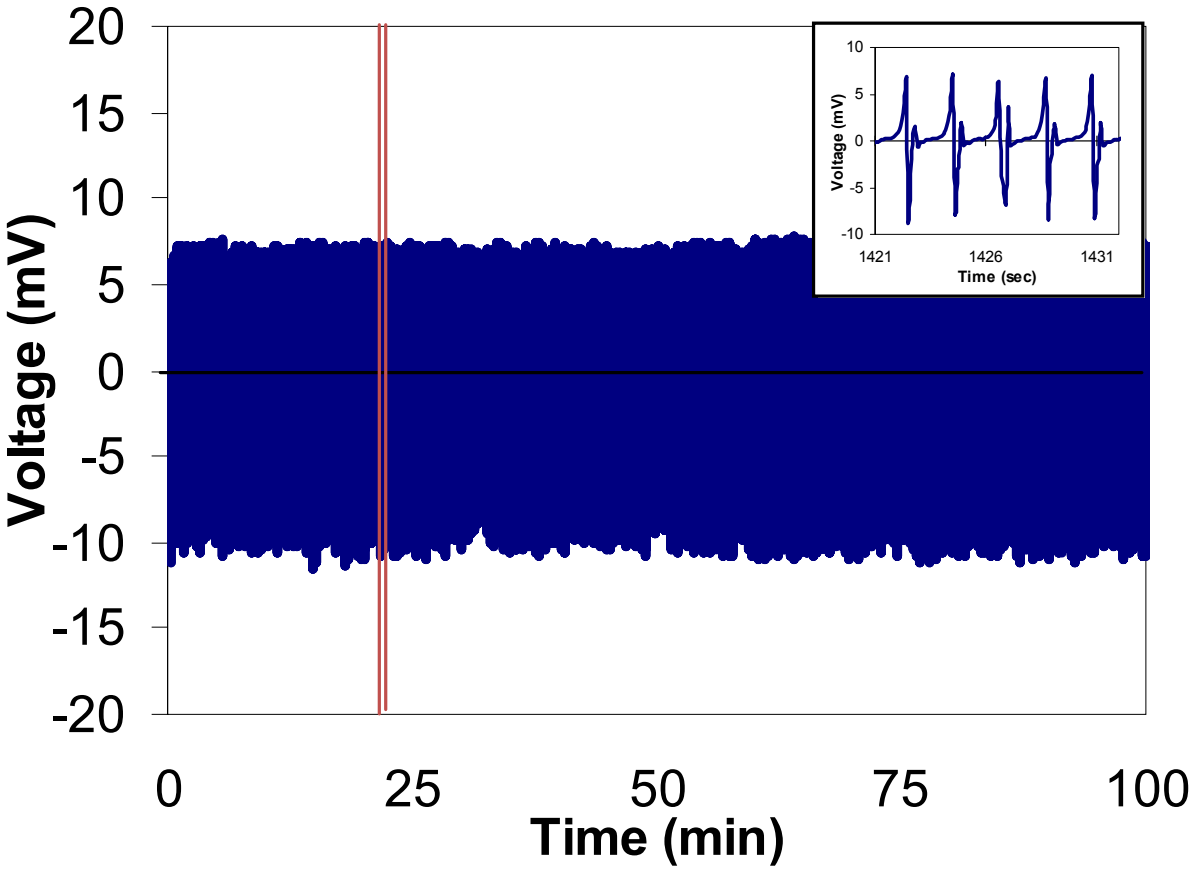

Figure 5.30. Output voltage of a PVDF nanogenerator under continuous stretch and release for 100 minutes.

5.6.5.2. Limitations of Conventional Electrospinning

The conventional electrospinning process produces randomly oriented nanofibers such that the piezoelectric outputs mostly cancel out one another as shown in Figure 5.31. By different electrode pattern design in conventional electrospinning [32], the electrostatic forces can guide PVDF nanofibers across the gap of two electrodes (Figure 5.32). However, the PVDF nanofiber arrays do not have controlled polarity. The polarities of these PVDF nanofibers were still cancelling out one another such that the overall electric outputs were close to zero (Figure 5.33).

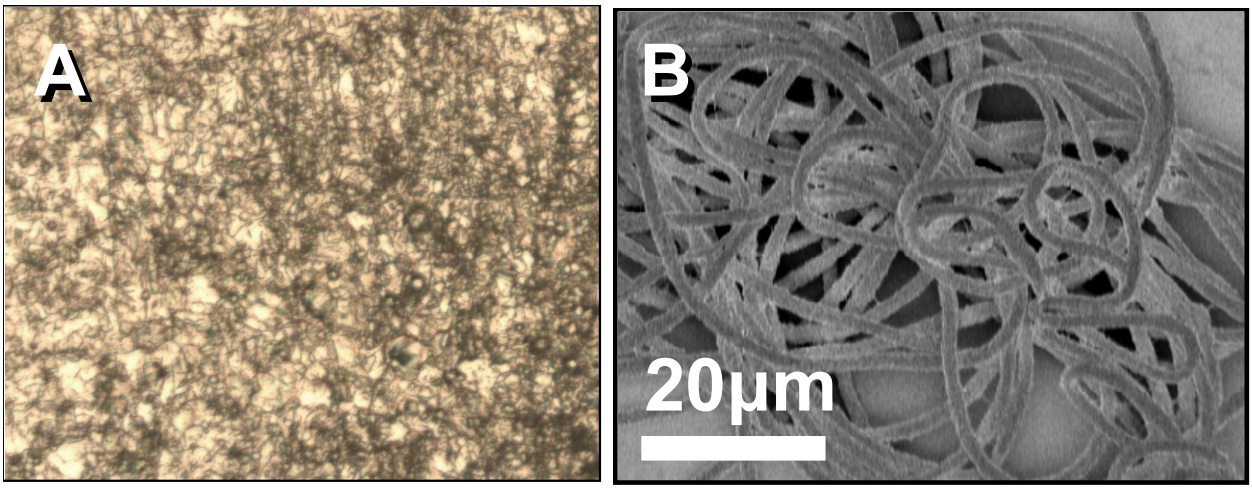

Figure 5.31. (A) Optical image and (B) Scanning electron microscope (SEM) image showing spiraling and random patterns of as-spun PVDF nanofibers as the result of the conventional electrospinning process.

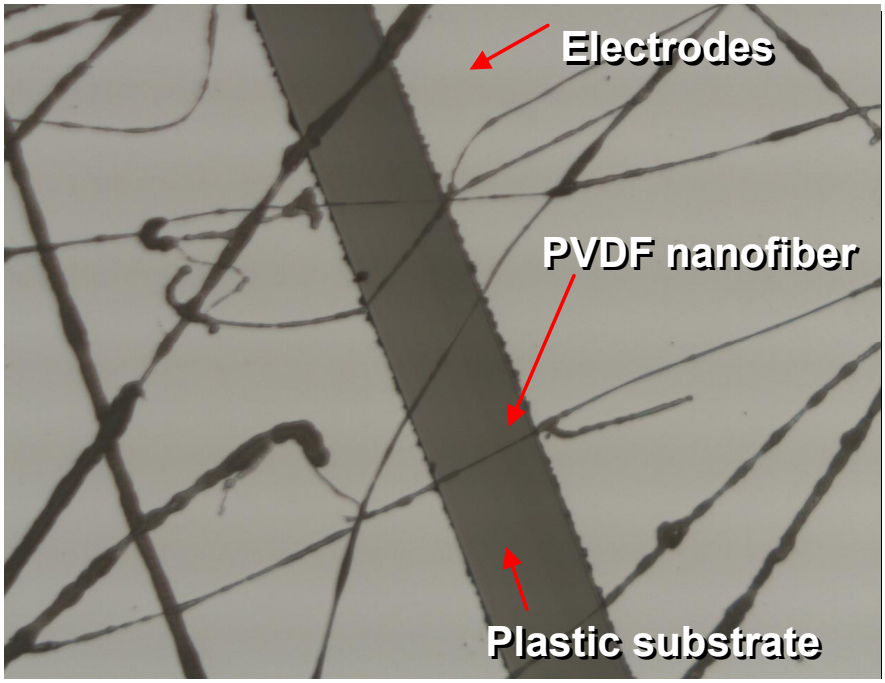

Figure 5.32. Optical image of PVDF nanofibers deposited between two metal electrodes by conventional electrospinning.

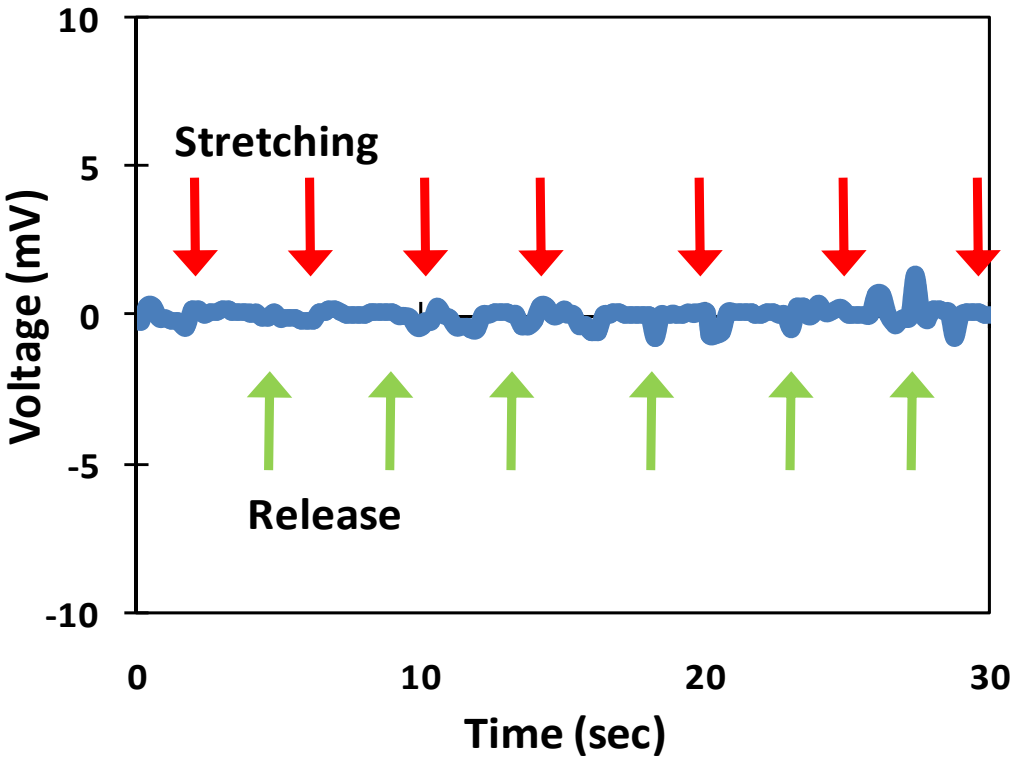

Figure 5.33. Voltage output of the random PVDF nanofibers subject to continuous stretch and release.

5.6.5.3. Validation of Piezoelectric Response

To verify that the electrical outputs were generated from piezoelectric properties of PVDF nanofibers, we performed the same experiments but change the nanofiber material from PVDF to the non-piezoelectric polymer, poly(ethylene oxide) (PEO). The output voltage (Figure 5.34) showed only noise with no visible peaks, indicating that PEO nanofibers did not produce piezoelectric behavior like the PVDF nanofiber (Figure 5.35). The data precluded the possibility of residual charges, friction, or contact potential as the cause of the observed electric outputs for the PVDF nanofibers.

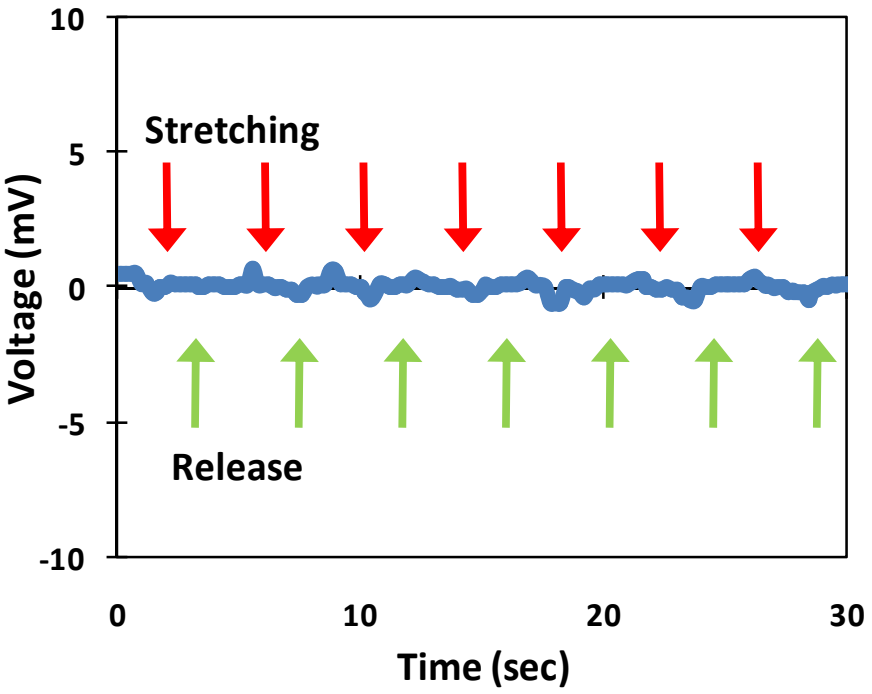

Figure 5.34. Voltage output of a single PEO nanofiber subject to continuous stretch and release.

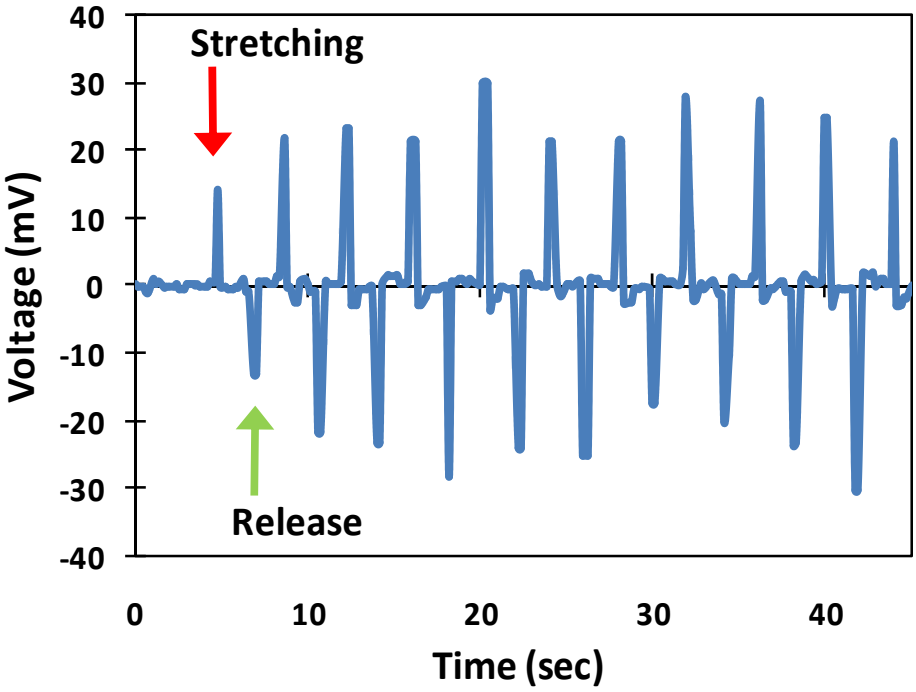

Figure 5.35. Voltage output of a single PVDF nanofiber subject to continuous stretch and release.

To confirm the validity of the recorded piezoelectric responses, various combinations of probe connections and experiments on stretching/compressing of the nanogenerators were characterized. We first examined if our PVDF nanofibers met the "switching polarity" criterion, which would confirm that the measured outputs were indeed generated by the piezoelectric response [8]. In forward connections, the positive and negative probes were connected to the positive and negative potential of the PVDF nanofiber, respectively. In the reverse connection, this connection is reversed as shown in Figure 5.36. Since the polarity of the PVDF nanofiber was fixed, this switching polarity test generated electrical outputs (Figure 5.37) with opposite polarity of those in Figure 5.23.

In our experiments, compressing the PVDF nanofiber generated electrical outputs (Figure 5.38) with polarities opposite to those of the stretch experiments. This further confirmed the piezoelectric properties of our PVDF nanofiber. We also performed polarity switching tests in compression experiments to verify the piezoelectric response. The polarity of electrical outputs in the forward and reverse connections had opposite polarities as shown in Figure 5.38 and Figure 5.39.

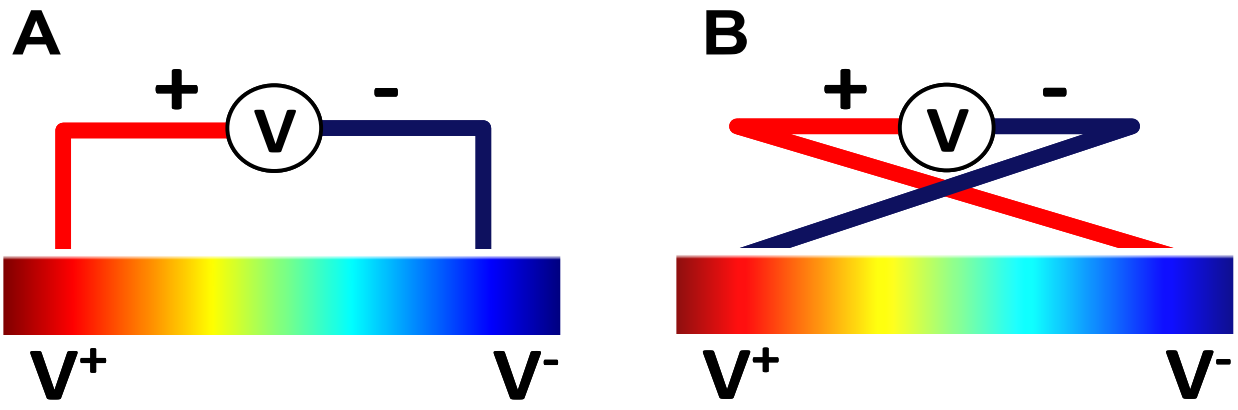

Figure 5.36. (A) Forward connection and (B) reverse connection for switching polarity tests.

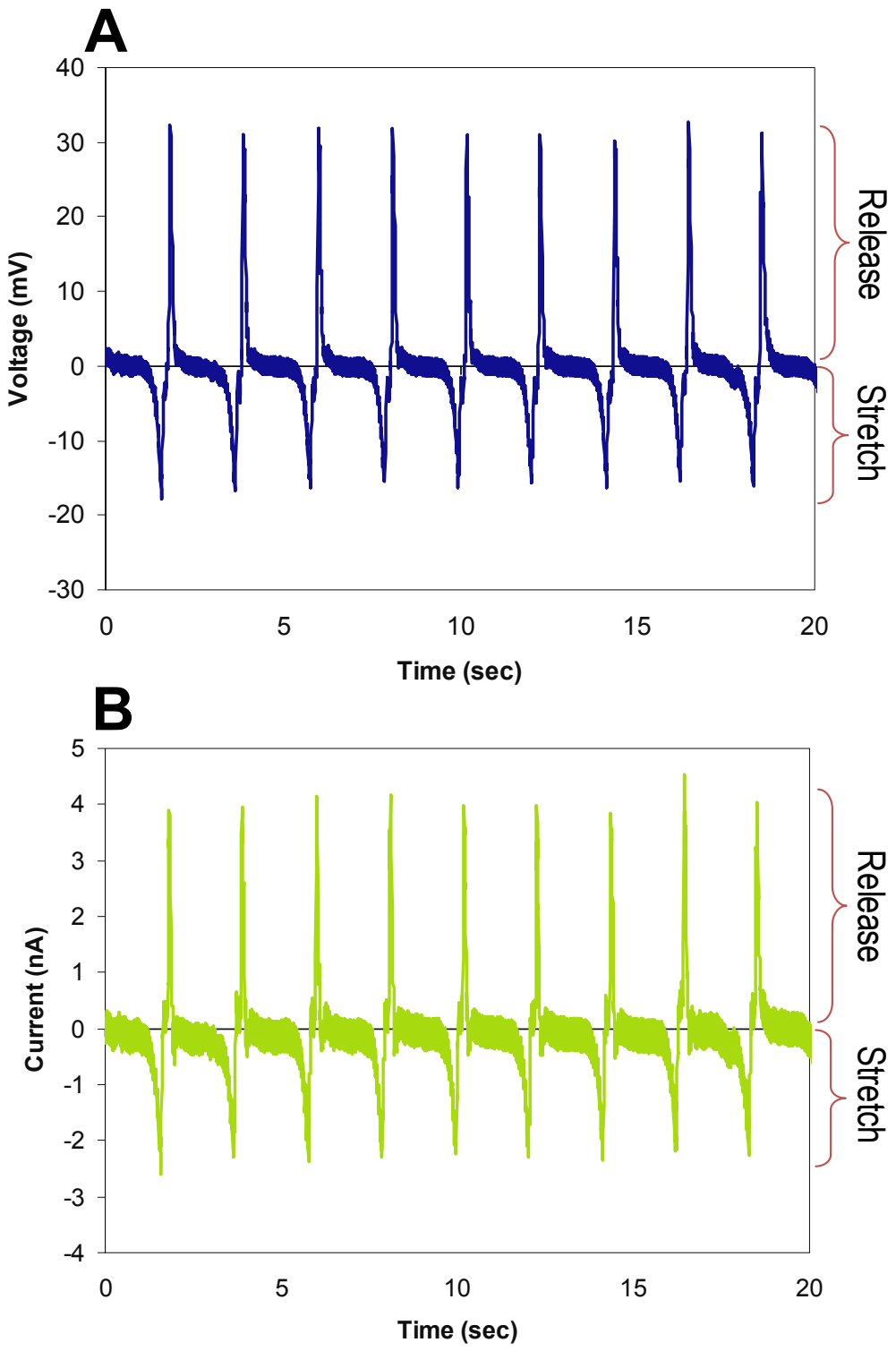

Figure 5.37. Electrical outputs of a PVDF nanogenerator subject to continuous stretch and release when reversely connected to the measurement system. (A) Output voltage. (B) Output current.

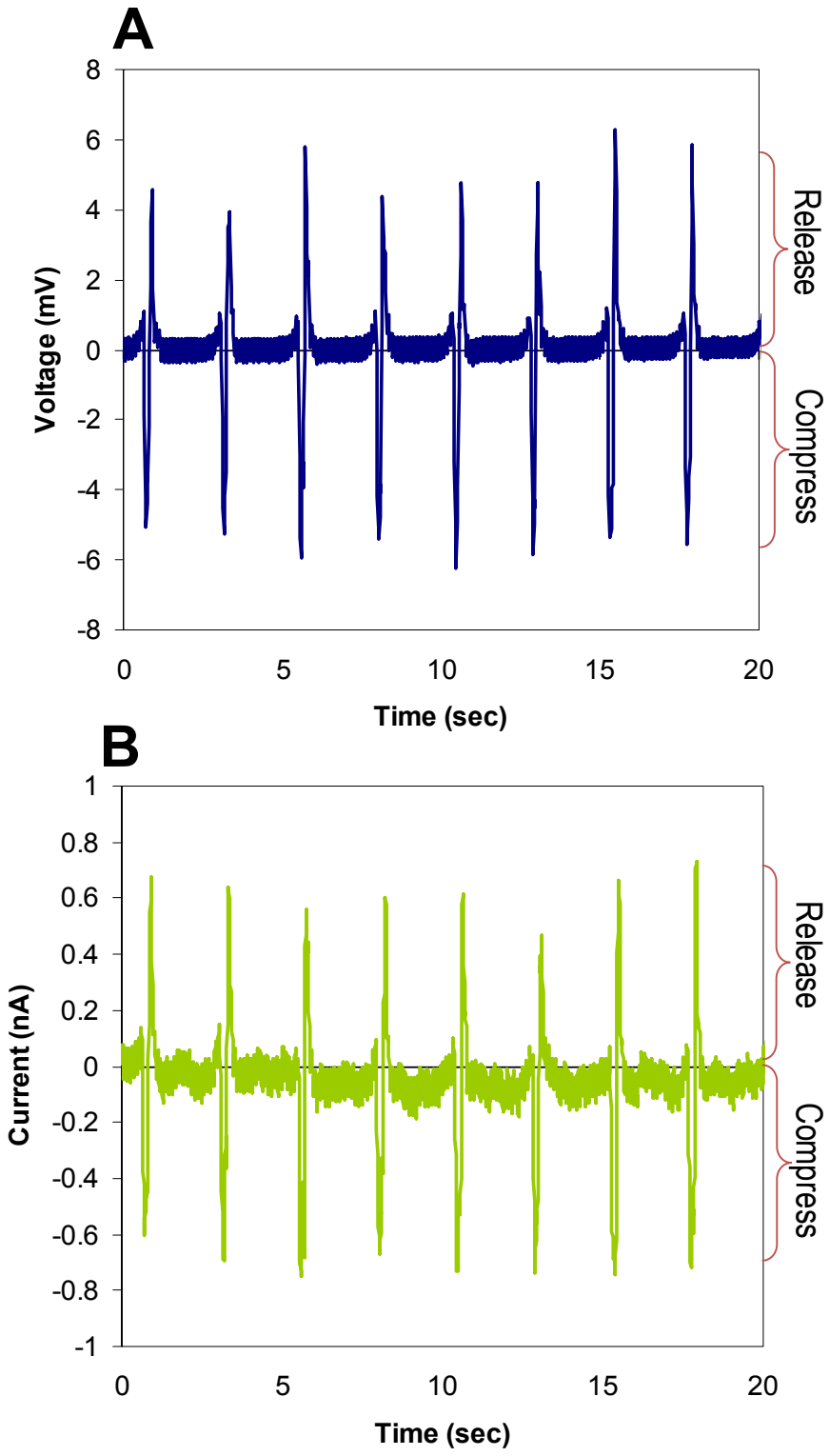

Figure 5.38. Electrical outputs of a single piezoelectric PVDF nanofiber subject to continuous compress and release. (A) Output voltage. (B) Output current.

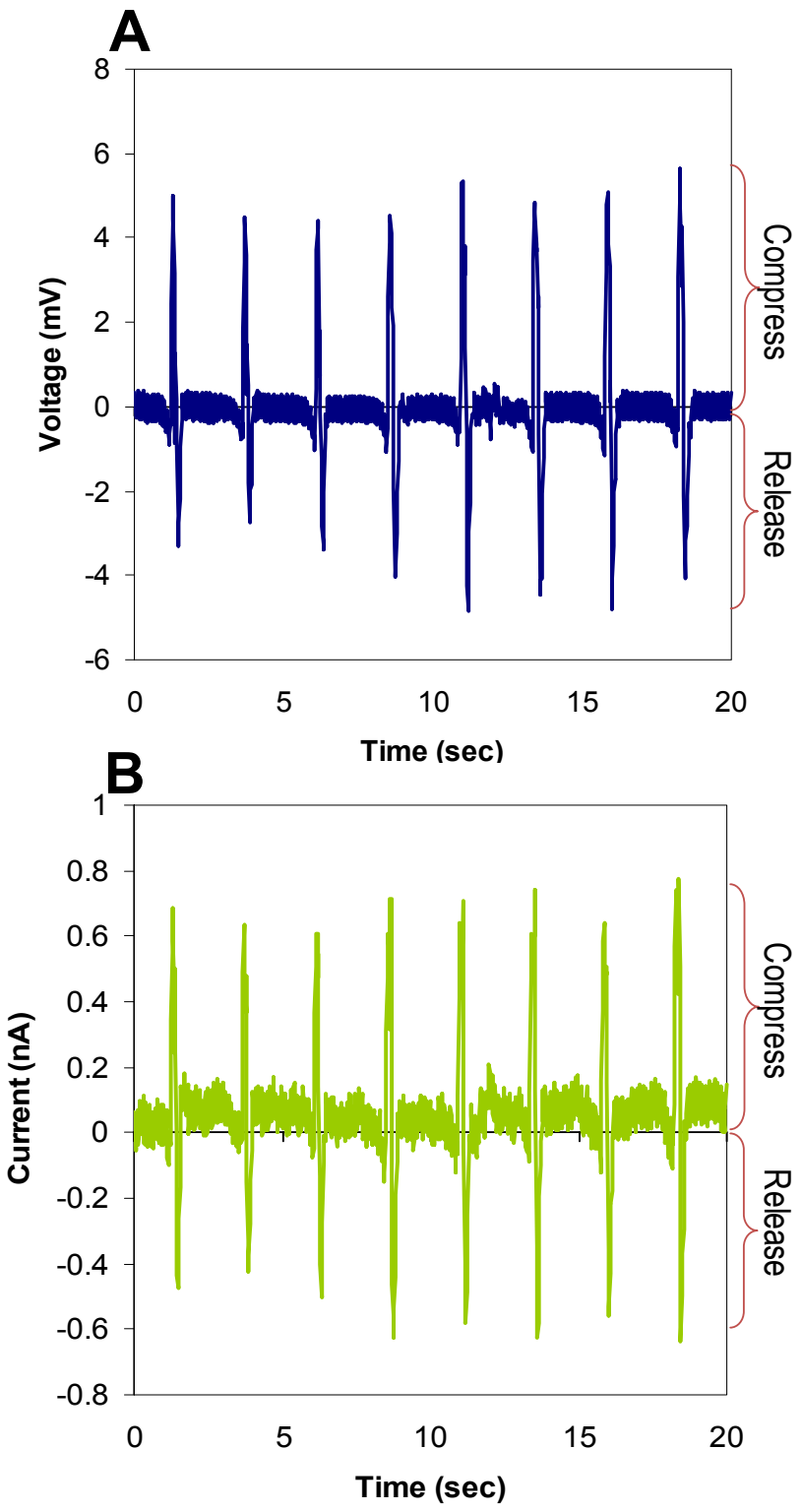

Figure 5.39. Electrical outputs of a single piezoelectric PVDF nanofiber subject to continuous compression and release when reversely connected to the measurement system. (A) Output voltage. (B) Output current.

It was also found that the output voltage and current of the PVDF nanogenerator could be enhanced by serial and parallel connections, respectively (Figure 5.40). The electrical outputs of serial and parallel connections are approximately the sum of the two individual nanogenerators, which satisfies the "linear superposition" criterion proposed by Yang *et al* [8] to confirm the true piezoelectric responses. This is achieved by the direct-write characteristics of NFES, as the placement and polarity of the PVDF nanofibers can be manipulated such that nanofibers are in either serial or parallel connections during the fabrication process.

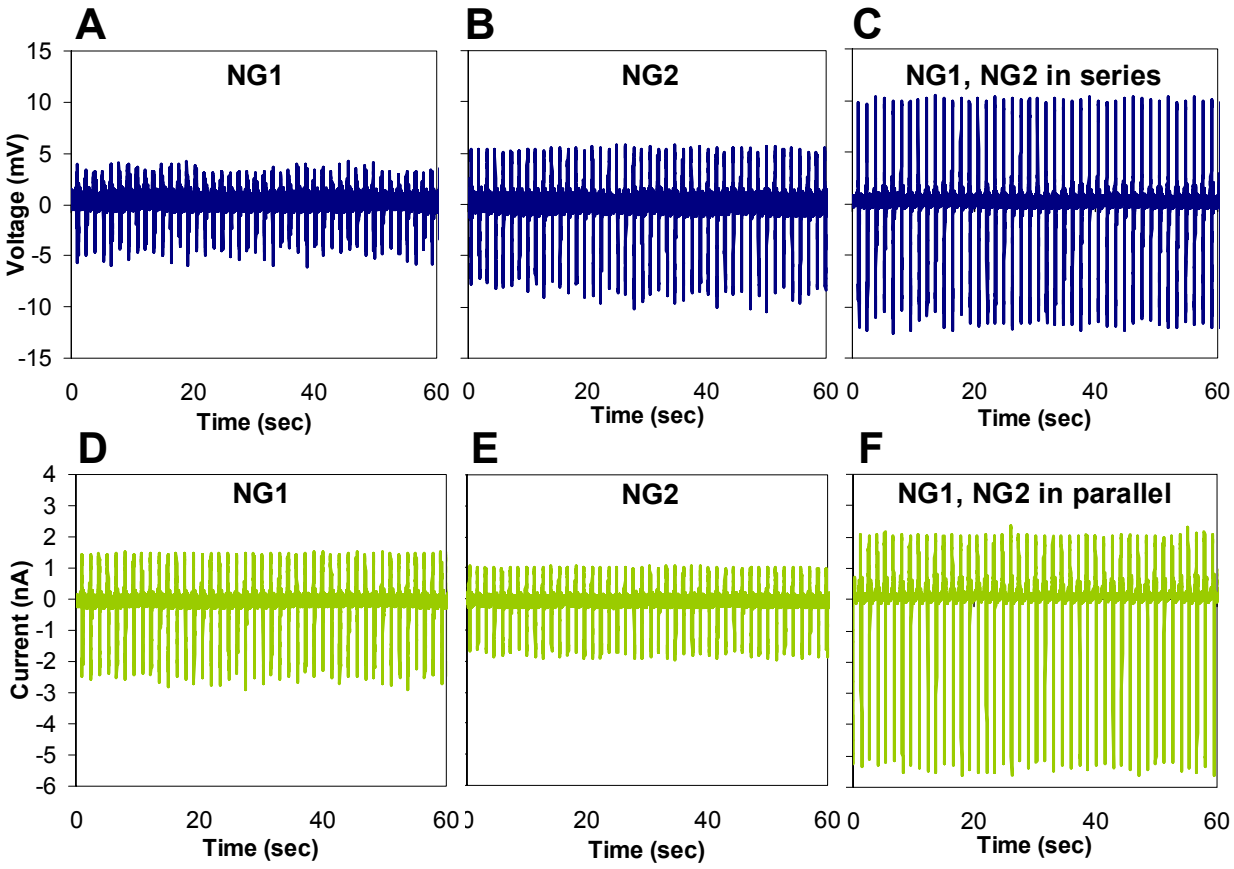

Figure 5.40. Output voltages of (A) nanogenerator #1 and (B) nanogenerator #2 subject to continuous stretch and release. (C) Output voltages constructively add when two nanogenerators are in serial connection. Output currents of (D) nanogenerator #1 and (E) nanogenerator #2 subject to continuous stretch and release. (F) Output currents constructively add when two nanogenerators are in parallel connection. All data are measured when the two nanogenerators are operated in the same strain, strain rate, and frequency.

5.6.5.4. Energy Conversion Efficiency

The energy conversion efficiency (ECE) in this section was defined as

$$\text{ECE} \equiv \frac{\textit{Electric energy generated}}{\textit{Mechanical energy applied}} = \kappa^2$$

where κ is the electromechanical coupling coefficient of the piezoelectric material. The electric energy W_e was estimated by integrating the product of output voltage and current of the PVDF nanogenerator when stretched. The elastic strain energy was estimated by using

$$W_s = \frac{1}{2} EA\varepsilon^2 L_0$$

where E is Young's modulus of the material, A is cross-sectional area, ε is the strain applied on the material, and L_0 is the length of the material. The dimensions of the PVDF nanofibers were measured with SEM after the energy generation experiments. There were more than 45 PVDF nanogenerators used in our experiments to estimate the energy conversion efficiency. Among all samples in the energy conversion efficiency experiments, the nanofibers were 600 nm – 6.5 μm in diameter, 100 – 600 μm in length, and the Young's modulus was estimated as 1.4 GPa [33].

By analyzing 45 samples, the energy conversion efficiency of our nanogenerators was found to be as high as 21.8% with an average of 12.5%, a value that is much greater than typical power generators made from experimental piezoelectric PVDF thin films (0.5 – 4%) [34, 35, 36, 37] and commercial PVDF thin films (0.5 – 2.6%) tested under the same conditions in this work (Figure 5.41).

The efficiency of the PVDF thin film was estimated using the same method as the PVDF nanogenerators. However, d_{31} mode was utilized in PVDF thin film instead of d_{33} mode to accommodate for the strain loading setup. In the experiments, the output voltage and current of the PVDF thin film were *c.* 60 mV and *c.* 60 μA, resulting in a energy conversion efficiency of 0.5 – 2.6% (average 1.3%). We realized that the energy conversion efficiency of d_{31} mode would be smaller than d_{33} mode (d_{33} = 30 pC/N and d_{31} = 22 pC/N from the company's data sheet [29]). If taken into account, the efficiency would be enhanced by ~1.8 times, resulting in an average efficiency of 2.3%. However, it is noted that the real strain applied on the PVDF thin film would be larger than the strain on the top surface of the plastic substrate, which was measured by a strain gauge. Therefore, the energy conversion efficiency of the PVDF thin films would become smaller if we used the real strains on the PVDF thin films to calculate the efficiency. The energy conversion efficiency of PVDF thin film provided by the company was 1.96%, which was close to the estimation from our experiment. This demonstrated that the approach we used in calculating the energy conversion efficiency was reasonable.

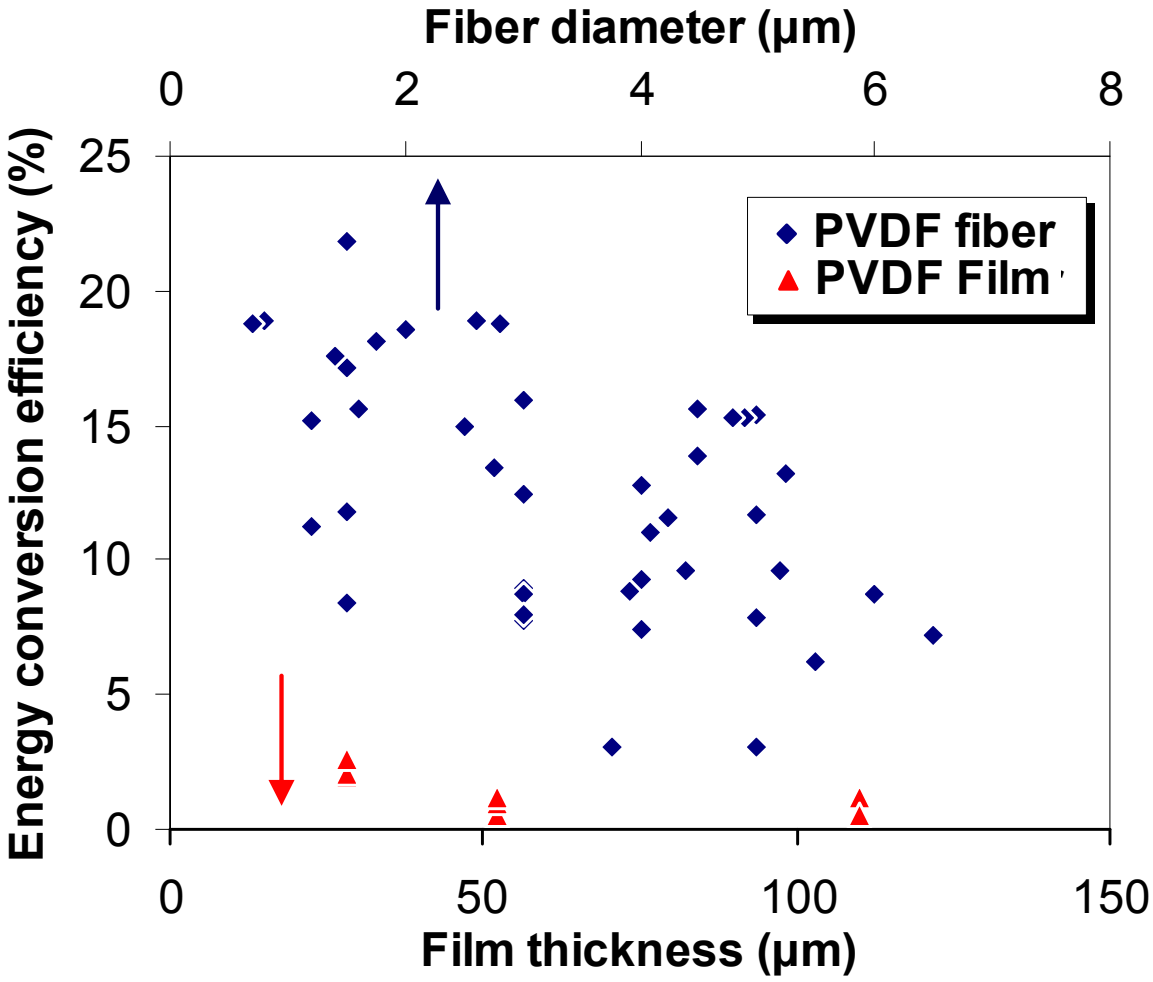

Figure 5.41. Plots of measured energy conversion efficiency of PVDF nanogenerators and thin films with different feature sizes.

The error analysis was performed to examine the repeatability and accuracy of our measurement system. First, we estimated the electrical energy error by calculating the average and standard deviation of electric energy generated from the same PVDF nanogenerator under the same operating conditions. As shown in Figure 5.42 and Table 5.3, the calculated electric energy had an average of 4.07×10^{-13} J and a standard deviation of 8.74×10^{-14} J, corresponding to an error ($\Delta W_e / W_e$) of 21.5%. The elastic strain energy error mainly came from the mechanical strain variations, which was caused by the strain loading machine and plastic substrate. We estimated this error by continuously bending the plastic substrate by the same amount and measuring the strains to obtain the average and standard deviation. In our experiment, the measured strain had an average of 0.085% and a standard deviation of 0.0013%, corresponding to a strain error ($\Delta\varepsilon/\varepsilon$) of 1.5% and an elastic strain energy error ($\Delta W_s / W_s$) of 3.0%. Therefore, the total error of the energy conversion efficiency (ΔECE / ECE) was *c.* 21.71%.

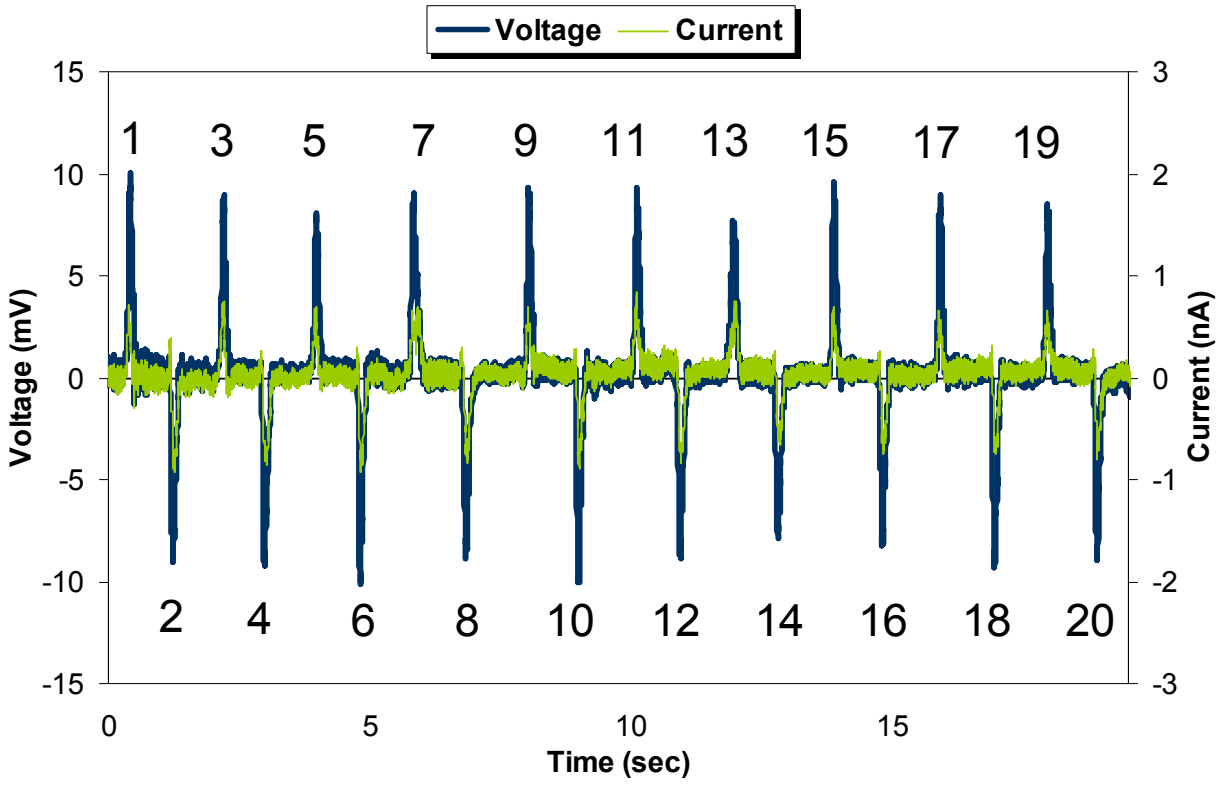

Figure 5.42. Output voltage and current of a PVDF nanogenerator subject to continuous stretch and release under the same strain.

Table 5.3. Calculated electric energy of PVDF nanogenerator.

No. of peaks	Electric energy (J)
1	3.23E-13
2	5.10E-13
3	3.28E-13
4	5.06E-13
5	3.03E-13
6	5.47E-13
7	4.76E-13
8	4.56E-13
9	3.09E-13
10	5.38E-13
11	3.93E-13
12	4.83E-13
13	4.06E-13
14	3.86E-13
15	3.03E-13
16	4.21E-13
17	2.64E-13
18	4.51E-13
19	2.89E-13
20	4.39E-13
Average	**4.07E-13**
Standard deviation	**8.74-14**

The general trend in Figure 5.41 indicates that nanogenerators with smaller diameters exhibit higher energy conversion efficiencies, even with variable piezoelectric properties resulting from slight changes in processing conditions. Several possible reasons could have contributed to the observed enhanced electromechanical response. For example, previous reports have demonstrated a drop in the piezoelectric coefficient due to internal defects in ultrathin PZT films [38], while nanogenerators made by the NFES process could possibly have fewer defects than the PVDF thin film due to a higher degree of crystallinity and chain orientation [39]. The difference in elastic boundary conditions (thin film/bulk samples have metal electrodes on both ends as constraints) [40] and the physical size of the nanogenerators could promote size dependent piezoelectricity such as "flexoelectricity", which is caused by strain gradients that locally break inversion symmetry and induce polarization [41].

Furthermore, piezoelectric thin films could have a significant fraction of the measured responses coming from extrinsic contributions collectively known as "domain wall motion" [42]. PVDF thin film material has a domain wall motion barrier at *c*.0.3% strain [43], under which the piezoelectric response results from the mostly linear, intrinsic response (the responses of single domains). Once the applied strain increases beyond the barrier, the piezoelectric response is dominated by the remarkably large, nonlinear extrinsic responses due to domain wall motion [43].

We observed a much smaller domain wall motion barrier in PVDF nanofibers (*c*.0.01%) as shown in Figure 5.43 which results in large piezoelectric responses for strain higher than 0.01%. This could be caused by small concentrations of point and line defects in the nanofibers which improve the contribution of domain wall motion and lead to higher energy conversion efficiency.

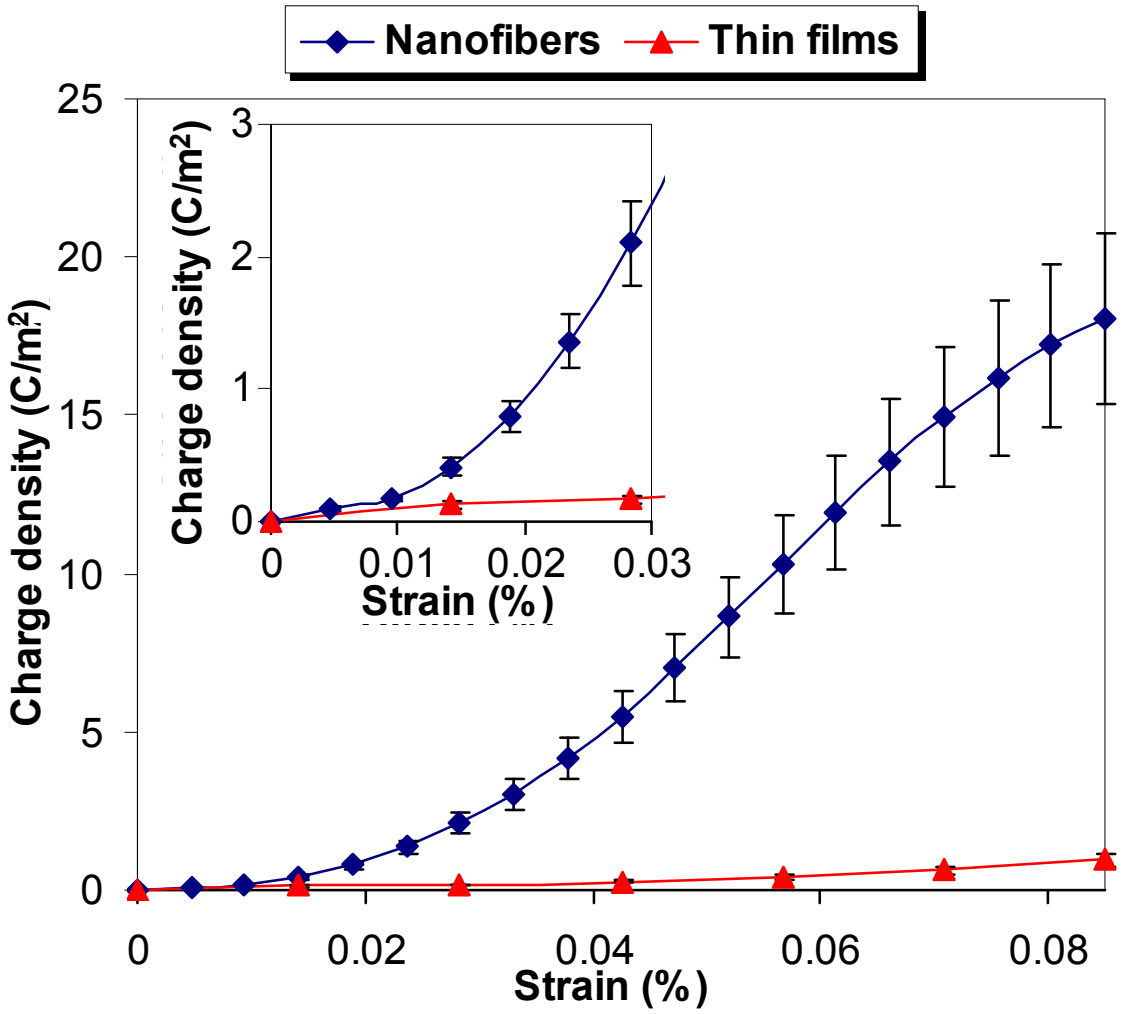

Figure 5.43. Experimental results of PVDF thin film and nanofiber charge density (generated charges divided by electrode area) with respect to applied strain. The charge density of PVDF nanofiber increases nonlinearly when the applied strain is larger than *c.* 0.01%. The inset shows the details under small strains.

5.7 Summary

In summary, we have demonstrated PVDF nanogenerators that are directly written onto flexible plastic substrate using NFES. The piezoelectric responses of single PVDF nanofibers were measured and multiple nanofibers were arranged to enhance the electrical outputs. The reported nanogenerator has several advantages over other maco-, micro-, and nanogenerators, including high energy conversion efficiency, manufacturability, and the capability of integration with other micro/nanofabrication processes. The principle and the nanogenerator demonstrated

could be the basis for integrated power source in nanodevices and wireless sensors or new self-powered textile by direct-writing nanofibers onto a large area cloth to boost the total power output for portable electronics.

References

[1] X. Lu, M. B. McElroy, and J. Kiviluoma, "Global potential for wind-generated electricity," *Proceedings of the National Academy of Sciences U.S.A.*, vol. 106**,** pp.10933-10938, 2009.

[2] J. Scruggs and P. Jacob, "Harvesting ocean wave energy," *Science*, vol. 323, no. 5918, pp. 1176-1178, 2009.

[3] J. A. Paradiso and T. Starner, "Energy scavenging for mobile and wireless electronics," *IEEE Pervasive Computing*, vol. 4, no. 1, pp. 18-27, 2005.

[4] J. M. Donelan, Q. Li, V. Naing, J. A. Hoffer, D. J. Weber, and A. D. Kuo, "Biomechanical energy harvesting: generating electricity during walking with minimal user effort," *Science*, vol. 319, no. 5864, pp. 807-810, 2008.

[5] Z. L. Wang and J. Song, "Piezoelectric nanogenerators based on zinc oxide nanowire arrays," *Science*, vol. 312, no. 5771, pp. 242-246, 2006.

[6] X. Wang, J. Song, J. Liu, and Z. L. Wang, "Direct-current nanogenerator driven by ultrasonic," *Science*, vol. 316, no. 5821, pp. 102-105, 2007.

[7] Y. Qin, X.Wang, and Z. L. Wang, "Microfibre-nanowire hybrid structure for energy scavenging," *Nature*, vol. 451, pp. 809-813, 2008.

[8] R. Yang, L. Qin, L. Dai, and Z. L. Wang, "Power generation with laterally packaged piezoelectric fine wires," *Nature Nanotechnology*, vol. 4, pp. 34-39, 2009.

[9] T. Hattori, M. Kanaoka, and H. Ohigashi, "Improved piezoelectricity in thick lamellar beta-form crystals of poly(vinylidene fluoride) crystallized under high pressure," *Journal of Applied Physics*, vol. 79, no. 4, pp. 2016-2022, 1996.

[10] Y. Ye, Y. Jiang, Z. Wu, and H. Zeng, "Phase transitions of poly(vinylidene fluoride) under electric fields," *Integrated Ferroelectrics*, vol. 80, no. 1, pp. 245-251, 2006.

[11] P. Sajkiewicz, A.Wasiak, and Z. Golclowski, "Phase transitions during stretching of poly(vinylidene fluoride)," *European Polymer Journal*, vol. 35, no. 3, pp. 423-429, 1999.

[12] A. Salimi and A. A. Yousefi, "FTIR Studies of β-Phase Formation in PVDF Stretched Films," *Polymer Testing*, vol. 22, no. 6, pp. 699-704, 2003.

[13] M. Neidhöfer, F. Beaume, L. Ibos, A. Bernès, and C. Lacabanne, "Structural evolution of PVDF during storage or annealing," *Polymer*, vol. 45, no. 5, pp. 1679-1688, 2004.

[14] R. Gregorio and N. Chaves Pereira de Souza Nociti, "Effect of PMMA addition on the solution crystallization of the alpha and beta phases of poly(vinylidene fluoride)," *Journal of Physics D: Applied Physics*, vol. 28, no. 2, pp. 432-436, 1995.

[15] J. S. Andrew, J. J. Mack, and D. R. Clarke, "Electrospinning of polyvinylidene difluoride-based nanocomposite fibers," *Journal of Materials Research*, vol. 23, no. 1, pp. 105-114, 2007.

[16] J. S. Andrew and D. R. Clarke, "Effect of electrospinning on the ferroelectric phase content of polyvinylidene difluoride fibers," *Langmuir*, vol. 24, no. 3, pp. 670-672, 2008.

[17] K. Gao, X. Hu, C. Dai, T. Yi, "Crystal structures of electrospun PVDF membranes and its separator application for rechargeable lithium metal cells," *Materials Science and Engineering: B*, vol. 131, no. 1-3, pp. 100-105, 2006.

[18] M. Nasir, H. Matsumoto, T. Danno, M. Minagawa, T. Irisawa, M. Shioya, and A. Tanioka,

"Control of diameter, morphology, and structure of PVDF nanofiber fabricated by electrospray deposition," *Journal of Polymer Science: Part B: Polymer Physics*, vol. 44, no. 5, pp. 779-786, 2006.

[19] M. Nasir, H. Matsumoto, M. Minagawa, A. Tanioka, T. Danno, and H. Horibe, "Formation of β-phase crystalline structure of PVDF nanofiber by electrospray deposition: additive effect of ionic fluorinated surfactant," *Polymer Journal*, vol. 39, no. 7, pp. 670-674, 2007.

[20] X. Ren and Y. Dzenis, "Novel continuous poly(vinylidene fluoride) nanofibers," *Materials Research Society Symposium Proceedings*, vol. 920, pp. 0920-S03-03, 2006.

[21] W. A. Yee, M. Kotaki, Y. Liu, and X. Lu, "Morphology, polymorphism behavior and molecular orientation of electrospun poly(vinylidene fluoride) fibers," *Polymer*, vol. 48, no. 2, pp. 512-521, 2006.

[22] L. Yu and P. Cebe, "Crystal polymorphism in electrospun composite nanofibers of poly(vinylidene fluoride) with nanoclay," *Polymer*, vol. 50, no. 9, pp. 2133-2141, 2009.

[23] Z. Zhao, J. Li, X. Yuan, X. Li, Y. Zhang, and J. Sheng, "Preparation and properties of electrospun poly(vinylidene fluoride) membranes," *Journal of Applied Polymer Science*, vol. 97, no. 2, pp. 466-474, 2004.

[24] J. Zheng, A. He, J. Li, and C. C. Han, "Polymorphism control of poly(vinylidene fluoride) through electrospinning," *Macromolecular Rapid Communications*, vol. 28, no. 22, pp. 2159-2162, 2007.

[25] Z.-M. Huang, Y.-Z. Zhangb, M. Kotakic, and S. Ramakrishna, "A review on polymer nanofibers by electrospinning and their applications in nanocomposites," *Composites Science and Technology*, vol. 63, no. 15, pp. 2223-2253, 2003.

[26] L.D. Morgret, K.J. Pawlowski, J. A. Hinkley, "Electrospinning of polyvinylidene fluoride and polyetherimide from mixed solvents," *NASA Technical Report*, NASA/TM-2005-213786, 2005.

[27] D. Li and Y. Xia, "Electrospinning of nanofibers: Reinventing the wheel?" *Advanced Materials*, vol. 16, no. 14, pp. 1151-1170, 2004.

[28] Q.P. Pham, U. Sharma, and A.G. Mikos, "Electrospinning of polymeric nanofibers for tissue engineering applications: a review," *Tissue Engineering*, vol. 12, no. 5, pp. 1197-1211, 2006.

[29] http://www.acoustics.co.uk/static/pdf/PVdF-properties.pdf

[30] M. Alexe, S. Senz, M. A. Schubert, D. Hesse, and U. Gösele, "Energy harvesting using nanowires?" *Advanced Materials*, vol. 20, no. 21, pp. 4021-4026, 2008.

[31] J. Sirohi and I. Chopra, "Fundamental understanding of piezoelectric strain sensors," *Journal of Intelligent Material Systems and Structures*, vol. 11, no. 4, pp. 246-257, 2000.

[32] D. Li, Y. Wang, and Y. Xia, "Electrospinning of polymeric and ceramic nanofibers as uniaxially aligned arrays," *Nano Letters*, vol. 3, no. 8, pp. 1167-1171, 2003.

[33] S. Vidhate, A. Shaito, J. Chung, and N. A. D'Souza, "Crystallization, mechanical, and rheological behavior of polyvinylidene fluoride-carbon nanofiber composites," *Journal of Applied Polymer Science*, vol. 112, no. 1, pp. 254-260, 2009.

[34] J. Kymissis, C. Kendall, J. Paradiso, and N. Gershenfeld, "Parasitic power harvesting in shoes," *Second IEEE International Symposium on Wearable Computers*, pp. 132-139, 1998.

[35] E. Häsler, L. Stein, and G. Harbauer, "Implantable physiological power supply with PVDF film," *Ferroelectrics*, vol. 60, no. 1, pp. 277-282, 1984.

[36] T. Starner, "Human powered wearable computing," *IBM Systems Journal*, vol. 35, no. 3-4, pp. 618-629, 1996.

[37] V. H. Schmidt, "Piezoelectric energy conversion in windmills," *Proceedings of IEEE Ultrasonics Symposium*, vol. 2, pp. 897-904, 1992.

[38] S. Dunn, "Determination of cross sectional variation of ferroelectric properties for thin film (ca. 500 nm) PZT (30/70) via PFM," *Integrated Ferroelectrics*, vol. 59, no. 1, pp. 1505-1512, 2003.

[39] S.-Y. Gu, Q.-L. Wu, J. Ren, and G. J. Vancso, "Mechanical properties of a single electrospun fiber and its structures," *Macromolecular Rapid Communications*, vol. 26, no. 9, pp. 716-720, 2005.

[40] M.-H. Zhao, Z.-L. Wang, and S. X. Mao, "Piezoelectric characterization of individual zinc oxide nanobelt probed by piezoresponse force microscope," *Nano Letters*, vol. 4, no. 4, pp. 587-590, 2004.

[41] M. S. Majdoub, P. Sharma, and T. Cagin, "Enhanced size-dependent piezoelectricity and elasticity in nanostructures due to the flexoelectric effect," *Physical Review B*, vol. 77, no. 12, pp. 125424-1-125424-9, 2008.

[42] N. Bassiri-Gharb, I. Fujii, E. Hong, S. Trolier-McKinstry, D. V. Taylor, and D. Damjanovic, "Domain wall contributions to the properties of piezoelectric thin films," *Journal of Electroceramics*, vol. 19, no. 1, pp. 47-67, 2007.

[43] Y. Wang, K. Ren, and Q. M. Zhang, "Direct piezoelectric response of piezopolymer polyvinylidene fluoride under high mechanical strain and stress," *Applied Physics Letters*, vol. 91, no. 22, pp. 222905-1-222905-3, 2007.

CHAPTER 6

CONCLUSION AND FUTURE DIRECTIONS

6.1. Conclusion

6.1.1. Near-Field Electrospinning

A near-field electrospinning (NFES) process has been developed to deposit solid nanofibers in a direct and controllable manner. Specifically, a tungsten electrode with tip diameter of 25 μm is used to construct nanofibers of 50~500 nm line-width on silicon based collectors while the liquid polymer solution is supplied in a manner analogous to that of a dip pen. The minimum applied bias voltage is 600 V and minimum electrode-to-collector distance is 500 μm for achieve position controllable deposition. Charged nanofibers can be orderly collected, making NFES a potential tool in direct write nanofabrication for a variety of materials. NFES is a simple yet powerful method for direct-write deposition of nanofibers with unprecedented controllability at resolutions comparable to those achieved with much more expensive and sophisticated lithography tools. It should be especially useful for the heterogeneous integration of nanoscale materials to devices prepared by conventional lithographic and manufacturing methods, such as microelectronics and MEMS structures. Furthermore, NFES could play a key role in building up ordered non-woven nanofibers for various applications.

6.1.2. Continuous Near-Field Electrospinning

To compensate for the discontinuity issue of NFES, a continuous near-field electrospinning process has been developed to deposit solid nanofibers with orderly patterns over large areas. Before the onset of electrospinning, a bias voltage is applied to a semi-spherical shaped polymer droplet outside of a syringe needle, and a probe tip mechanically draws a single fiber from the droplet to initiate continuous NFES. Contrary to the conventional electrospinning process, we show that decreasing electrical field in continuous NFES results in smaller line-width deposition, and nanofibers can be assembled into controlled, complex patterns such as circular shapes and grid arrays on large and flat areas. The concept and demonstration of continuous NFES make possible applications that were difficult to achieve by conventional electrospinning. We believe that the ability to deposit polymeric materials at precise locations with specific patterns can open up opportunities for cost-effective, heterogeneous integration of a variety of materials.

6.1.3. Direct-Write Piezoelectric PVDF

Nanogenerators capable of converting energy from mechanical sources to electricity with high effective efficiency using low-cost, non-semiconducting, organic nanomaterials are attractive for many applications, including energy harvesters. In this dissertation, near-field electrospinning is used to direct-write polyvinylidene fluoride (PVDF) nanofibers with *in-situ* mechanical stretch and electrical poling characteristics to produce piezoelectric properties. Under mechanical stretching, nanogenerators have shown repeatable and consistent electrical outputs with energy conversion efficiency an order of magnitude higher than those made of PVDF thin films. The early onset of the nonlinear domain wall motions behavior has been identified as one mechanism responsible for the apparent high piezoelectricity in nanofibers, rendering them potentially advantageous for sensing and actuation applications.

The reported nanogenerator has several advantages over other maco-, micro-, and nanogenerators, including high energy conversion efficiency, manufacturability, and the capability of integration with other micro/nanofabrication processes. The principle and the nanogenerator demonstrated could be the basis for integrated power source in nanodevices and wireless sensors or new self-powered textile by direct-writing nanofibers onto a large area cloth to boost the total power output for portable electronics.

6.2. Future Directions

6.2.1. Near-Field Elecgtrospinning

The concept and initial demonstrations of near-field electrospinning make possible new applications that were impossible by conventional electrospinning. In addition to the nanogenerator demonstrated in this dissertation, there are many other interesting directions that can be implemented by NFES. The following sections will give several examples.

6.2.1.1. Integrated Nanofiber Sensors

The ability of depositing polymeric materials at specific locations can open up opportunities for heterogeneous integration of sensing materials with microelectronics. Figure 6.1 shows the schematic diagram of a simple way to complete the heterogeneous integration of nanofiber materials with prefabricated contact electrodes for possible sensing applications. The chaotic nature of conventional electrospinning prevents the possibility of site specific deposition. The SEM microphoto shows preliminary results. A nanofiber of 100 nm in diameter made of polypyrrole conducting polymer was deposited by NFES in a suspended fashion over two micro bridges made of heavily-doped polysilicon. The nanofiber was deposited with good control over a 10-μm wide air gap as shown. Initial IV characteristics show rectifying behavior under negative voltage input and this phenomenon still needs further investigation. Nevertheless, one may imagine the possible expansion of the proposed architecture to have integrated circuitry underneath the contact pads for transduction, readout, processing, and communications. Furthermore, there are a wide variety of material selections for the electrospinning process such that different kinds of sensors can be constructed by the proposed method.

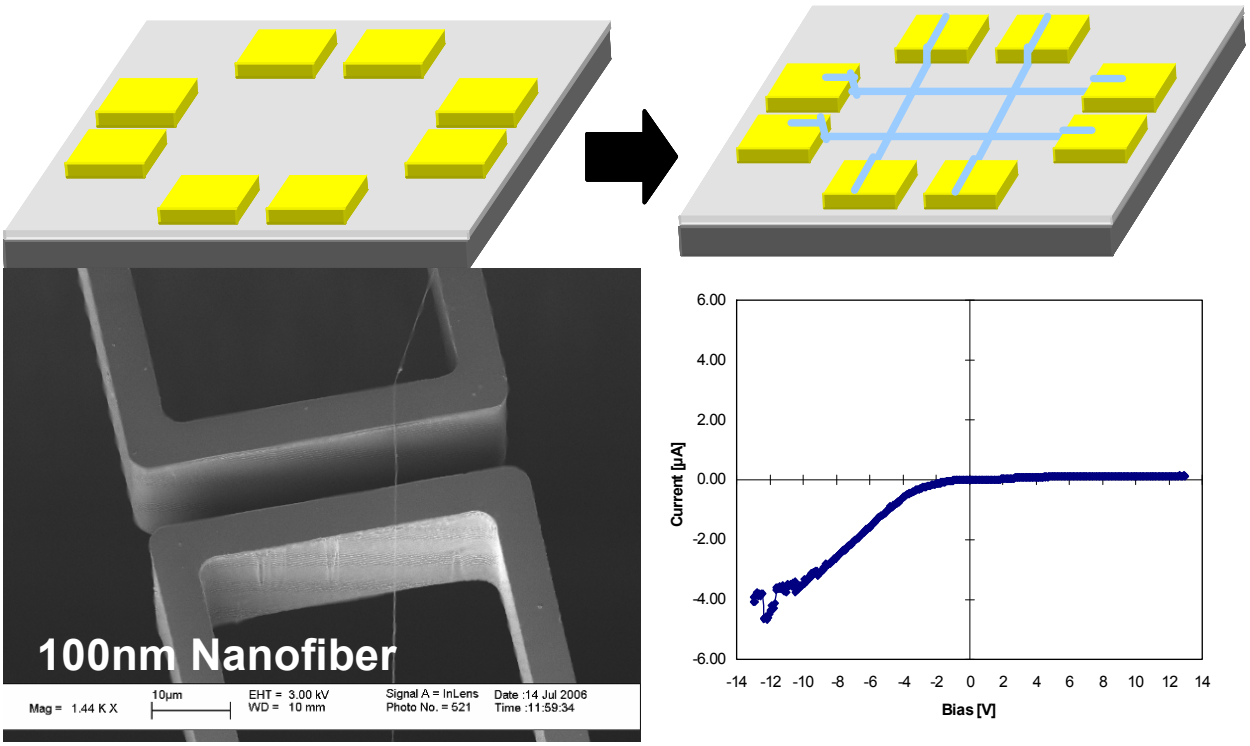

Figure 6.1. Schematic diagram showing a simple way to complete the heterogeneous integration of nanofiber materials with prefabricated contact electrodes for possible sensing applications. The SEM microphoto shows preliminary results that 100 nm in diameter polypyrrole conducting polymer was deposited by NFES over two suspended micro bridges made of heavily-doped polysilicon. This single nanofiber was deposited with good control over a 10 µm wide air gap. Initial IV characteristics show rectifying behavior under negative voltage input.

6.2.1.2. One Dimensional Sub-Wavelength Waveguide

The smallest diameter of an optical beam propagating in dielectric waveguides is of the order of the wavelength because of optical diffraction limits. This limits the size of integrated optical devices and the spatial resolution of the optical measurements. If there were a way to decrease the smallest beam diameter beyond diffraction limit, it would make a great contribution to optical devices in the nanometer range. The structure of proposed one dimensional sub-wavelength waveguide is like rolling a two dimensional optical waveguide into cylinders as shown in Figure 6.2A. The structure can be easily fabricated by coating a thin metal layer around the electrospun nanofibers as shown in Figure 6.2B. The light propagates in one dimensional optical waveguide in transverse electromagnetic mode (TEM), which has the advantage of no cutoff frequency. The attenuation is dominated by resistive loss in metal and light can be guided around sharp corners.

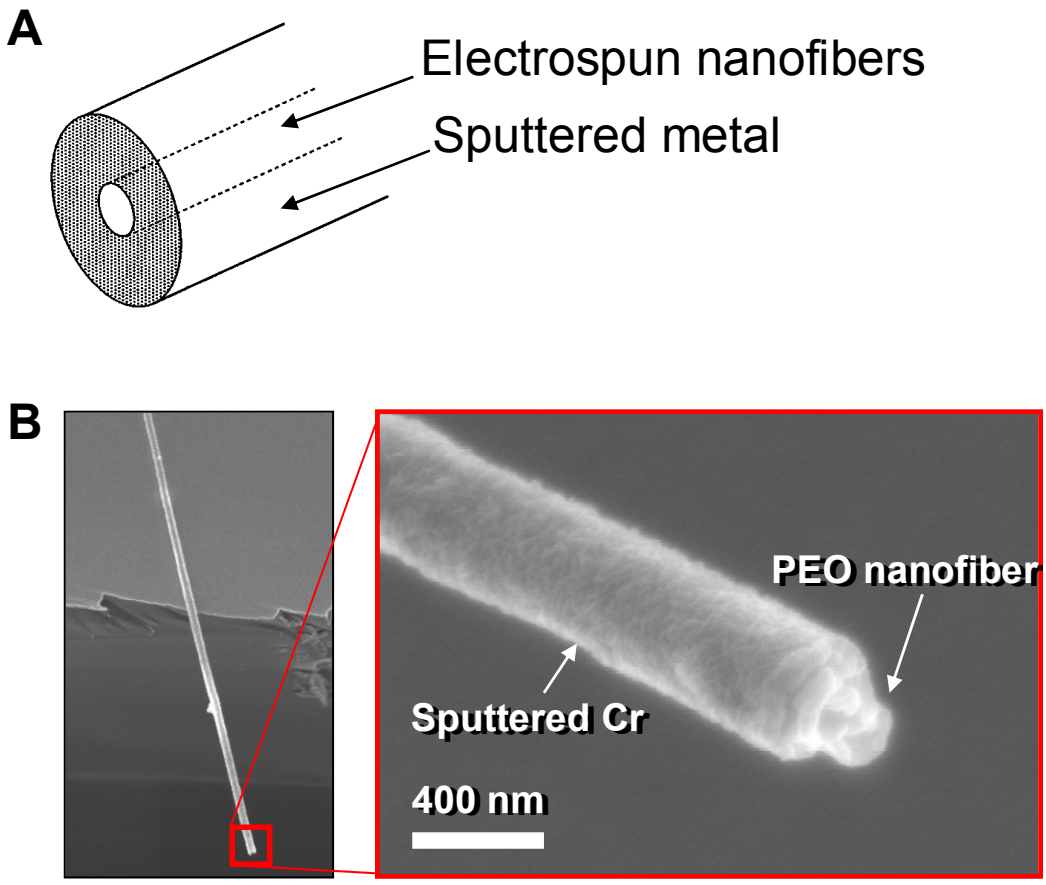

Figure 6.2. (A) Illustration of a one dimensional sub-wavelength optical waveguide. (B) The SEM microphoto shows the fabricated optical waveguide.

6.2.1.3. Biological Applications

NFES can enable bioengineers and biologists to create highly tailored and functionalized culture substrates quickly and at low cost by varying the concentration of factors such as biological compounds (e.g. growth factors/inhibitors, enzymes, proteins), conductivity, porosity, and surface chemistry (e.g. hydrophobicity) in polymeric solutions. Possible applications include drug tests, neuron guidance, stem cell differentiation, proliferation, and apoptosis, focal adhesion and migration, cell growth and cessation, and tissue engineering.

In recent years, artificial tissue and organs have gained great attention due to the drastic mismatch between numbers of tissue and organ donors to the patients requiring transplants. For example, conventional electrospinning [1] have been used to create scaffolds to mimic extracellular matrices (ECMs) for tissue engineering for studying cell behavior such as attachment and proliferation. However, these techniques are non-ideal for tissue engineering because the highly ordered and specialized structures found in real tissues and organs [2] are unachievable. NFES has the potential to not only create ordered structures through automated

processes, but to also specifically functionalize different parts of these structures through the use different materials. The ability to develop and customize ordered 3D structures (Figure 6.3) would enable bioengineers to create 3D scaffolds in vitro that are highly representative of real ECMs. Such scaffolds could extend current tissue engineering techniques to develop previously unachievable organs types and increase the viability of these tissues.

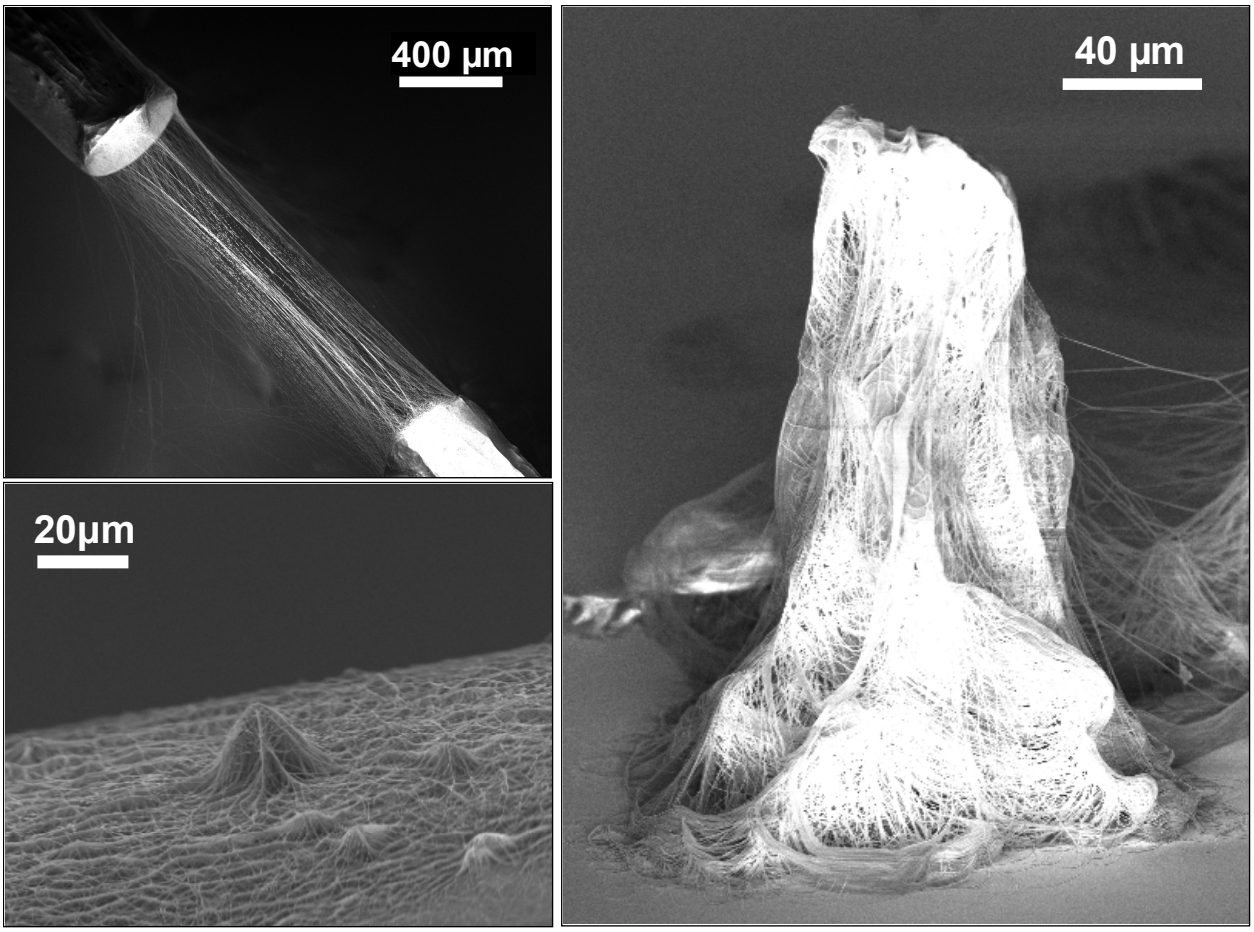

Figure 6.3. The SEM microphoto shows preliminary result of 3D structures fabricated by continuous NFES shows promising potential for bio-scaffolds/substrates applications.

6.2.2. Direct-Write Piezoelectric PVDF

The current experimental results in this dissertation lead to several directions that can be exploited in the future. First, what are the geometry and material effects on the energy generation? These are complex issues as fiber diameter control, material properties, and manufacturing parameters are related to each other and should be investigated at the same time. Processing parameters such as electrical field strength, viscosity of the polymer solution, and environmental conditions will all affect the fiber diameter and piezoelectric properties. Second,

piezoelectric nanofibers have never been studied or demonstrated before and it could present interesting potentials in various applications beyond power scavenge, including piezoelectric sensing and actuation. In this dissertation, we aim to start our studies on manufacturing protocols, material properties and optimizations. A prototype energy harvester demonstration using the proposed electrospun nanofibers is definitely needed for its practical applications. For example, can a single nanofiber be a power source itself for nanosensors that may require low power? Can one make a bundle of these nanofibers for larger power output? Future research should extend the investigations on large scale demonstrations for several possible placements, including buildings, automobiles, bridges etc. Because the natural geometry of nanofibers resembles fabrics, the demonstration of a wearable nanogenerator on clothes could be a starting point.

References

[1] W.-J. Li, C.T. Laurencin, E.J. Caterson, R.S. Tuan, and F.K. Ko. “Electrospun nanofibrous structure: A novel scaffold for tissue engineering.” *Journal of Biomedical Materials Research*, vol. 60, no. 4, pp. 613-621, 2002.

[2] M.P. Lutolf and J.A. Hubbell. “Synthetic biomaterials as instructive extracellular microenvironments for morphogenesis in tissue engineering.” *Nature Biotechnology*, vol. 23, no. 1, pp. 47-55, 2005.